Exploration of astatine chemistry in solution : focus on the Pourbaix diagram in noncomplexing medium and characterization of astatine-mediated halogen bonds

Lu Liu

UNIVERSITE MATIERE BRETAGNE MOLECULES LOIRE ET MATERIAUX

IMT Atlantique
Bretagne-Pays de la Loire
École Mines-Télécom

THESE DE DOCTORAT DE

L'ÉCOLE NATIONALE SUPERIEURE MINES-TELECOM ATLANTIQUE
BRETAGNE PAYS DE LA LOIRE - IMT ATLANTIQUE

ECOLE DOCTORALE N° 596
Matière, Molécules, Matériaux
Spécialité : Chimie Analytique et Radiochimie

Par

Lu LIU

Exploration de la chimie de l'astate en solution : Focalisation sur le diagramme de Pourbaix en milieu non complexant et caractérisation de liaisons halogènes induites par l'astate

Thèse présentée et soutenue à Nantes, le 28 octobre 2020
Unité de recherche : SUBATECH, UMR 6457
Thèse N° : 2020IMTA0205

Rapporteurs avant soutenance :

Claire LE NAOUR	Chargée de recherche, HDR, CNRS, IJCLab
Jean AUPIAIS	Directeur de recherche, CEA, DAM

Composition du Jury :

Président :	Christophe DEN AUWER	Professeur, Université de Nice, ICN
Rapporteurs :	Claire LE NAOUR	Chargée de recherche, HDR, CNRS, IJCLab
	Jean AUPIAIS	Directeur de recherche, CEA, DAM
Examinateurs :	Philippe MOISY	Directeur de Recherche, CEA, Marcoule
	Bernd GRAMBOW	Professeur, IMT Atlantique, SUBATECH
Dir. de thèse :	Gilles MONTAVON	Directeur de recherche, CNRS, SUBATECH
Encadrants :	Julie CHAMPION	Maître de conférences, IMT Atlantique, SUBATECH
	Rémi MAURICE	Chargé de recherche, CNRS, SUBATECH

Acknowledgements

My Ph.D. project was realized in the radiochemistry group at SUBATECH under the direction of Dr. Gilles Montavon, Dr. Julie Champion and Dr. Rémi Maurice. As arriving at the end of this Ph.D. project, I would like to express my gratitude to all those people who made this work possible and an unforgettable experience for me.

I owe my deepest gratitude to my supervisors, Gilles, Julie and Rémi. During this three-year period of my doctoral stage, they have all been very enthusiastic, reactive and complementary to each other concerning my research activities. I would like to thank them for the very nice and close daily guidance for designing, executing, analyzing and enhancing the research works. Their help delivered me a strong scientific background and prepared me for the forthcoming scientific journey.

My special words of thanks should also go to my colleagues in SUBATEH, especially to Sylvain Pardoue, Véronique Baty, Céline Bailly, Guillaume Blain, Nicolas Bessaguet, Katy Perrigaud, Anne Piscitelli, Karine David and Valérie Bossé, for their help on the use of experimental equipment and devices such as the HPLC, COT meter, glove boxes, *etc.* I also would like to thank Romain Berny, Ronald Jahké, Maxime Birot, for the radioprotection service.

I would like to acknowledge my coauthors of articles, Ning Guo, Cecilia Gomez Pech, Nicolas Galland, Seyfeddine Rahali, Jérôme Graton and Jean-Yves Le Questel, for their efforts and expertise on astatine, halogen bonds and quantum mechanical calculations, which lead to the publication of ours articles.

I wish to express my sincere gratitude to all the jury members of my defense, Dr. Claire Le Naour, Prof. Christophe Den Auwer, Prof. Philippe Moisy, Dr. Jean Aupiais and Prof. Bernd Grambow. I am very grateful that they took much time to review my thesis very carefully

and gave me many suggestions to improve my dissertation.

I would like to deliver my special thanks to my schoolmates in Subatech, Haohan, Fengqi, Yifeng, Yajing, Yuwei, Anne-Laure, Yahaya, Emeline, and my friends Ziling, Kan, Zijun, Zijie, Yajun. They helped me a lot to integrate into life in France and they make my life in this country more colorful.

Last but not least, I would like to thank my whole family, who have supported me in carrying a Ph.D. study abroad. And special thanks to my boyfriend, Liangzhao, who has always accompanied me, encouraged me and supported me during my Ph.D. studentship.

Contents

List of abbreviations and symbols

At_{ox}	Astatine species presenting in alkaline and non-reductive conditions
At_{red}	Astatine species presenting in alkaline and reducing conditions
BFC	Bifunctional Chelating agent
$(BuO)_3PO$	Tributyl phosphate
Bu_2SO	Dibutyl sulfoxide
Bu_3PO	Tributylphosphine oxide
CAS	Chemical Abstracts Service
CFRP	Chromatography at Fixed Redox Potential
cHex	Cyclohexane
cHexanone	Cyclohexanone
D_{At}	Distribution coefficient of astatine
DFT	Density Functional Theory
DIPE	Diisopropyl ether
DMAc	Dimethylacetamide
DMAM	Dimethylcyanamide
DTPA	Diethylenetriaminepentaacetic acid
DTT	DL-dithiothreitol
E	Potential
EAS	Electrophilic Aromatic Substitution
EC	Electron Capture
EDTA	Ethylenediaminetetraacetic acid
Et_2O	Diethyl ether
Et_2S	Diethyl sulfide

Hept	Heptane
HPGe	High-Purity Germanium
HPIEC	High-Performance Ion Exchange Chromatography
HSAB	Hard and Soft Acids and Bases
I	Ionic strength
IC	Inorganic Carbon
LET	Linear Energy Transfer
LLC	Liquid/Liquid Competition
LLNL	Lawrence Livermore National Laboratory
M	$mol \cdot L^{-1}$
$Me(EtO)_2PO$	Diethyl methylphosphonate
Me_2Se	Dimethyl selenide
Me_6Ph	Hexamethyl benzene
MePh	Toluene
NAS	Nucleophilic Aromatic Substitution
NHE	Normal Hydrogen Electrode
NTA	Nitrilotriacetic acid
OS	Oxidation State
PBS	Phosphate-Buffered Saline
PET	Positron Emission Tomography
Ph_3PS	Triphenylphosphine sulfide
PIPPS	Piperazine-1,4-bis(propanesulfonic acid)
pK_{BI2}	Diiodine basicity scale
PrCOOEt	Ethyl butyrate
RP	Radiopolarography
SAB	Succinimidyl astatobenzoate
SLC	Solid/Liquid Competition

SPECT	Single Photon Emission Computed Tomography
TAT	Targeted Alpha-particle Therapy
TC	Total Carbon
ThioAcetamide	Thioacetamide
ThioCamph	Thiocamphor
TLC	Thin-Layer Chromatography
TMeThioUrea	Tetramethylthiourea
TMeUrea	Tetramethylurea
TOC	Total Organic Carbon
tSIE	Transformed Spectral Index of External Standard
UV	Ultraviolet
XB	Halogen bond

List of figures

List of tables

Introduction

In 1869, when Dmitri Mendeleev published his periodic table, the space under iodine, *i.e.* the element 85, was empty. In 1940, Dale R. Corson, Kenneth R. MacKenzie, and Emilio G. Segrè synthesized for the first time the element 85 by bombarding bismuth-209 with accelerated alpha particles in a cyclotron at University of California, Berkeley (USA).[1] This element was named "astatine" (with chemical symbol "At") afterward, from the Greek astatos (ἄστατος), meaning "unstable".[2,3] As reflected by its name, astatine is a radioelement. Since its discovery, 39 isotopes have been experimentally identified, all of them being radioactive and actually short-lived ($t_{1/2} \leq 8.1$ h).[4] Astatine is one of the rarest naturally occurring element in the Earth's crust. The total amount is estimated at less than 30 grams at any given time.[5] Thus, it is difficult to collect it, and the major route for obtaining astatine is through production *via* nuclear reactions, in fact in minute quantities. All the chemical studies on astatine are conducted at ultra-trace concentrations (typically between 10^{-10} and 10^{-15} mol·L^{-1}), which makes the classic spectroscopic tools inapplicable to scrutinize astatine chemistry at the molecular level. Even 80 years after the discovery of astatine, its chemistry remains poorly known.

Among its isotopes, astatine-211 (^{211}At) has attracted some particular attention owing to its potential application in nuclear medicine. Indeed, ^{211}At has a half-life of 7.2 hours. It decays through a double-branched pathway producing overall one α particle per decay.[6] The average energy of the emitted α-particles is 6.8 MeV, and the mean linear energy transfer (LET) in tissues is 97 keV·µm^{-1},[7] thus being powerful enough for destroying the diseased cells. These favorable properties make ^{211}At a promising candidate for targeted alpha-particle therapy (TAT). It is based on the injection of radioactive isotopes undergoing alpha decay into the patient to treat diseased tissue at close proximity. A prerequisite for the application is to label ^{211}At in a stable manner to a carrier-targeting

agent, which requires knowledge on astatine chemistry, in particular on its speciation and reactivity in solution.

The high-energy ARRONAX cyclotron in Nantes is capable of producing ^{211}At, which has led several teams, notably radio-, theoretical, and synthetic chemists, to gather for investigating its chemistry and radiolabeling. The project developed at the Subatech laboratory (UMR 6457), in collaboration with the CEISAM laboratory (UMR 6230), aims at exploring the chemistry of astatine in solution by combining experimental and computational approaches. Subatech has initiated this research more than fifteen years ago. The efforts made by Julie Champion and Ning Guo, the first Ph.D. students on this project at Subatech, led to important advances in the speciation of astatine in aqueous solution and in the reactivity of basic astatine species. More precisely, they have identified three oxidation states (OS) in the aqueous medium (–1, +1 and +3) as At^-, At^+, AtO^+,[8–10] and also hydrolysis products of AtO^+,[11,12] which are key information to construct the Pourbaix diagram of astatine. They have also investigated the reactivity of the cationic species of astatine with some inorganic ligands (Cl^-,[13] Br^-,[13,14] I^-,[14] and SCN^-[15]) and also to some organic ones,[15,16] which led to the study on the halogen bonds involving astatine. The present Ph.D. project has two main objectives. The first one is to complete the lacking information of the Pourbaix diagram of astatine in alkaline conditions by actually characterizing the speciation change between $AtO(OH)_2^-$ and At^-. The second objective is to study the capacity of astatine, in particular inside the AtI unit, to form halogen bonds with different Lewis bases.

This dissertation is organized in four main chapters, briefly introduced in the following paragraphs.

The first chapter presents a literature survey on the general property of astatine, the application of ^{211}At in nuclear medicine, and the chemistry of astatine in solution.

The primary constraint for studying astatine, regarding its low availability, is to work at ultra-trace scales (10^{-10} – 10^{-15} mol·L^{-1}). The nature of the species proposed in the

literature is thus deduced from indirect methods based on radiochemistry techniques, such as electromobility, chromatography, or competition methods. The general methodology applied in the framework of this thesis will be presented in the second chapter.

Knowledge on the Pourbaix diagram is essential for chemists. Information is lacking in alkaline conditions because the passage between the two supposed species, At^- and $AtO(OH)_2^-$, has not been directly characterized. This aspect will be exposed in the third chapter.

As a member of the halogen family of elements, halogen-bonded adducts between astatine and Lewis bases have been recently evidenced. The fourth chapter focus on completing the work on At-mediated halogen bonds by extending the preliminary basicity scale with a larger set of Lewis bases and halogen-bond strengths.

Chapter 1. Literature survey

The objective of this chapter is to illustrate the importance of knowing chemical properties of astatine compounds, especially for nuclear medicine applications. Firstly, a brief summary of astatine features will be presented, from its discovery to its general physical properties. Then, the keen interest of astatine in nuclear medicine will be discussed and, in this context, several recent developments on labeling strategies will be highlighted. Although some approaches appear efficient for starting clinical trials, problems are yet to be resolved, emphasizing the urgent need to better understand the basic chemistry of this element. The objectives of the thesis topic will be finally presented in the light of current knowledge of the chemistry of astatine.

1.1 Generality of astatine

Astatine is a radioactive chemical element with the symbol At and atomic number 85. In the periodic table, it belongs to the halogen group, below iodine. This part will focus on the generality of this element, including the history of discovery and the general physical properties, in order to gain overall information of this element.

1.1.1 Discovery of astatine

When Dmitri Mendeleev published his periodic table in 1869, the space underneath iodine, *i.e.*, the element 85, was empty. It was called “eka-iodine” because of its position. Scientists tried to look for it in nature, while considering its extreme rarity, these attempts resulted in several refuted discoveries.

The first widely popularized claim was reported by American physicist Fred Allison in 1931 at the Alabama Polytechnic Institute. He developed a new method called the magneto-optic method. He examined some typical halogen-containing matrices such as

seawater and monazite sand. He claimed to find the element 85 and named it "alabamine".[17] However, his method and the validity of his discovery were disproved by MacPherson in 1934.[18]

Inspired by the work of Allison, Indian chemist Rajendralal De tried to search for eka-iodine in monazite sand by chemical separation. He detected a black substance and named it "dakin" in 1937.[19] Nevertheless, the description of dakin is inconsistent with the chemical properties of astatine identified afterward.

In 1936, Romanian physicist Horia Hulubei and French physicist Yvette Cauchois claimed to have discovered the element 85 through X-ray analysis of radon samples and named it "dor" later. Even though Hulubei and Cauchois's samples did contain astatine, their means to detect it were too weak to be accepted as a firm identification.[19]

In 1940, Swiss chemist Walter Minder announced the discovery of the element 85 as the beta decay product of radium A (polonium-218) by α-particle detection of radon samples, choosing the name "helvetium".[20] In 1942, Minder, in collaboration with the English scientist Alice Leigh-Smith, announced the detection of another isotope of the element 85, presumed to be the product of thorium A (polonium-216) beta decay. They named this substance "anglo-helvetium".[21] These discoveries were disproved by Karlik and Bernert because they were unable to reproduce the experiments.[19]

The first reliable report of the discovery and identification of eka-iodine appeared in 1940 by D. R. Corson, K. R. MacKenzie, and E. Segrè. Instead of searching in nature, the scientists synthesized the element 85 by bombarding bismuth-209 with alpha particles in a cyclotron of University of California in the USA.[1] They suggest the name "astatine", from the Greek *astatos* (ἄστατος), meaning "unstable".[2,3] This work is still considered as the true discovery of astatine, thus credited to Corson, MacKenzie and Segrè.

1.1.2 General properties of the astatine atom

1) Physical properties

Astatine is the Block p, Group 17, Period 6 element. Its ground-state atomic electron configuration is [Xe]$4f^{14}5d^{10}6s^{2}6p^{5}$. Its Van der Waals radius is 202 pm.[22] In its elemental form, astatine's Chemical Abstracts Service (CAS) number is 7440-68-8.

2) Isotopes

There are 39 known isotopes of astatine, with atomic masses (mass numbers) of 191–229. Theoretical modeling suggests that 37 more isotopes could exist.[4] Neither stable or long-lived astatine isotope has been observed, nor is one expected to exist.[23]

3) Natural occurrence

Four of astatine's isotopes can be found in nature as a result of the decay of radioactive thorium and uranium ores, and trace quantities of ^{237}Np. ^{215}At and ^{219}At exist in the decay chain of ^{235}U. ^{218}At can be found in the decay chain of ^{238}U. ^{217}At is produced through the decay of ^{237}Np. However, the total amount of astatine in the Earth's crust is estimated to be at most 30 grams at any given time.[5,24] Astatine is considered as the rarest naturally occurring element.

1.1.3 Two representative isotopes: ^{210}At and ^{211}At

1) ^{210}At

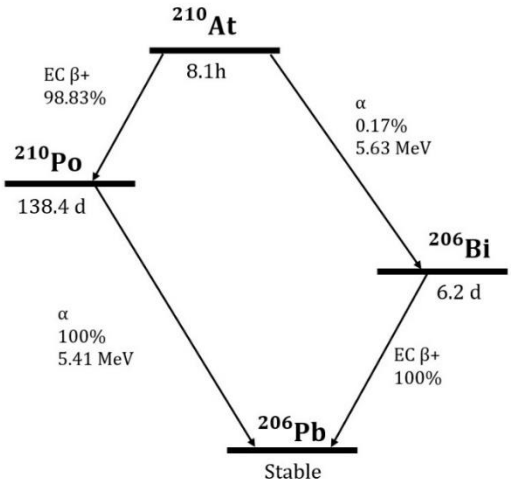

Figure 1.1 Simplified scheme illustrating the decay of ^{210}At with data from IAEA Nuclear Data Section.

^{210}At is the most stable isotope of astatine with a half-life time of 8.1 hours. As shown in Figure 1.1, ^{210}At decays *via* two branches. The primary decay mode (98.83%) is by electron capture (EC) with positron emission to ^{210}Po. The latter possesses a half-life of 138.4 days and decays to stable ^{206}Pb by the emission of 5.41 MeV α-particles. The other route (0.17%) is by direct emission of 5.63 MeV α-particles to ^{206}Bi, and then decays to stable ^{206}Pb by EC with positron emission. One should note that among the decay products of ^{210}At, ^{210}Po is extremely toxic to humans (it has been used as a poison[25]).

2) ^{211}At

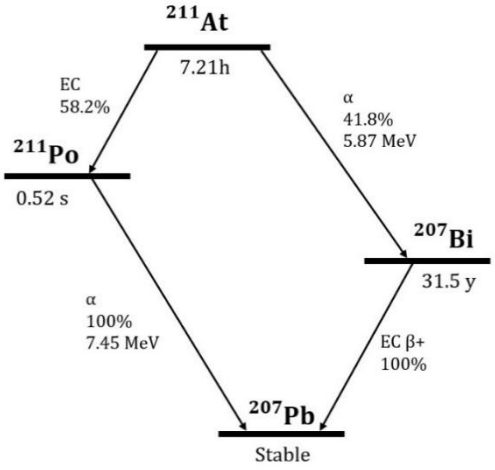

Figure 1.2 Simplified scheme illustrating the decay of 211At with data from IAEA Nuclear Data Section.

^{211}At is the second long-lived isotope of astatine. It has a half-life of 7.2 hours and decays through a double-branched pathway (see Figure 1.2) producing one α particle per decay. The first route (58.2%) is by EC to ^{211}Po with a half-life of 0.52 seconds, which is immediately excited by the emission of 7.45 MeV α-particles to stable ^{207}Bi. The second route (41.8%) is by direct emission of 5.87 MeV α-particles to ^{207}Bi, which has a long half-life of 31.5 years, and then decays to stable ^{207}Pb by EC with positron emission.

1.2 Medicinal perspective for ^{211}At

The ^{211}At radionuclide is considered as a promising candidate as a radiation source in TAT. In this section, for the sake of completeness, a short introduction of nuclear medicine will

be firstly given, with a focus on its two branches — the imaging (diagnostic) and the targeted radiation therapy. Then, the characteristics that make ^{211}At a good candidate for TAT as well as the trials to label targeting agents with ^{211}At will be presented. Finally, the actual difficulties related to the application of ^{211}At will be discussed.

1.2.1 Nuclear medicine

The principle of nuclear medicine is to make use of radioactivity for diagnosis and/or therapy. In "molecular" nuclear medicine (by opposition to direct beam irradiation), radioactive isotopes are conditioned so as to target specific organs to diagnose or treat disease.

Several types of radioactive emissions are distinguished, leading to general features for their interactions with the human body depending on the radiation type. Table 1.1 summarizes the characteristics of different types of radioactive missions.

Table 1.1 Characteristics of different radiation types.

Radiation type	Identity	Energy transfer	Penetrating power
α-particle	Helium nucleus	Very high	Very short, will not penetrate skin
β^--particle	Electron	Intermediate	Short, will slightly penetrate skin and tissues
β^+-particle	Positron, generating γ-rays after annihilation with electron	Very low	Deep, will deeply penetrate tissues
γ-ray	Electromagnetic radiation	Very low	Deep, will deeply penetrate tissues
Auger (e^-)	Electron	Very low	Minimal

Based on these properties, two main axes of nuclear medicine were distinguished: imaging and therapy. Imaging is possible for isotopes whose decay leads to direct or indirect emission of gamma radiation. Indeed, it is the most energetic radiation in the

photonic spectrum and therefore has a high-penetrating power which allows them to "leave" the body and thus be detected for imaging purposes. For therapy, the concept is different: the energy resulting from radioactive decays must be localized at the level of the area to be treated. In this case, "particulate" radiations are preferred, in particular α-particle emission in the context of astatine.

Figure 1.3 shows the elements with potential interests for nuclear medicine in the periodic table.

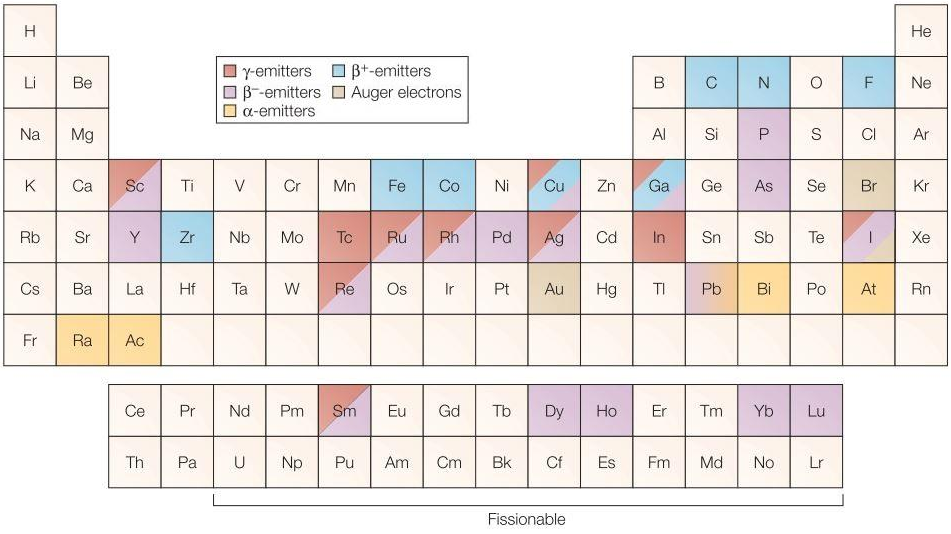

Figure 1.3 A representation of the periodic table, highlighting the elements of interest in nuclear medicine. The color defines the emission type.[26]

1.2.1.1 Nuclear medical imaging

Nuclear medical imaging techniques are based on the use of a radioactive tracer, which emits radiations detectable by a radiosensitive device. In general, the biological vectors of radioisotopes are chosen to ensure the preferential fixation on a particular type of cell according to the established diagnosis. Once the organ or the tissue is targeted, the radiation directly emitted by the radionuclide or resulting from a subsequent decay event is captured by an external detector and formed pictures of the target. The images obtained allow notably to diagnose the state of health of the patient. To this end, the radiation emitted by the radiotracer should have a high penetration ability to pass through the body

to reach the detector, usually being γ-rays. Therefore, the radiotracers applied are either those directly emitting γ-rays, such as ^{99m}Tc, ^{123}I, ^{131}I, ^{111}In, or those emitting β^+-particles and generate γ-rays after annihilation with the electrons, like ^{18}F, ^{11}C, ^{82}Rb, ^{13}N, ^{15}O and ^{68}Ga, and ^{89}Zr. Actually, based on this principle, two major nuclear medical imaging techniques, Single Photon Emission Computed Tomography (SPECT) and Positron Emission Tomography (PET) have been developed as standard nuclear medicine services.

Figure 1.4 A PET scanner used to take images of a specific area of a patient.

1.2.1.2 Targeted radiation therapy

Considering that most tumors can be diagnosed by the imaging methods mentioned above, it is important to develop an effective approach to treat these diseases. The targeted radiation therapy, delivering a high dose of radiation into the patient to treat tumors at close proximity, presents great interests. The essential of this approach is to eliminate cancerous cells efficiently while reducing the damage to the surrounding healthy cells. Though some radionuclides present intrinsic properties for the targeting, such as I^- for the thyroid or Ra^{2+} for the bones, in the most of cases, the targeting is carried out *via* a biological vector (antibody, antibody fragment, peptide, sugar, *etc.*). In this framework, antibody fragments are potential candidates of radioisotope carriers to tumors since they are known to be used by the immune system to target and inhibit specific antigens located either at the tumor surface or inside it. Therefore, the selection of the radionuclide becomes an important issue that should meet several criteria such as emission type, energy transfer, penetration range, half-life, ability to be fixed on the biological vector, and

also the toxicity of the daughter radionuclides. Regarding to the emission type, the α- and β-particle emitters have received much attention. Due to the relative long penetration and sparse scattering transfer of β-particle, they are appropriate for large tumors. The typical radionuclides are ^{90}Y, ^{131}I, ^{177}Lu, ^{186}Re, ^{212}Pb. However, these properties can also be disadvantages because they can lead to harmful radiation of healthy tissues beyond the targeted cells when the tumor is small. Compared to β-particle emitters, the short penetration range α-emitting nuclides are ideal for the treatment of small tumors or residual diseases after surgery. Table 1.2 lists promising candidates of α-emitting radionuclides applied in nuclear medicine. To date, a drug containing the α-particle emitting nuclide ^{223}Ra, Alpharadin® (radium-223 chloride), is already available on the market for use on patients with bone metastases.

Table 1.2 Potential candidates of α-emitting radionuclides for the application in nuclear medicine.

Radionuclides	Half-life	α-emission energy (MeV)	Advantages	Disadvantages
^{212}Bi	60.6 min	7.8	Production yield can be controlled	2.6 MeV γ-ray exposure
^{225}Ac	10 d	6 – 8.4	5 α-emissions	Immense α-particle recoil energy
^{213}Bi	45.6 min	6 – 8.4	Labeling reaction rapid and effective	Radiation damage to the biological vectors
^{211}At	7.21 h	6.8	Appropriate half-life	Production is facility-dependent
^{223}Ra	11.4 d	6	4 α-emissions	Gaseous product ^{219}Rn distributes *in vivo*
^{149}Tb	4.15 h	4	Weak specific irradiation	Decay products may deposit in bone mineral
^{227}Th	18.7 d	6	5 α-emissions	Gaseous product ^{219}Rn distributes *in vivo*

1.2.2 Radiolabeling

For most cases, once the best couple of biological vector and radionuclides is selected, it is important to link them together; this process is called the radiolabeling. The goal of this

step is to achieve a biological vector-radionuclide system with adequate *in vivo* stability. Current radiolabeling protocols are usually based on the following two strategies.

a) Direct radiolabeling

The direct radiolabeling mechanism is meant to link the radionuclide directly to a biological vector as shown in Figure 1.5 a. This mechanism is strongly dependent on the basic chemistry of the applied radionuclide. A good example is the straightforward integration of ^{131}I into phenyl rings of terminal tyrosine groups of antibodies through electrophilic substitution.[27,28]

b) Indirect radiolabeling

The indirect radiolabeling mechanism involves the application of a bifunctional chelating agent (BFC) who serves as a linker for the radionuclide and the biological vector, as shown in Figure 1.5 b.

In this mechanism, as suggested by its name, the BFC plays a double role: through one functional group it binds the radionuclide, and through the other one it sticks to the biological vector.[26,29] It is worth noting that BFCs are quite specific to given radionuclides, as for instance the preferred coordination number(s) may depend on the radionuclide.[26]

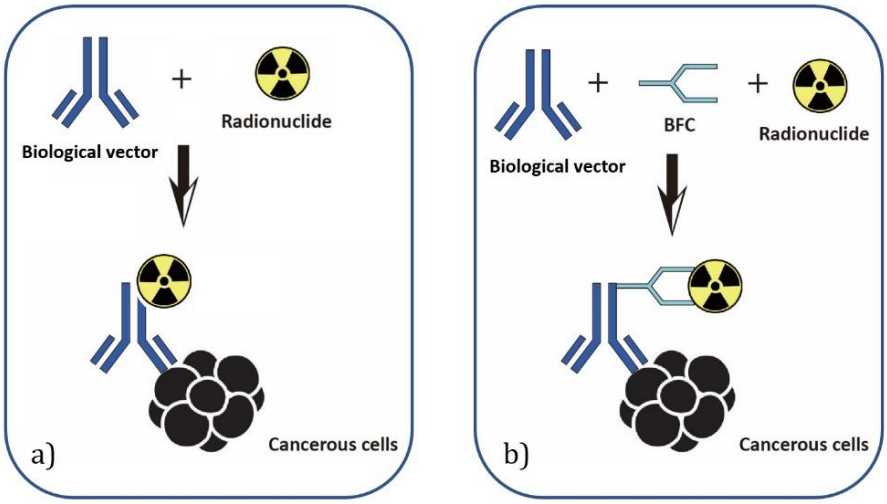

Figure 1.5 Schemes of radiolabeling through a) direct radiolabeling, b) indirect radiolabeling.

1.2.3 Application of ^{211}At in targeted alpha-particle therapy

1.2.3.1 Characteristics of the ^{211}At radionuclide

As previously discussed, TAT involving an α-particle emitter is on the paper preferred for treating small tumors or the residual diseases after surgery. Among the α-emitting radionuclides, ^{211}At is considered to be a promising candidate due to the following assets:[30–32]

- ^{211}At has a half-life of 7.21 h, which is long enough to complete the complicated radiolabeling strategies, and short enough to control what happens after injection.
- ^{211}At is a 100% α-particle emitter with sufficient energy, on average 6.8 MeV.
- The LET of its α-particles is, on average, 97 keV·μm^{-1}, is close to the value needed to achieve the highest relative biological effectiveness of ionizing radiation.
- The energy range of its α-particles corresponds to 55–80 μm, limiting the additional damage to adjacent healthy tissues.
- The X-rays generated through the EC decays of ^{211}At to ^{211}Po, with energy up to 92 keV, provide a valuable means for tracking ^{211}At in laboratory studies. The ^{211}At activity distribution can be imaged and quantified by planar and SPECT imaging.

1.2.3.2 Radiolabeling with ^{211}At

Medicinal chemists and oncologists have started (or at least attempted) to make profit of the favorable characteristics of ^{211}At to treat cancers for decades. So far, two phase I clinical tests have already been completed[33,34] and one phase II one is ongoing (NCT03128034). More radiopharmaceuticals are in development, and the challenge is still the establishment of an efficient and reliable radiolabeling protocol. Guided by the radiolabeling with iodine radioisotopes, three main strategies have been envisaged: radiolabeling through At-C bonds, through At-B bonds, and through At-metal bonds.

1) Radiolabeling through At-C bond

Since the direct electrophilic aromatic substitution (EAS) approach is used to directly label iodine radioisotopes to the aryl C atoms of terminal tyrosine residues in antibodies, the same approach for the radiolabeling of ^{211}At has been considered.[27,28] However, the ^{211}At-labeled compounds by this approach has shown to be highly unstable *in vivo*, presumably due to the rather weak bond formed between At and C atoms.[35] Therefore, it is more reasonable to label ^{211}At to biological vectors through BFCs or to targeting agents than direct radiolabeling.

To this end, a lot of targeting agents and BFCs, retaining ^{211}At *via* an At-C bond have started to be developed. Interesting compounds have been successfully synthesized with At^+ through EAS, or with At^- through nucleophilic aromatic substitution (NAS). For example, ^{211}At-astatobenzylguanidine (MABG, Figure 1.6 a) was found to be able to bind selectively to neuroblastoma tumors.[36] ^{211}At-labeled methylene blue (Figure 1.6 b) is a targeting agent that binds almost exclusively to melanoma tumors.[37] Succinimidyl ^{211}At-astatobenzoate (SAB, Figure 1.6 c) has been successfully linked to specific antibodies, and the complex has been attempted clinically.[38,39]

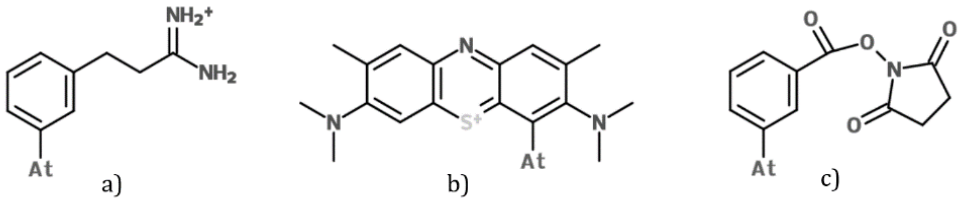

Figure 1.6 Examples of ^{211}At-targeting agents and ^{211}At-BFCs: a) MABG, b) ^{211}At-labeled methylene blue and c) SAB.

2) Radiolabeling through At-B bond

Boron compounds have been successfully used for cancer treatment within the boron neutron capture therapy. They can be easily conjugated to targeting agents if they are

appropriately functionalized. Since the I-B bonds are known to be significantly stronger than the I-C ones, it led to the idea that radiolabeling through ^{211}At-B bonds will be more stable than ^{211}At-C bonds.[40] Based on this chemistry, Wilbur *et al.* developed and tested several boron cluster reagents, such as *nido*- and *closo*-carboranes, for radiohalogenation of biomolecules.[40,41] These reagents have also been implemented in protein labeling and were found to be more stable *in vivo* compared with the corresponding astatinated proteins labeled by aromatic reagents.[42–44] Recently, a phase I/II clinical trial is ongoing, using a ^{211}At-labeled monoclonal antibody conjugate produced with the B10-NCS, a *closo*-decaborate compound.[45]

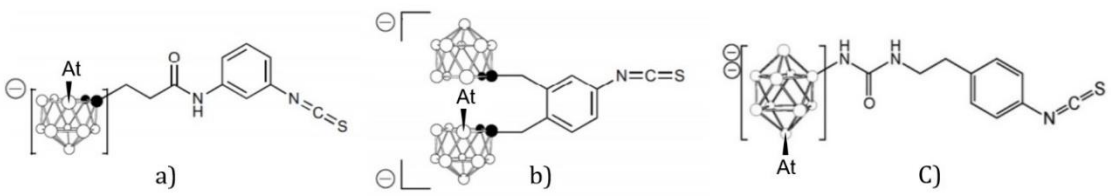

Figure 1.7 Examples of astatinated and functionalized boron clusters: a) a *nido*-carborane derivative, b) a bis-*nido*-carborane derivative and c) a *closo*-decaborate derivative. Filled circles represent C atoms while empty ones represent B atoms.

3) Radiolabeling through At-metal bond

A novel strategy to retain ^{211}At in stable complexes has been recently proposed by Pruszyński *et al.*[46–48] By extrapolating from I^-, they assumed that At^- would have soft anion properties and be able to form strong interactions with soft metal cations, according to the hard and soft acids and bases (HSAB) theory of Pearson[49]. Therefore, their idea is to attach At^- to metal cations, which are themselves chelated by BFCs. Pruszyński has notably reported the complexation of ^{211}At with Rh(III) and Ir(III) metal cations retained on a thioether chelating agent (see Figure 1.8), which could form the basis for a BFC.

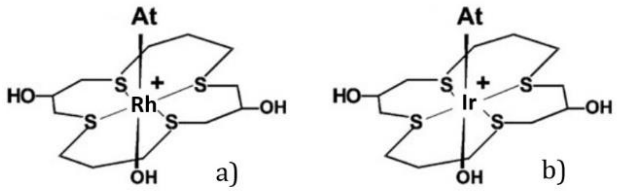

Figure 1.8 Examples of stable complexes with $^{211}At^{-}$ attached to a) Rh (III), and b) Ir (III) soft metal cations.

1.2.3.3 *In vivo* stability of ^{211}At-labeled complexes

The synthesis of ^{211}At-labeled complexes with adequate *in vivo* stability is a critical step for the application of ^{211}At in TAT, because free ^{211}At in the human body will cause undesired toxicity to patients. As mentioned in the previous section, different methodologies developed for radioiodine have been applied to astatine. Unfortunately, different extent of *in vivo* deastatination occurs in most of the cases, notably when the biological vector is metabolized, for uncertain reasons.[50] It becomes clear that the improvement of the actual radiolabeling strategy and the development of specific strategies for ^{211}At are crucial. This demands at least a decent understanding of the chemical behavior of At in various conditions, allowing to apply the particular chemistry of astatine for the development of novel radiolabeling protocols while not the chemistry of iodine.

1.3 The chemistry of astatine in solution

Unraveling the fundamental chemistry of At is of great importance for the development of potential novel ^{211}At radiolabeling strategies. Nevertheless, the current understanding of its chemistry is very limited, even 80 years after the discovery of At, mainly due to its rarity and its radioactive nature. Referring to its position in the periodic table, At may act as a chemical chameleon. On the one hand, as a member of the halogen group, At should share properties with the other halogens. On the other hand, At may also bear some metallic characters as its neighbor, polonium, which is condensed in the “metalloid” flag. The

following part will describe the current understanding of the chemistry of At, starting from the production methods, to the analytical methods, and finally to the current "thermodynamic database" of At.

1.3.1 Production of ^{211}At

Although ^{210}At is the longest-lived isotope of At, it is not frequently used in chemistry studies, principally because of its extremely radiotoxic decay product – ^{210}Po. In fact, ^{210}Po is an α-emitter with a half-life time of 138.4 days. Therefore, it will interfere the identification of At (who is also an α-emitter) and severely complicate the waste management. Instead, ^{211}At is more "easy going", thus it is usually the selected radionuclide. Since ^{211}At exists in minimal quantity in the Earth's crust, it is impossible to collect it from nature. Therefore, the typical way to get access to ^{211}At sources is through intentional production.

1) Production through nuclear reaction ^{209}Bi(α, 2n)^{211}At by cyclotron

Currently, the most used method for producing ^{211}At is direct production *via* the bombardment of ^{209}Bi with energetic α-particles.

The incident energy of the α-particles beam should satisfy several conditions. As shown in Figure 1.9, according to the excitation function of the ^{209}Bi(α, 2n)^{211}At reaction, the reaction threshold is about 21 MeV and the maximum production yield is reached by using an α-beam of about 30 MeV. However, starting from 29 MeV, the competing reaction ^{209}Bi(α, 3n)^{210}At occurs, producing undesired ^{210}At. In order to avoid the contamination of ^{210}At, the incident α-particles energy should be below the threshold for the ^{209}Bi(α, 3n)^{210}At. Usually, the energy used is around 28 MeV.

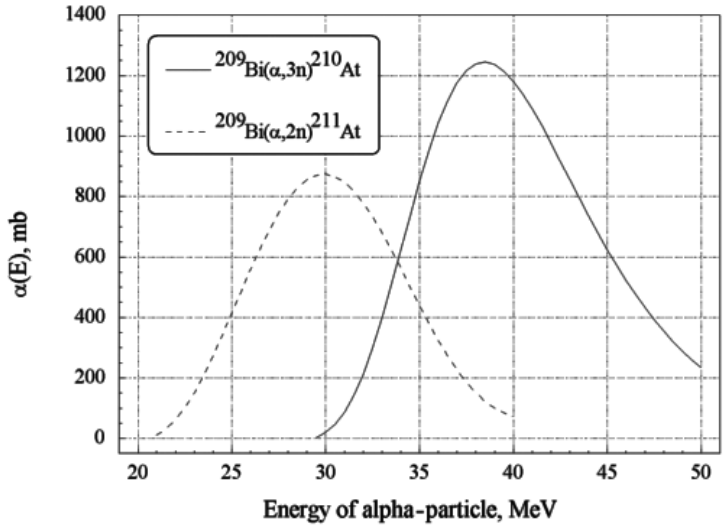

Figure 1.9 Fit of the cross-sections for ^{209}Bi(α, 2n)^{211}At and ^{209}Bi(α, 3n)^{210}At reactions.[51]

According to a recent review, 29 cyclotrons around the world are identified as having a characteristic α-particle beam to produce ^{211}At. However, only a few of them routinely produce ^{211}At, which has led to a commercial shortage of At source.[52]

After the cyclotron irradiation, astatine needs to be isolated from the bismuth target. Generally, there are two approaches for the recovery of astatine: wet harvesting and dry distillation. In the former, the bismuth target is dissolved in concentrated acids, such as HNO_3 or $HClO_4$. Then astatine is extracted into an organic solvent such as butyl or isopropyl ether.[53] Astatine partitioning between nitric acid and conventional solvents have been recently investigated in order to improve the recovery efficiency.[54–56] After that, astatine also has to be back-extracted from the organic phase to aqueous media to achieve a chemically useful form for further labeling.[56] Though this method results in good yields, it is time-consuming because it involves multiple radioactive manipulation steps. The commonly used approach to isolate astatine from the bismuth target is dry distillation. The target is heated to around 650°C in a quartz vessel. Astatine is sublimated selectively and entrained using a stream of nitrogen or argon. The vaporized astatine is finally condensed and recovered by a small volume of a preferred solvent such as chloroform.[57,58]

2) Production by $^{211}Rn/^{211}At$ generator

Another possible route for producing ^{211}At is through a $^{211}Rn/^{211}At$ generator. The advantage of the generator is the longer half-life of ^{211}Rn compared with ^{211}At (14.6 h *vs.* 7.2 h). This will increase the distribution area of ^{211}At from the production site with maintained astatine activity compared with the delivery of ^{211}At alone. The production of ^{211}Rn can be made through nuclear reaction $^{209}Bi(^{7}Li, 5n)^{211}Rn$ or by the decay of ^{211}Fr.[59–61] However, these productions necessitate the heavy-ion high-energy beam irradiation and careful isolation and containment of the produced ^{211}Rn, which is more technically demanding than the former route.[52]

1.3.2 Speciation studies

1.3.2.1 Experimental methods

Though At is available through artificial productions, the source is still limited to minute quantities. For research purposes, one may work with astatine only at ultra-trace concentrations, typically below 10^{-10} mol·L^{-1}, making the conventional spectroscopic tool barely applicable. Therefore, in order to investigate the chemical properties of astatine in solution, indirect methods couple with a radioactivity detection system were used in the literature. These methods are mainly based on electromobility, chromatography and competition, and are presented in the following.

1) Electromobility measurements

In the electromobility measurements, a (high) voltage is applied in an electrolyte solution, creating a homogenous electric field. The sample containing At is injected into the electrolyte. Scanning by a γ-ray detector, the position of At can be recorded. At ions will move to cathode or anode, which gives the evidence of its charge. Moreover, the change of At position in function of time offers an evaluation of the mobility of the At ions in the sample, being a character of the charge/size ratio of these ions.[62]

2) High-performance ion exchange chromatography (HPIEC)

The principle of HPIEC measurements relies on the use of a column containing an ion exchange resin (served as the stationary phase). The column is coupled a γ-ray detector which produces radio-chromatogram signals due to the elution of species that contain ^{211}At. In a typical HPIEC-based experiment, an eluent which contains the desired medium (mobile phase) is first equilibrated with the system. The sample containing ^{211}At is then introduced and is taken by the eluent to pass through the column. The target analytes (anions or cations) are retained on the stationary phase, but can be detached from it by adding a similar kind of charge to the eluent. Depending on the eluent flow rate and the affinity of an At species for the exchange resin, it takes some time for that species to exit the column. This time is defined as the retention time and can be visualized on the radio-chromatogram. Important information such as the number of species and their charge (for ion exchange chromatography) can be obtained.

3) TLC measurements

Thin-Layer Chromatography (TLC) is a chromatography technique similar to HPIEC technique. TLC experiments use a sheet of glass, plastic, or aluminum foil, which is coated with a thin layer of adsorbent material, usually being silica gel, aluminum oxide, or cellulose, as the stationary phase. At sample is applied on the plate, a solvent or solvent mixture (known as the mobile phase) is drawn up the plate *via* capillary action. Because different analytes ascend the TLC plate at varying rates, separation is achieved. The distribution of At can be visualized by a γ radiation imaging system. To quantify the results, the distance traveled by the substance being considered is divided by the total distance traveled by the mobile phase. This ratio is called the retardation factor.

4) Competition experiments

This approach is based on the method described by Schubert adapted to the study of the elements present at trace levels.[63,64] The underlying principle is that an At species is

characterized by a given distribution coefficient in an immiscible biphasic system. If a change in the experimental conditions causes a change in the At speciation, then the distribution coefficient of astatine between the two phases may change. If a change in the distribution coefficient is observed, it must indicate a speciation change. This method is called liquid/liquid competition (LLC) when the biphasic system consists of two liquid phases, while if it refers to a solid and a liquid, then the method is classified as solid/liquid competition (SLC). By analyzing the change in the distribution coefficient as a function of key parameters, it is possible, by modelling, to identify the type of species present as well as the quantitative description of their formation.

1.3.2.2 Quantum chemistry methods

Theoretical chemistry based on quantum mechanical methods is nowadays performed almost routinely by computational chemists to understand, rationalize and even predict various properties concerning atoms, molecules, including chemical reactions. For astatinated species, quantum chemistry methods have to be applied in a context where experimental studies cannot lead to a full range of information. In particular, the absence of spectroscopic data severely limits the experimental knowledge of the nature and structures of molecules. However, a few key indices may pave the way for the computational study.

From the stoichiometry of a compound, quantum calculations coupled to an energy minimization algorithm allow to access the structure of a conformer of a compound by determining structural parameters such as inter-atomic distances and bond angles between different atoms, *etc.* These algorithms are said “local”, meaning that the optimized geometry depends on the starting geometry. Because of this, several starting geometries have to be considered, and several guesses for the electronic structure may also have to be considered for each starting geometry. The discrete set of optimizations may lead to only one stable structure, the minimum, or to various conformers, with one global minimum and at least one local minimum. Depending on the energy difference

between the conformer, the Gibbs free energy may be governed by the global minimum, or an ensemble of conformers may have to be considered.

At is a heavy main-group element; therefore, its computational treatment requires the consideration of relativistic effects, at least the scalar relativistic ones and also in general the spin-orbit coupling. The former ones cause corrections to the one-electron energies due to the mass-velocity dependence of electrons close to heavy nuclei. The latter one causes further energy corrections and changes in the ground-state wave function due to the effective interaction between the spin of the electrons and the magnetic field induced by their motion around the nuclei.[65] In order to deal with relativistic effects as well as electron correlation, wave-function-based methods and density functional theory (DFT) methods within two-component frameworks may be employed.

In summary, the experimental methods mentioned above can offer some characteristics of At species, with their own advantages and disadvantages. However, they can only give information at the macroscopic scale, quantum chemistry methods represent a cost-effective tool to obtain information at microscopic scale, in order to help in analyzing the experimental outcomes, as illustrated in the article of Champion *et al*.[13] Details of the methods will be given in the next chapter. Concrete examples of their use to better understand the chemistry of astatine are given below.

1.3.3 Speciation of astatine in aqueous solutions in the absence of a complexing agent

Identifying the chemical forms of At in different physicochemical conditions, in particular pH and redox conditions, is of fundamental interest for chemists, so that one can proceed more straightforwardly with the assessment of its reactivity towards other chemical species. The diagram mapping the predominant species as a function of both pH and redox potential (E) of a given media is called the Pourbaix diagram. Knowledge of this diagram is of particular importance for the development of TAT based on ^{211}At, since it determines

the type of redox species that can exist in aqueous solution. Knowing their chemical properties, it is therefore possible to apply it for the synthesis of targeting agents and BFCs, and for controlling their *in vivo* behaviors.

In the literature, the related works were mainly reported by Johnson *et al.*,[66] Appelman,[67–70] Visser and Diemer,[71] Dreyer *et al.*,[72–76] Cavallero[77–79] from the 1960s to the 1980s, and summarized by Berei *et al.*[80] and Ruth *et al.*[81]. In recent years, Champion *et al.*[8–12] and Nishinaka *et al.*[82,83] have brought some new results.

Investigations of the chemical forms of At were generally based on the behaviors in coprecipitation, electromigration measurements and competition experiments in a biphasic system, *etc.*, with the knowledge of iodine chemistry as a guide. Most experiments were conducted with dilute solutions; therefore, attempts to test specific reaction mechanisms are often hampered by competing reactions with solvent impurities, leading to irreproducible results. Thus, as such, the experiments alone are incapable of leading to a firm identification of the observed chemical species. In this context, DFT may be of great help since it can provide extra information from theory.[13] The experimental results can be then compared with the theoretical ones, in order to validate (or not) the nature of the observed species.[9–12]

To date, six OSs have been identified or hypothesized: –1, 0, +1, +3, +5, and +7. In the following paragraphs, the speciation of At will be presented according to the physicochemical conditions (pH, redox potential, *etc.*). For given conditions, the species proposed in the literature will be discussed, as well as the investigation of its characterizations (charge, mobility, *etc.*) and the thermodynamic constants for the speciation changes.

1) In reducing conditions

In a solution with the presence of sufficiently strong reducing agents such as SO_3^{2-}, Zn and hydrazine, it is generally assumed that At is in –1 OS and the chemical form is At^-, by

analogy with the other halogens elements. Lighter halogens all present this species while with a trend that the heavier the halogen, the smaller E-pH range of existence of this species. At^- is probably the most clearly established form of At. The characterizations of At^- have been deduced by coprecipitation with AgI, TlI and PbI_2, its inability to be extracted into nonpolar organic solvents such as carbon tetrachloride or benzene,[81] and the similar retardation factor with I^- measured by TLC.[82] Quantitatively, the negative charge has been evidenced by its migration to the anode in electric fields,[9,66,73,74,76,84] and its ability to be retained by anionic exchanger Aminex A27[78,85] and Dionex AS20[8]. The –1 charge has been confirmed by HPIEC measurements comparing the behavior of At^- with I^- and Br^- ones.[8] Moreover, the first absolute mobility value of At^- in acidic and reducing conditions, being $(-8.26 \pm 0.59) \cdot 10^{-4}$ $cm^2 \cdot V^{-1} \cdot s^{-1}$, was reported by Guo *et al*. in 2018.[9] This value, close to the I^- one, was also confronted with computational chemistry ones based on an *ad-hoc* force-field generated out of quantum mechanical calculations.[9] A summary of investigations for the mobility of At^- in the literature can be found in Table 1.4.

2) In acidic and slightly oxidizing conditions

In the presence of inorganic acids (HNO_3, $HClO_4$, HCl, H_2SO_4) without additional reagents, another At species was proposed. In the literature, two possibilities of OS have been attributed: 0 or +1.

Generally, the freshly distilled species from a target or left in acid solution without the presence of oxidizing agents, or the species that cannot be readily attributed to an oxidation number, is considered to be At^0. It is the least characterized species of At. The only consistent characteristics of At^0 is the ability to be extracted in nonpolar solvents (carbon tetrachloride, benzene, toluene, cyclohexane, *etc.*) and the high affinity for various types of surfaces (glass, aluminum, nickel, copper, *etc.*).[81] It is hypothesized that astatine can be obtained as At^0 in the gas phase during the preparation processes, which is recently supported by TLC experiments.[83] However, Visser *et al.* proposed that the "At^0"-like

behaviors in solution came from the product of At^+ with organic purities presented in the aqueous solution, according to a detailed investigation.[71] The possibility of organic astatine formation is supported by the observation of CH_3At^+ through mass spectrometry.[68]

Other studies proposed as well the possible existence of At^+ in acidic and slightly oxidizing conditions.[10,79,84] From the electromigration experiments of Dreyer *et al.*, the At species in 0.02 M $HClO_4$ solution migrated indeed to the anode, which indicates the positive charge.[84] However, the contrary behavior was observed by Johnson *et al.* that At migrated as an anion in acidic solutions.[66] The contradict behavior may also be explained by the reaction between At and impurities of the initial solvent of At source.[81] The details of electromigration experiments for At species in acidic conditions are summarized in Table 1.4.

Although the direct characterization of At species gives irreproducible outcomes, information can be alternatively obtained from the speciation change evidence. By changing the experimental conditions, which results in the change of redox potential of the solution, a speciation change from At^- is indeed evidenced, through various experiments, such as radiopolarity measurements, chromatography measurements and competition experiments.[10,69,78,79] The common point of these investigations is that all the authors considered only electron exchange occurred in the redox reaction and the redox potential is in agreement with each other (between 0.30 and 0.37 V *vs.* Normal Hydrogen Electrode (NHE)), though the number of exchanged electrons considered is different (see Table 1.5). Among them, Champion *et al.* demonstrated that the redox reaction involves two electrons exchange but without protons (of water) from the competition experiments, implying the formation of At_2 or At^+. The redox potential being 0.36 ± 0.01 V, from which the hypothesis of At_2 is eliminated according to the quantum mechanical calculations.[10] Furthermore, At_2 molecule is highly unlikely in solution due to the extremely low concentration of At, which is generally agreed by scientists.[81]

3) In acidic and oxidizing conditions

In acidic solution with the presence of oxidizing agent $Cr_2O_7^{2-}$, another At species is observed. In particular, from the electromigration experiments of Dreyer *et al.*, they discovered that for the same At stock solution prepared in 0.1 M HNO_3/5·10^{-3} M $K_2Cr_2O_7$ environment, the mobility is very different when the electrolyte contains or not $K_2Cr_2O_7$ (see Table 1.4).[84] Therefore, the species in acidic conditions with the presence of $Cr_2O_7^{2-}$ must be different from the one without the presence of $Cr_2O_7^{2-}$. According to different authors, the OS in these conditions is +1 or +3 and the corresponding chemical form being At^+, At^{3+}, or AtO^+.

The positive charge of this species has been evidenced by electromigration measurements.[84,86] The monovalent character has been demonstrated by ion exchanger chromatography as shown in Table 1.3.[85,87,88] Therefore, the hypothesis of At^{3+} appears quite unlikely.

Table 1.3 Chromatography measurements for At species in acidic solution oxidized by $Cr_2O_7^{2-}$.

Ref	Resine	Solution for preparation of At	Charge
[87]	Dowex 50X8	0.005 M $H_2Cr_2O_7$, 0.3–1.25 M HNO_3	+1 compared with Cs^+
[88]	Dowex 50X8	0.01 M $H_2Cr_2O_7$, heat to 100°C for 0.5 h	+1 compared with Tl^+
[85]	Aminex A7	0.1 N HNO_3+CrO_3	+1, but probably unlike to be AtO^+

Moreover, from several investigations on redox reaction (Table 1.5), a speciation change is evidenced, in agreement with the electromigration experiments of Dreyer.[84] According to the previous discussion in acidic conditions, the At species being At^+, turns to another species in the present discussing conditions, which eliminates the possibility for At^+. Champion *et al.*[10] show that the redox reaction not only involves the exchange of two electrons but also is pH-dependent, which implies the exchange of protons (of water); therefore, the At^{3+} form can be excluded (in accordance with the charge +1 identified by

ion exchange). Consequently, the form of AtO^+ is identified. In terms of the standard potential, the values in the literature are at variance. In 1960, Appelman proposed 1.0 V at pH = 1 from coprecipitation and solvent extraction experiments.[69,70] Later, Cavallero *et al.* reported 0.80 ± 0.05 V from CFRP measurements.[78] More recently, Champion *et al.* reported 0.74 ± 0.01 V for the At^+/AtO^+ couple.[10]

4) In strong oxidizing conditions

In the presence of strong oxidizing agents, such as hot acidic solutions containing $S_2O_8^{2-}$, neutral solutions containing KIO_4, or alkaline solution containing HClO, At(V) in the form of AtO_3^- is recognized.[66,69,82,83] The AtO_3^- ion was originally proposed by its tendency to coprecipitate with $AgIO_3$, $Ba(IO_3)_2$ and $Pb(IO_3)_3$.[66,69] Similar behaviors to IO_3^- have been observed by various techniques such as HPIEC measurements,[85] electromigration measurements,[74,84] and TLC measurements,[82,83] indicating the existence of AtO_3^- species.

Regarding the redox equilibrium between different OSs, Appelman considered the equilibrium between AtO^- and AtO_3^-, and gave the redox potential being 1.5 V. However, the reducing form involved in this redox reaction is not guaranteed, as stated in the article of Appelman, it is probably to be At(I) in the form of AtO^-, but also possible to be At(III) with the chemical form being AtO^+.[69,70] Later, Visser *et al.* refined the works of Appelman and Cavallero[77], and proposed that the oxidation potential of 1.5 V should assigned for the couple At(III)/At(V).[71,89]

5) In strong oxidizing and neutral or alkaline conditions.

It is reported that AtO_4^- presents in neutral or alkaline solution with the presence of KIO_4 or XeF_2.[74,82,83] Similar to IO_4^-, AtO_4^- is not stable in acidic medium and easily reduced to AtO_3^-.[74]

The AtO_4^- anion is identified and characterized by its coprecipitation with KIO_4 and $CsIO_4$[80], electromigration measurements[74,84] and TLC measurements[82], *etc.*, as a

similar form with IO_4^-. However, no quantitative data have been proposed so far in the literature to describe the formation of this possible species.

6) In weak acidic and mild oxidizing conditions

As described in the above section, in acidic solution with the presence of $Cr_2O_7^-$, the cationic ion AtO^+ is observed. Milanov and co-workers found that the mobility of this species is pH-dependent, indicating the reaction with H_2O and proposed the formation of a neutral hydrolyzed species AtO(OH) with an apparent hydrolysis constant of $10^{-1.5}$ (at ionic strength I = 0.4 M) and $10^{-4.1}$ (at I = 0.25 M).[86,90] A constant of $10^{-5.23}$ (I = 0.1 M) was also proposed by Schumann *et al.* for the pH range of 1−10 through electro migration experiments.[91] Champion *et al.* confirmed the non-charge character of this species by the HPIEC measurements.[11] The speciation change between AtO^+ and AtO(OH) is evidenced by competition methods and confronted by quantum mechanical calculations, giving a hydrolysis constant of $10^{-1.9}$ (I = 0 M).[11]

7) In alkaline and non-reducing conditions

Though it is generally assumed that At^- is the predominant species in alkaline condition, Sergentu *et al.*[12] recently observed a species, carrying −1 charge. Nevertheless, it is demonstrated to be different from At^-, predominating in alkaline and non-reducing conditions (more precisely, in 10^{-3} M NaOH solution) by HPIEC measurements. Using competition experiments, an equilibrium constant value of $10^{-6.9}$ has been determined for the formation of this species from AtO(OH) with the exchange of one proton, giving the possible form of AtO_2^- or $AtO(OH)_2^-$. The quantum mechanical calculations ruled out the formation of the AtO_2^- species, while leading to a similar hydrolysis constant of AtO(OH) when the $AtO(OH)_2^-$ species is considered. This study is thus a net example of the added value of the quantum mechanical calculations: the confrontation of the experimental and computational results may lead to the discrimination of speciation hypotheses.

Table 1.4 Electromobility investigations of At species in different media.

Ref	Solution of At	Electrolyte	Mobility* (10^{-4} $cm^2 \cdot V^{-1} \cdot s^{-1}$)	Comment
[66]	Concentrated nitric acid	SO_2 in 0.1 M HNO_3	At migrates as a negative ion	Mobility of At^-
		Na_2SO_3 in 0.1 M NaOH		
[74]	Hydrazine	0.04 M KNO_3	−6.0	
[73]	0.2 M HNO_3 + 0.02 M $K_2Cr_2O_7$, then + 0.5–1 M NaOH (heat 100°C 1h)	0.04 M KNO_3	−6.1 ± 0.2	
		0.02 M $(NH_4)_2CO_3$ + 0.015 M NH_4OH		
[73]		0.02 M $(NH_4)_2CO_3$, 0.015 M NH_4OH	−7.2 ± 0.2	
[76]		0.05 M NaOH	−7.4 ± 0.2	
		0.10 M NaOH	−7.2 ± 0.2	
[9]	0.1 M NaCl, 0.01 M HCl, and 10^{-3} M $Na_2S_2O_3$	Solution of At + 10^{-3} M $MgCl_2$	−8.26 ± 0.59	Absolute mobility of At^-
[66]	Concentrated nitric acid	1 M HNO_3	At migrates as a negative ion	At^+ complexed with organic impurities
		0.1 M HNO_3		
[84]	0.1 M HNO_3, 0.005 M $K_2Cr_2O_7$ (heat 10 min at 100°C)	0.02 M $HClO_4$	9.2 ± 0.2	$At(x)^+$ turn to At^+ in the electrolyte without $Cr_2O_7^{2-}$
[87]		0.005 M $H_2Cr_2O_7$, 1.25 M HNO_3	At migrates as a positive ion	Species notes $At(\theta)^+$, supposed to be AtO^+ and it reacts with OH^-
[84]	0.1 M HNO_3, 0.005 M $K_2Cr_2O_7$ (heat 10 min at 100°C)	0.02 M $HClO_4$ + 10^{-3} M $K_2Cr_2O_7$	1.9 ± 0.2	
[86]	0.4 M $H(Na)ClO_4$ pH=1.68	0.4 M $H(Na)ClO_4$ 10^{-4} M $K_2Cr_2O_7$	1.17	

	10^{-4} M $K_2Cr_2O_7$			
[86]	0.4 M H(Na)ClO_4 pH=0.63 10^{-4} M $K_2Cr_2O_7$	0.4 M H(Na)ClO_4 10^{-4} M $K_2Cr_2O_7$	2.67	
[84]	0.1 M HNO_3, 0.005 M $K_2Cr_2O_7$ (heat 10 min at 100°C)	Neutral and alkaline medium	Non migration	At(θ)$^+$ converts to non-migrating form
[73,84]	5–10 mg/mL XeF_4 0.5 M $HClO_4$ + $Na_2S_2O_8$ (heat at 100°C)	0.02 M $HClO_4$ + 0.02 M $Na_2S_2O_8$	3.3 ± 0.2	AtO^+(?)
[73,84]	0.1 M HNO_3, 0.005 M $K_2Cr_2O_7$ (heat 10 min at 100°C) + 1 M NaOH heat for 60 min	0.04 M KNO_3 0.02 M $(NH_4)_2CO_3$ + 0.015 M NH_4OH	−4.6 ± 0.2	AtO_2^- (?)
[74]	10^{-3} M KIO_4 in a neutral or alkaline medium, and acidify with H_2SO_4 KClO in alkaline condition	0.04 M KNO_3	−2.3	AtO_3^-
[74,84]	10^{-3} M KIO_4 in a neutral or alkaline medium	0.04 M KNO_3	−3.4	AtO_4^-

*Apparent mobility if not indicated otherwise.

Table 1.5 Redox potential of At species in the literature. Data obtained through different methods: electromigration (Elc), the liquid/liquid competition (LLC) method, solid/liquid competition method (SLC), radiopolarography (RP) and chromatography at fixed redox potential (CFRP).

Reaction	Method and ref	Redox agents	Studies potential range (V)*	Redox potential (V *vs.* NHE)
At(0) / At^-	LLC, coprecipitation[69]	I^-/I_2 $Fe(CN)_6^{4-}/Fe(CN)_6^{3-}$, As^{III}/As^{V}	0.3 – 0.6 (at different pH)	0.3 at pH 1
At + e^- / At^-	CFRP[78]	SO_3^{2-} / SO_4^{2-}, $Fe(CN)_6^{4-}/Fe(CN)_6^{3-}$ Eluant = 1M $NaNO_3$	0.27 – 0.65	0.32 ± 0.02
At + e^- / At^-	RP[79]	Na_2SO_3	–0.15 – 0.55	> 0.23
At^+/At^-	LLC, TLC[71,89]	Data of Appelman[69] and Cavallero[77]	Not applicable	0.35
At^+ + $2e^-$ / At^-	LLC[10]	SO_3^{2-}/SO_4^{2-}	0.20 – 0.55 (pH 1)	0.36 ± 0.01
HOAt(?) / At(0)	LLC, coprecipitation[69]	VO^{2+} / VO_2^+	0.87 – 1.04 (pH 1)	1.00 ± 0.05 at pH 1
At^+ + e^- / At	CFRP[78]	Cr^{3+} / $Cr_2O_7^{2-}$ Eluant = 1M $NaNO_3$	0.84 – 1.1 (approx.)	0.80 ± 0.05
At^{3+} /At^+	LLC, TLC[71,89]	Data of Appelman[69] and Cavallero[77]	Not applicable	0.85
AtO^+ / At^+	SLC[10]	Fe^{2+} / Fe^{3+}	0.5 – 0.9 (pH 0 – 2)	0.74 ± 0.01
AtO_3^-/HAtO (?)	LLC, coprecipitation[69,70]	IO_4^- / IO_6^{5-}	1.40 – 1.60 (pH 1)	1.5 at pH 1
AtO_x^- + ne^- / At^+	CFRP[78]	Ce^{3+} / Ce^{4+} Eluant = 1M $NaNO_3$	1.5 – 1.6	>1.5
At^{5+}/At^{3+}	LLC, TLC[71,89]	Data of Appelman[69] and Cavallero[77]	Not applicable	1.5

*Estimation from the graphs of articles

8) Pourbaix diagram of At

According to previous discussions, the current Poubaix diagram of At can be constructed starting from At^- in reducing conditions. With the increasing redox potential in acidic conditions, two At species with the OS = +1 and +3 corresponding to At^+ and AtO^+ predominate. By increasing the pH while remaining in oxidizing conditions, two hydrolyzed forms of AtO^+ appear, namely AtO(OH) and $AtO(OH)_2^-$, respectively. At high redox potential while may be out of the range of water stability, AtO_3^- exists over the whole pH rang and AtO_4^- exists only at neural and alkaline conditions. The quantitative behaviors of the couples At^-/At^+, At^+/AtO^+, AtO^+/AtOOH and AtOOH/$AtO(OH)_2^-$ have notably been investigated through a dual experimental-computational approach at Subatech and CEISAM laboratories.[10–12] Accordingly, the equilibria of At^+/AtO(OH), At^-/AtO(OH) and $At^-/AtO(OH)_2^-$ can be deduced. Concerning AtO_3^- and AtO_4^- species, quantitative parameters are still not confirmed (for the speciation change between AtO^+ and AtO_3^- [69,71,78,89]) or missing. Finally, the Pourbaix diagram of At can be constructed as Figure 1.10.

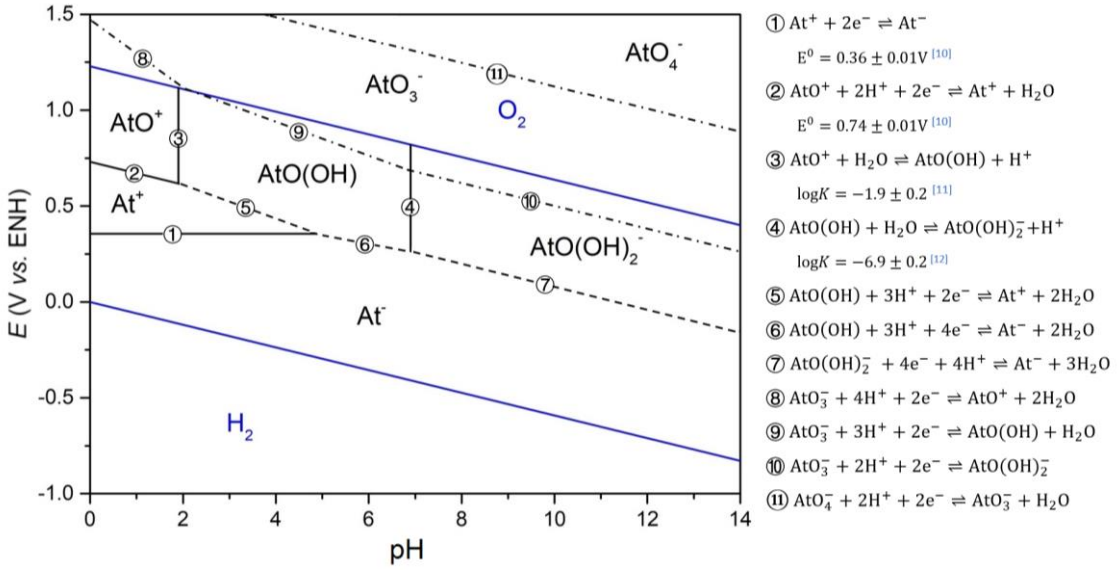

Figure 1.10 Pourbaix diagram of astatine (25°C). The blue solid lines refer to the stability zone of water; the black solid lines correspond to directly determined boundaries with data reported by Champion *et al.*[10–12]; the dashed lines indicate the boundaries deduced from known equilibria; the dashed dot lines relate to undetermined or uncertain boundaries.

9) Radiolytic effects on the speciation of ^{211}At

Two characteristics α-particles make ^{211}At a potential candidate for the targeted alpha-particle therapy. However, the emission of these particles may induce some negative consequences, such as the radiolytic effects on itself and the surrounding solvents, making the astatine speciation in solution more complicated.

In the literature, two works have investigated this aspect. Pozzi *et al.*[92] have studied the effect of radiation dose on the speciation of ^{211}At in methanol. The results indicate that with the increase of radiation dose, the predominant astatine species indeed change, to be a reduced form of astatine (presumably At^-). Aneheim *et al.*[93] have investigated the radiochemical behavior of ^{211}At in chloroform – an important intermediate solvent for the recovery of astatine after production. It is shown that radiolysis of chloroform plays an important role in the formation of multiple At species.

1.3.5 Complexation between astatine cations and inorganic ligands

As discussed in the previous section, At exists in cationic forms in some conditions, and the "metallic" character can be revealed by the reactions with complexing ligands. In recent decades, scientists used different indirect methods to evidence and analyzed the interactions between $At(x)^+$ and inorganic ligands such as Cl^-, Br^-, I^-, SCN^-. In the 1960s, Appelman investigated the interactions of At with the halogen ligands through the solvent extraction.[67] He proposed the existence of interhalogen species such as AtI, AtBr, AtI_2^-, $AtBr_2^-$, $AtCl_2^-$, $AtIBr^-$ and $AtICl^-$, and provided the associated equilibrium constants. Time-of-flight mass spectrometry was used to identify the At species and gave the first direct evidence of AtCl, AtBr and AtI.[68] The research team of Dubna worked on At reactions in acid solution by a cation exchange method to obtain the equilibrium constants of AtCl and $AtCl_2^-$ formation.[94,95] Later in the 1980s, the electromobility method was repeatedly applied to explore the reactions between astatine and halides (Cl^-, Br^-, I^-) or pseudo-

halide (SCN^-) at different pH and ionic strength by Dreyer *et al.*[72,75,76,96,97] More recently, Champion *et al.* studied the reactions of the cationic forms $At(x)^+$ species with Cl^-, Br^- and SCN^- through competition experiments and quantum mechanical calculations, indicating the formation of both 1:1 and 1:2 complexes.[13,15] Furthermore, the $\beta_{m,X}$-values obtained from the experiments are in good agreement with theoretical ones. It is found that the efficiency of the $At(x)^+$ interaction with the inorganic ligands increases in the order Cl^- < Br^- < SCN^-, regardless of the considered stoichiometry. According to the HSAB theory, the astatine metallic species can be considered as soft acids. Guo *et al.* interested in evidencing the existence of the trihalogen species $IAtBr^-$. The predominance domain of this species is predicted by the theoretical computations and checked by competition experiments.[14]

All the related equilibrium constants are presented in Table 1.6.

Table 1.6 Overview of the reactions between At cationic species and inorganic ligands through different methods: electromigration (Elc), the liquid/liquid competition (LLC) method or solid/liquid competition method (SLC).

Method	Medium	Equilibrium	Equilibrium constant
SLC[95]	0.1 M $H_2Cr_2O_7$	$At(x)^+ + NO_3^- \rightleftharpoons At(x)(NO_3)$ $At(x)^+ + SO_4^{2-} \rightleftharpoons At(x)SO_4^-$ $At(x)^+ + 2SO_4^{2-} \rightleftharpoons At(x)(SO_4)_2^{3-}$	$Log\beta_{1,NO_3^-} = 0.13^*$ $Log\beta_{1,SO_4^{2-}} = 0.23^*$ $Log\beta_{2,SO_4^{2-}} = 0.50^*$
LLC[10]	0.1 M $HClO_4$ 0.1 M $NaClO_4$		$Log\beta_{1,SO_4^{2-}} = 1.0 \pm 0.1$
SLC[95]	1 M $HClO_4$	$At(x)^+ + Cr_2O_7^{2-} \rightleftharpoons At(x)(Cr_2O_7)^-$	$log\beta_{1,Cr_2O_7^{2-}} = 1.34^*$
SLC[95]	0.3 M $HClO_4$ 0.005 M $H_2Cr_2O_7$	$At(x)^+ + Cl^- \rightleftharpoons At(x)Cl$ $At(x)^+ + 2Cl^- \rightleftharpoons At(x)Cl_2^-$	$log\beta_{1,Cl^-} = 3.10^*$ $log\beta_{2,Cl^-} = 3.42^*$
	0.5 M $HClO_4$ 0.005 M $H_2Cr_2O_7$		$log\beta_{1,Cl^-} = 3.20^*$ $log\beta_{2,Cl^-} = 3.40^*$
SLC[94]	0.5 M HNO_3 0.005 M $H_2Cr_2O_7$		$log\beta_{1,Cl^-} = 2.85^*$ $log\beta_{2,Cl^-} = 5.40^*$
LLC[13]	0.1 M $HClO_4$ 0.1 M $NaClO_4$		$log\beta_{1,Cl^-} = 1.9 \pm 0.2$ $log\beta_{2,Cl^-} = 2.3 \pm 0.1$
	0.1 M $HClO_4$ 0.1 M $NaClO_4$ 0.005 M $K_2Cr_2O_7$		$log\beta_{1,Cl^-} = 2.5 \pm 0.2$ $log\beta_{2,Cl^-} = 3.0 \pm 0.3$
LLC[67]	0.1 M $HClO_4$	$At(x)Br + Br^- \rightleftharpoons At(x)Br_2^-$ $At(x)^+ + Br^- \rightleftharpoons At(x)Br$ $At(x)^+ + 2Br^- \rightleftharpoons At(x)Br_2^-$	$logK_{2,Br^-} = 2.50^*$
Elc[76]	0.5 M HNO_3 0.05 M $K_2Cr_2O_7$		$logK_{2,Br^-} = 2.40^*$
LLC[13]	0.1 M $HClO_4$ 0.1 M $NaClO_4$		$log\beta_{1,Br^-} = 3.0 \pm 0.2$ $log\beta_{2,Br^-} = 4.1 \pm 0.3$
	0.1 M $HClO_4$ 0.1 M $NaClO_4$ 0.005 M $K_2Cr_2O_7$		$log\beta_{1,Br^-} = 2.7 \pm 0.2$ $log\beta_{2,Br^-} = 5.0 \pm 0.2$
LLC[14]	0.1 M $HClO_4$		$log\beta_{1,Br^-} = 2.7 \pm 0.2$ $log\beta_{2,Br^-} = 3.8 \pm 0.3$

LLC[67]	0.8 M $NaClO_4$	$At(x)I + I^- \rightleftharpoons At(x)I_2^-$ $At(x)^+ + I^- \rightleftharpoons At(x)I$ $At(x)^+ + 2I^- \rightleftharpoons At(x)I_2^-$	$\log K_{2,I^-} = 3.30^*$
Elc[76]	0.5 M HNO_3 0.05 M $K_2Cr_2O_7$		$\log K_{2,I^-} = 3.20^*$
LLC[14]	0.1 M $HClO_4$		$\log\beta_{1,I^-} = 6.1 \pm 0.2$ $\log\beta_{2,I^-} = 8.8 \pm 0.2$
Elc[97]	0.01 M $HClO_4$ 0.04 M $NaClO_4$		$\log\beta_{1,I^-} = 6.17$ $\log\beta_{2,I^-} = 9.42$
Elc[75]	0.5 M HNO_3 0.5 M $K_2Cr_2O_7$	$At(x)SCN + SCN^- \rightleftharpoons At(x)SCN_2^-$ $At(x)^+ + SCN^- \rightleftharpoons At(x)SCN$ $At(x)^+ + 2SCN^- \rightleftharpoons At(x)(SCN)_2^-$	$\log K_{2,SCN^-} = 2.60^*$
LLC[13,15]	0.1 M $HClO_4$ 0.1 M $NaClO_4$		$\log\beta_{1,SCN^-} = 3.8 \pm 0.2$ $\log\beta_{2,SCN^-} = 5.9 \pm 0.3$
LLC[13]	0.1 M $HClO_4$ 0.1 M $NaClO_4$ 0.005 M $K_2Cr_2O_7$		$\log\beta_{1,SCN^-} = 2.8 \pm 0.2$ $\log\beta_{2,SCN^-} = 5.3 \pm 0.2$
LLC[67]	0.1 M $HClO_4$	$At(x)I + Br^- \rightleftharpoons At(x)IBr^-$	$\log K = 2.08^*$
LLC[67]	0.1 M $HClO_4$	$At(x)I + Cl^- \rightleftharpoons At(x)ICl^-$	$\log K = 0.95^*$
Elc[72]	0.05 M HNO_3 0.005 M $K_2Cr_2O_7$	$At(x)C(CN)_3 + C(CN)_3^- \rightleftharpoons$ $At(x)(C(CN)_3)_2^-$	$\log K_2 = 2.83^*$

* Apparent values.

1.3.6 Complexation between astatine cations and organic ligands

The metalloid-like behaviors of At were investigated by the interaction between $At(x)^+$ and organic ligands. Some well-known chelating agents for the sequestration of metals, such as EDTA (ethylenediaminetetraacetic acid)[98], DTPA (diethylenetriaminepentaacetic acid)[99], NTA (nitrilotriacetic acid)[91], have been studied by Milesz and co-workers. The complexes formed with $At(x)^+$ were evidenced by electromigration measurements. In particular, DTPA was considered as a chelating agent for the radiolabeling with ^{211}At and antibody, while the *in vivo* stability was proved to be too low for biomedical applications.[100] The interactions between $At(x)^+$ and thioureas, acyl thiourea and selenoureas have been investigated through electromigration measurements by Dreyer *et al.*[96,101] The complexes were assumed to be of the $At(L)_2$ form. Se-donors were also found to coordinate more strongly to $At(x)^+$ than ligands containing carbamide and thiocarbamide. Soft-donor ligands containing phosphorus have also been considered. The interactions were shown to occur only at acid conditions due to the speciation change of At.[102] It is observed that $At(x)^+$-PPh_3 complex is more stable than the $AtBr_2^-$ complex, which is coherent with the soft acids character of At cations, while the complex with OEt_3P is of low stability. Ludwig *et al.* investigated the interactions between $At(x)^+$ and linear nitrogen-, oxygen-, and sulfur-containing ligands by electromobility measurements, demonstrating that complexes of the type (AtXL) (with X^- = Cl^- and Br^-) are formed.[103] The related formation constants are provided.[103] Stronger interactions were evidenced with the sulfur-containing compounds. Sulfur-containing calixarene, such as tetramercaptocalix[4]arene[104] and thiacalix[4]arenetetrasulfonate,[15] have been synthesized and investigated through HPIEC and competition methodologies. ^{211}At-tetramercaptocalix[4]arene is found to be unstable *in vivo* and cannot be applied to nuclear medicine.[104] At(I) and At(III) can form 1:1 and 1:2 complexes with thiacalix[4]arenetetrasulfonate; the associated equilibrium constants are detailed in the

same work. It was also shown that the interaction strength for At (I) is slightly higher than for At (III).[15] All the related equilibrium constants are presented in Table 1.7.

Table 1.7 Formation constant between $At(x)^+$ species and organic compounds

Method	Medium	Ligand	Equilibrium	log *K*
Elc[103]	0.05M NaBr+$NaClO_4$ $HClO_4$ (pH=3) EtOH	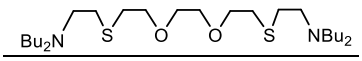	$AtBr + L \rightleftharpoons AtBrL$	$3.99 \pm 0.02^*$
		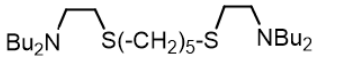		$3.64 \pm 0.02^*$
		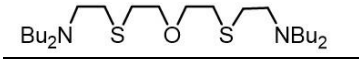		$3.60 \pm 0.04^*$
		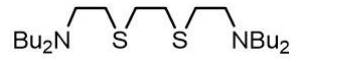		$3.59 \pm 0.03^*$
		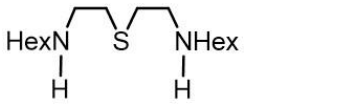		$3.63 \pm 0.04^*$
		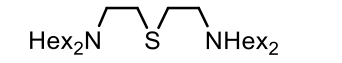		$3.42 \pm 0.04^*$
		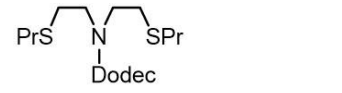		$3.83 \pm 0.02^*$
		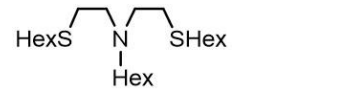		$3.71 \pm 0.03^*$
		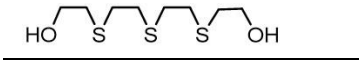		$3.49 \pm 0.02^*$
		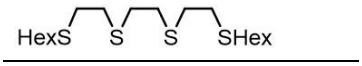		$2.75 \pm 0.04^*$
		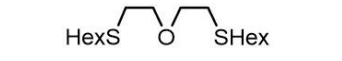		$2.24 \pm 0.04^*$
SLC, LLC[15]	0.1 M $HClO_4$ 0.1 M $NaClO_4$	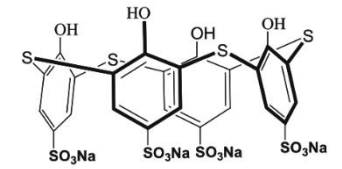	$At^+ + L \rightleftharpoons AtL^+$	4.5 ± 0.4
	0.1 M $HClO_4$ 0.1 M $NaClO_4$ 0.005 M $K_2Cr_2O_7$		$AtO^+ + L \rightleftharpoons AtOL^+$	3.3 ± 0.3

*Apparent values

1.3.7 Halogen bonding with Lewis bases

An important property of halogen elements is the ability to form halogen bonds (XB) with Lewis bases. The halogen bonds correspond to the highly directional interactions between an electrophilic region (called σ-hole due to the local symmetry and its propensity to partially accept electrons) of a halogenated R-X compound (called XB donor) and a Lewis base (called XB acceptor, though it is the actual electron donor).[105]

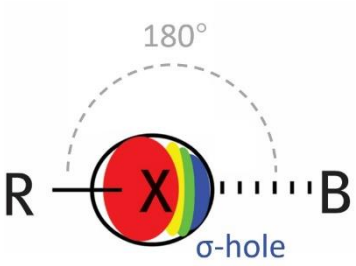

Figure 1.11 Schematic representation of an R−X···B halogen bond.[106]

Belonging to the non-covalent interactions, XBs have been recognized to be strongly impactful for the molecular design.[107–109] To establish the propensity of XB acceptors to engage in XBs, the diiodine basicity scale (pK_{BI2}) was notably proposed in 2011 by Laurence *et al.*,[110] which is based on complexation constants measured between a reference XB donor (I_2) and a broad set of Lewis bases.

As a member of halogen element, astatine has long been predicted to be the strongest XB donor atom,[111,112] despite the lack of experimental data. Recently, Guo *et al.* evidenced the first XBs involving At using experimental and computational approaches.[84] From liquid/liquid competition experiments, they have evidenced the interactions between AtI and nine Lewis bases and obtained the associated equilibrium constants from the analysis of distribution coefficient measurements (listed in Table 1.8). Quantum mechanical calculation shows that AtI interacts with these Lewis bases *via* At atom and, the formed species fully satisfy the features of XB compounds. Besides, the comparison between the measured equilibrium constants (log K_{BAtI}) and the available pK_{BI2} values for the same

Lewis bases, disclosed a quasi-proportional relationship: $\log K_{BAtI} \approx 1.56(22) \times pK_{BI2}$. This confirms again the halogen bonding interactions and proves that At is a stronger XB donor atom than I.

Table 1.8 Equilibrium constants of AtI with different Lewis bases[16]

Lewis base (B)	Molecular structure	Equilibrium	$\log K_{BAtI}$*
Toluene		$AtI + B \rightleftharpoons BAtI$	−0.67 ± 0.24
Ethyl butyrate	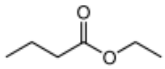		0.46 ± 0.56
Hexamethyl benzene	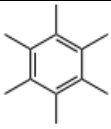		0.67 ± 0.64
Diethyl ether	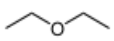		1.53 ± 0.46
Diethyl methylphosphonate	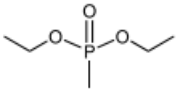		1.75 ± 0.44
Tributyl phosphate	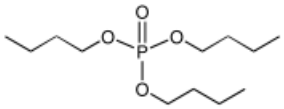		2.84 ± 0.26
Triphenylphosphine sulfide	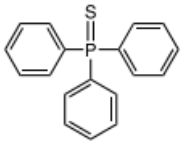		3.41 ± 0.76
Dibutyl sulfoxide	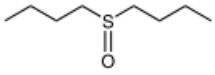		3.78 ± 0.40
Diethyl ether	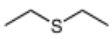		4.01 ± 0.62

*Constants in cyclohexane solution

1.4 Scientific motivations

^{211}At is a promising candidate for TAT. However, the poor understanding of At chemistry impedes the development of its medicinal use. Further research on the fundamental aspects of At chemistry, especially of its speciation in solutions and its reactivity to organic

compounds, are of great interest. The present Ph.D. project aims at purchasing and completing these two sides, with a focus on the Poubaix diagram of At and the At–mediated halogen bonds. The previously developed experimental methodologies (HPIEC, electromobility, competition methods) and the comparative experiment/theory approach[13] are applied.

The Pourbaix diagram is essential information for chemists. It can also be helpful for identifying the At speciation during the radiolabeling processes, and for developing novel radiolabeling strategies. Previous works allow the establishment of a primary version of the Pourbaix diagram of At in the range of stability of water. However, information is lacking in alkaline conditions because two species, At^- and $AtO(OH)_2^-$, are both supposed to be present, while their predominant zones have not been directly determined. The first objective of the thesis is therefore to study the passage from one species to the other. If the speciation change between At^- and $AtO(OH)_2^-$ is direct, the associated constant can be correctly determined by the combination of all the previously measured parameters (equilibrium constants for the couples At^-/At^+, At^+/AtO^+, $AtO^+/AtO(OH)$ and $AtO(OH)/AtO(OH)_2^-$), as hypothesized to build Figure 1.10. It would thus be possible to validate the Pourbaix diagram, at least in the range of water stability. If the change cannot be simply described, this would indicate the existence of another species of At.

As a member of halogen elements, At has been recently proved to be able to form halogen bonding interactions with Lewis bases. However, only a limited number of ligands have been investigated so far; it is of prime importance to extend this work and to (i) set the full range of equilibrium constants that can be reached and (ii) confirm the global trend and in particular check for the occurrence of significant deviations to it. This task will be the second objective of my Ph.D.

Chapter 2. Methodologies and materials

Because astatine is available only in ultra-trace quantities, indirect methods were mostly used in the literature to study its chemistry, for instance based on electromobility, chromatography, or competition between two phases.[10,62,76,78,82,87] The general idea is to associate each possible astatine species in given conditions with a parameter set that characterizes it, which may include the intrinsic mobility or its distribution coefficient between two phases. By tracking one or several parameters with changes in the experimental conditions, changes in astatine speciation may be evidenced. The nature of the species as well as the quantitative parameters that describe astatine behavior can be indirectly revealed by simulations that aim at modeling the experimental data based on the simplest possible (phenomenological) models, for instance by accounting for equilibrium constants in the case of a thermodynamic model.

In the framework of this thesis, three experimental methodologies were applied: electromobility, HPIEC and liquid/liquid competition. Different simulations of chemical processes were made, based on simple analytical expressions or on numerical thermodynamic codes. Since quantum chemistry appears as an alternative "speciation" method to help in establishing the nature of At species at the molecular level,[13] some of the experimental results and analyses will be compared to outcomes of such calculations. Actually, the link between these calculations and the previously mentioned simulations is made *via* quantitative comparisons of the same data (such as equilibrium constants), as shown in the works of Champion *et al*.[9–12,14,16] This chapter is devoted to giving a general description of these methodologies and simulations, including the related principle, devices, analytical tools and pretreatment of data. The materials used in these works will also be presented at the end of this chapter.

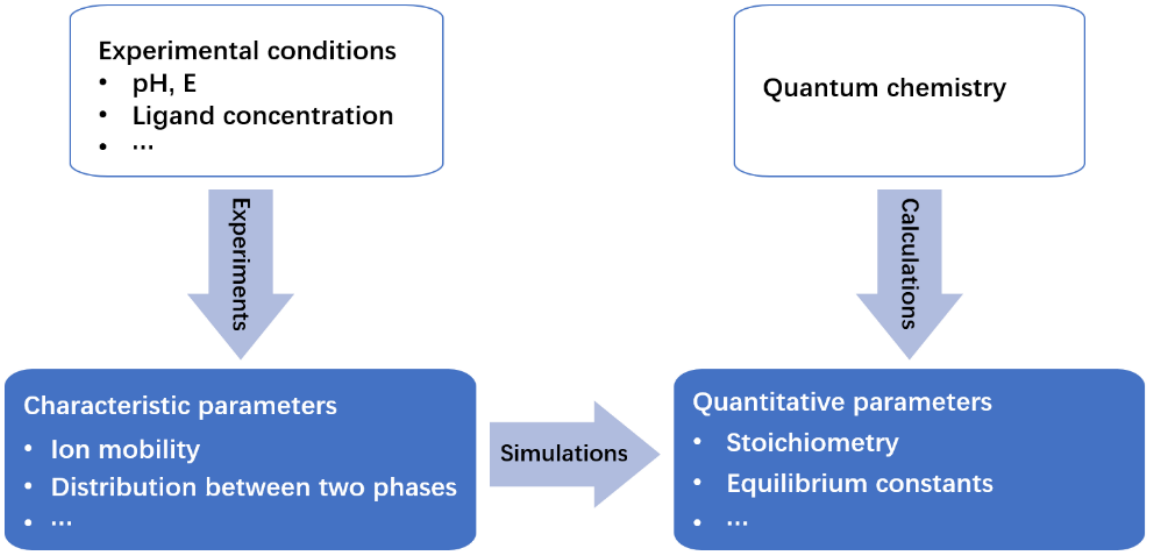

Figure 2.1 Schematic representation of the methodologies for studying the chemistry of astatine in the framework of this work.

2.1 Experimental methodologies

2.1.1 Electromobility

1) Principle

The electromobility measurement is based on the electrophoresis phenomenon.[113] When a voltage U is applied in a solution with distance d in the horizontal direction, an electric field E is created, being U/d (in $V \cdot m^{-1}$). For an ion with charge q in the solution, it will suffer two types of force in the horizontal direction. The first one is the electric field force qE (in $kg \cdot m \cdot s^{-2}$), driving the ion move to the opposite-charged side. The second one is the frictional force which impedes the movement of ions. In a homogeneous laminar flow, this term can be expressed as $6\pi\eta\nu r$ (in $kg \cdot m \cdot s^{-2}$) according to the Stokes' law, with η the dynamic viscosity of the solution ($kg \cdot m^{-1} \cdot s^{-1}$), ν the flow velocity relative to the ion ($m \cdot s^{-1}$) and r the radius of the ion (m). Note that the radius here refers to the Stokes radius, which is the effective radius of the moving ion including any molecules of water or other solvent that move with it. Under the effect of these two forces, the charged ion will be

accelerated until it reaches a constant drift velocity. At this moment, the total resulting force is zero. Therefore, the mobility of this ion μ (in $m^2 \cdot V^{-1} \cdot s^{-1}$), defined as the ratio of the drift velocity to the electric potential, can be expressed as:

$$\mu = \frac{v}{E} = \frac{q}{6\pi r \eta} \tag{2.1}$$

This parameter depends obviously on the charge/size ratio of the ion, affected only by ion-solvent interactions. Therefore, a change of mobility can reflect a change of At species, while two quite different species may accidentally have similar mobilities due to the effect of Stokes radius (see for instance Cl^- and ClO_4^-)[9]. In real cases, the limiting mobilities of ions are usually determined by extrapolation to zero concentration taking into consideration the values of mobilities at finite concentrations of electrolytes.

2) Device

The device for measuring a radioactive ion mobility in free electrolytes was developed by Milanov *et al.*[62] A similar equipment was built by the mechanical service of the Subatech laboratory in order to investigate the mobility of iodine and astatine ions.[9] The diagram of the device is shown in Figure 2.2.

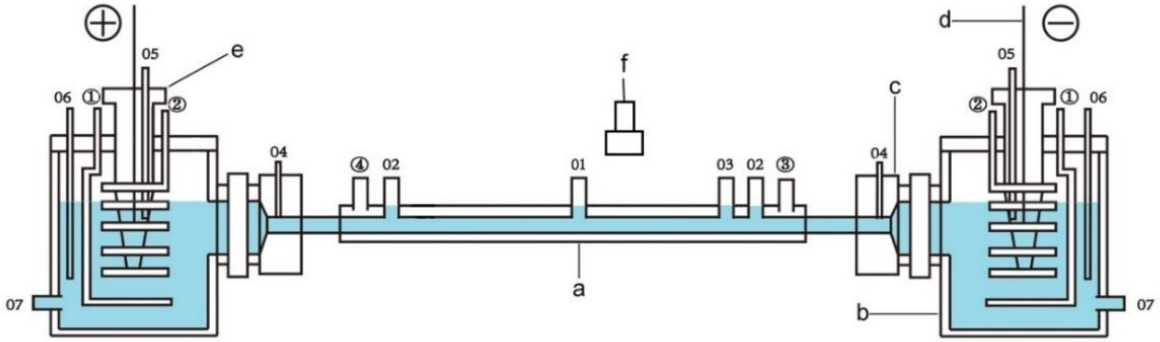

Figure 2.2 Diagram of the electromobility device. a. migration tube; b. electrolyte cells; c. hydrodynamic resistor; d. Pt-electrode; e. glass cylinder; f. γ-ray detector; 01. outlet for the injection of solution containing radioactive sample; 02. outlets used to insert the voltage-measuring electrodes; 03. outlets used to measure the temperature of the medium inside the migration tube with a thermometer probe;

04. outlet for filling the migration tube with the electrolyte; 05 and 06. outlets used to refresh the electrolyte in the cells; 07. outlets for the junction of the cells; ①, ②, ③, ④. outlets for the water bath.[9]

The electrolyte solution fills the horizontal glass tube (a), which is 500 mm long with an inner diameter of 3 mm, and the two electrolyte cells (b). In order to ensure the constancy of the electrolyte composition in the cells, especially the pH and ionic strength, the electrolyte solution inside the electrolyte cells can be refreshed by pumping out through outlets 05 and in through outlets 06 with a 4-channel tubing pump (ISMATEC). Furthermore, electrolyte cells are linked by a PVC tube through the bottom 07 to hinder the liquid flow caused by hydrostatic pressure. The hydrodynamic resistors (c, nitrocellulose membrane, 220 nm) are connected between the migration tube and the electrolyte cells to prevent the transfer of rotational and turbulent flows from the cells into the tube. A water bath system connecting a thermostat (LAUDA ECO Silver RE 420SN) and the outlets ①, ②, ③, ④, is used to maintain the electrolyte temperature in both the migration tube and the electrolyte cells. Additionally, a thermosensor connected to the thermostat is inserted into the electrolyte 03 to calibrate the temperature.

Pt-electrodes (d) with protective glass cylinders (e) are inserted into the cells, and connected to the power supplies (HCP series, FuG Elektronik GmbH) providing a high voltage in the range of 125–2000 V. The voltage-measuring electrodes are inserted into the electrolyte through the outlets 02 to measure the electric field intensity. The actual voltage applied in the migration tube is shown by a digital multimeter (Française d'Instrumentation).

The radioactive samples are injected through the outlet 01 and the migration occurs in the horizontal glass tube. A gamma-ray detector (g, Raytest, controlled by the modified GITA STAR system) moves all the time along the tube with a fixed speed of 37 seconds per scan, to monitor the distribution of radioactivity ions. The detector sensor is a BGO crystal with a photomultiplier tube that detects gamma radiation with a 15 mm tungsten collimator.

The computer program Elphi is used running under Windows for the online data recording. After each scan, the software reads the data from the detector.

The data obtained by the Elphi software are the activities of the radionuclide recorded at each position inside the migration tube at a given time. It shows the distribution of the radionuclide in the electrolyte as a function of the distance. Figure 2.3 a) presents an example of the activity distribution in the migration tube at different moments after the injection of ~500 kBq ^{123}I. The peak/species is initially located around the injection outlet. As time goes by, the peaks visually show the movement of the species to the positive electrode in the electric field, indicating the negative charge of ^{123}I species.

Then the maximum peak position (P, mm) can be obtained by peak fitting performed in Origin 9.0 software using the Gaussian model, as shown in Figure 2.3 b). Note that the small peak stuck in the middle of the tube corresponds to the activity remaining in the injection inlet. This activity is not considered for the data interpretation.

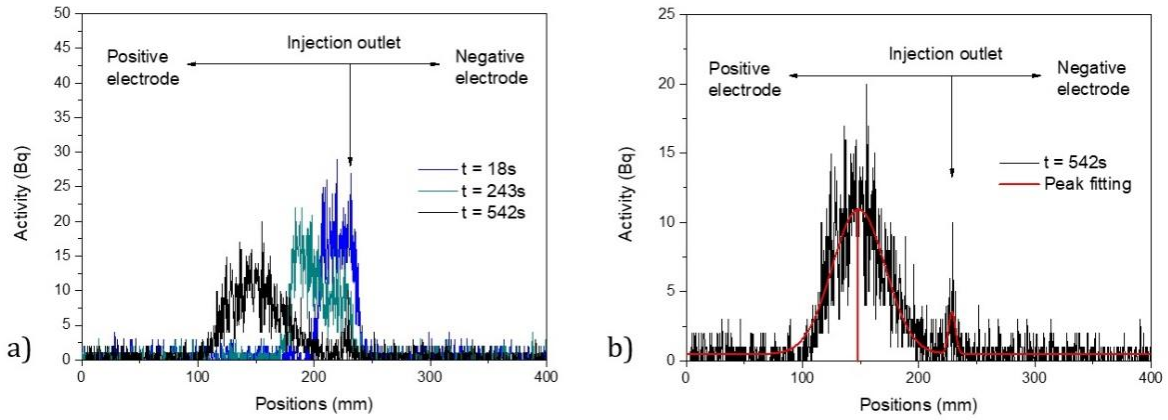

Figure 2.3 Activity of ^{123}I as a function of the position along the migration tube: ^{123}I ~ 500 kBq (10 µL), I = 0.1 M (0.1 M NaCl, 0.1 mM NaOH, 0.1 mM DTT), V = 7.9 ± 0.1 V·cm^{-1}, T = 25 ± 1°C. a) Activity distribution at different times; b) Peak fitting of the activity distribution.

The peak position (P, mm) is plotted as a function of time (t, s) in order to obtain the migration speed (v, cm·s^{-1}) of the investigated ion by the following equation:

$$P = a + v \times 10 \times t \qquad (2.2)$$

where a is the intercept of the line.

Finally, the apparent mobility of the ion (μ_{app}, 10^{-4} $cm^2 \cdot V^{-1} \cdot s^{-1}$) in the electrolyte is:

$$\mu_{app} = \frac{\nu \times d}{V} \tag{2.3}$$

The associated uncertainty is calculated as:

$$\sigma_{\mu_{app}} = \mu_{app} \times \sqrt{\frac{\sigma_\nu^2}{\nu^2} + \frac{\sigma_d^2}{d^2} + \frac{\sigma_V^2}{V^2}} \tag{2.4}$$

2.1.2 HPIEC

1) Principle

In an HPIEC-based experiment, a column consisting of an ionic exchange resin is used as a stationary phase. It attracts solutes with an opposite charge. A buffer solution (eluent) containing the desired media serves as a mobile phase, pushed by a pump under high pressure. The column is firstly equilibrated with the eluant. The sample is then injected and brought to traverse the column together by the eluent. The analytes in the sample (cations or anions depending on the used column) will be retained on the column and then be detached from it by the exchange of similar ions in the eluent freshly pumped in. Therefore, it takes certain time for the analytes in the sample to exit column and then be detected; this time is called retention time (t_r).

Taking the example of a cationic column, initially, the surface absorbed site $\equiv R^+$ is in equilibrium with the ions A^- in the eluent as equation (2.5).

$$A^- + \equiv R^+ \rightleftharpoons \equiv RX \tag{2.5}$$

When the sample is injected, the anions of interest in the sample X^- pass and interact with the column. The interaction can be expressed by the following ion exchange reaction:

$$X^- + \equiv RA \rightleftharpoons \equiv RX + A^- \tag{2.6}$$

As a result, X^- is retained in the column compared to a non-conservative tracer. This translates quantitatively into t_r. t_r depends on the affinity of the analyte to the stationary phase and the flow rate of the eluent, it is thus possible to separate different species.

The data are usually presented in terms of the retention factor (k), which is defined as the ratio between the analyte amounts in the stationary phase and those in the mobile phase. An easy way to calculate k is by the following equation:

$$k = \frac{t_r - t_d}{t_d} \tag{2.7}$$

with t_d being the dead time, meaning the time necessary for the non-retained species to pass through the column, which can be determined from the dead volume and the flow rate of eluent.

From equation (2.6), (2.7) and invoking a number of basic chromatographic principles, log$k$ can be expressed as a linear function of log[eluent]. The slope depends on the charge of analyte and of eluent.[114–116]

For the case of astatine, the retention time can be readily read from the radio-chromatogram produced by the measurement with a γ-ray detector coupled to the HPIEC device.[8,11] While two peaks indicate the occurrence of two distinct species, one peak may reveal one species or hide several species. Thus, HPIEC may not be capable of revealing some specific speciation changes, especially when one is limited in terms of nuclearized column.

2) Device

In this work, the HPIEC device used is a commercially available one, Dionex UltiMate3000.[8] Figure 2.4 represents a simplified schema of this device. The eluents are prepared and stocked in solvent reservoirs ①, then degassed and mixed by ②, ③, ④. The mixture is pushed under the high-pressure by a DGP-3600 MB pump ⑤. The samples are injected into the eluant by an AS3000 auto-sampler ⑥, ⑦. After that, the eluant

entertains the sample to pass through firstly the AG20 guard column ⑧, then the AS20 column ⑨. The temperature of the column is maintained by a TCC-3200B column oven. Finally, the samples are detected by an ultraviolet (UV) detector (⑩, DAD-3000 detector) and a γ-ray detector (⑩, Raytest type "GabiStar") successively.

The Dionex AS20 anionic exchange column (2 mm diameter × 250 mm length) consists of hydrophilic polymer grafted with quaternary alkanol ammonium, with a column capacity of 77.5 μeq. It is pre-protected by a Dionex AG20 guard column (2 mm diameter × 50 mm length), with a column capacity of 1.5 μeq. The γ-ray detector is piloted by Gina Software, and experimental data are acquired and processed by Chromeleon 6.80 Chromatography Software. The retention time is taken at the maximum of the peak that belongs to the specific species (known or unknown) from the chromatogram.

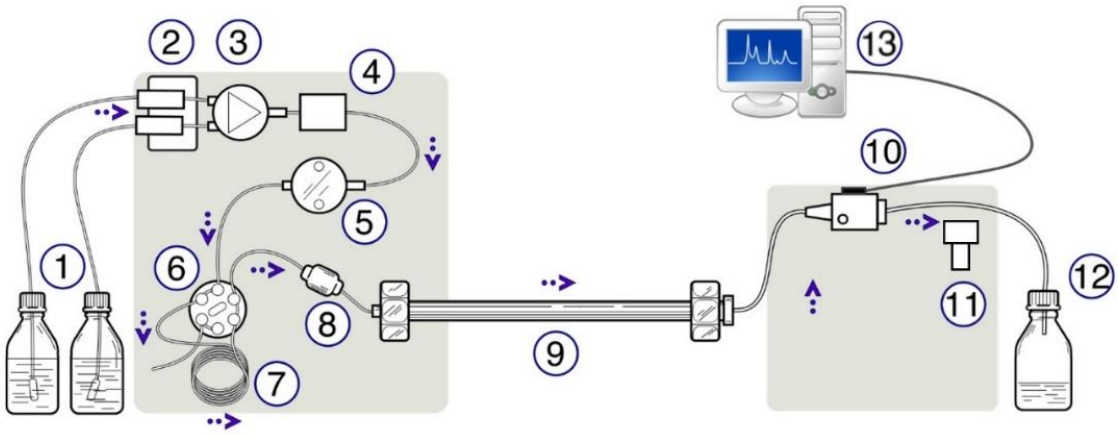

Figure 2.4 Schematic representation of an HPIEC unit. ① Solvent reservoirs, ② solvent degasser, ③ gradient valve, ④ mixing vessel for delivery of the mobile phase, ⑤ high-pressure pump, ⑥ switching valve in "inject position", ⑦ sample injection loop, ⑧ pre-column, ⑨ analytical column, ⑩ UV detector, ⑪ γ-ray detector, ⑫ waste collector, ⑬ data acquisition.

2.1.3 Liquid/liquid competition

1) Principle

In a given biphasic system, each astatine species is associated with a distribution

coefficient (D), which is the ratio of the concentration of this species to its concentration in the same form in the other phase at equilibrium.[117] Taking the example of a species At_{x1} in an organic/aqueous system, its distribution coefficient can be expressed as the following equation (the overlined species corresponding to the organic phase):

$$At_{x1} \overset{D_{At_{x1}}}{\rightleftharpoons} \overline{At_{x1}} \qquad D_{At_{x1}} = \frac{[\overline{At_{x1}}]}{[At_{x1}]} \tag{2.8}$$

Considering that it is barely possible to distingue astatine species in the same phase, the distribution coefficient of astatine (D_{At}) is more frequently used as a characterization in reals cases. It is calculated as the ratio of the sum of the concentrations of all forms of astatine in each of the two phases.

$$D_{At} = \frac{[\overline{At_{x1}}] + [\overline{At_{x2}}] + \cdots}{[At_{x1}] + [At_{x2}] + \cdots} \tag{2.9}$$

This parameter is ruled by the equilibria that are at play in the biphasic system, themselves characterized by equilibrium constants. These equilibria and the associated constants may correspond to one given phase (chemical equilibrium in this phase which may involve one or two astatine species, but also a ligand and/or water) or to the extraction/back-extraction process (chemical equilibrium ruling the distribution of one species between the two phases, being it an astatine one or a ligand for instance).

The principle of the liquid/liquid competition method is to track D_{At} between two liquid phases as a function of influent physiochemical parameters (pH, Eh, ligand concentration, *etc.*). A variation of D_{At} value caused by the change of experimental conditions must reveal an astatine speciation change in at least one of the two phases.[10,16] By simulating the behaviors of D_{At}, the occurrence of chemical equilibria can be revealed and the associated equilibrium constants can be determined.

2) Experimental protocol

According to different experiments, 5 mL (or 4 mL) aqueous phases containing ^{211}At species and 5 mL (or 2 mL) organic phases (pre-equilibrated with the aqueous phases

without the presence of At) are put together in a Pyrex tube. The mixture is shaken for two hours to ensure the equilibrium. After that, the two phases are separated, and an aliquot of 1 mL of each phase is taken to measure their radioactivity by a liquid scintillation counter. The distribution coefficient of At is defined as:

$$D_{\mathrm{At}} = \frac{A_{\mathrm{org}} \times V_{\mathrm{aq}}}{A_{\mathrm{aq}} \times V_{\mathrm{org}}} \tag{2.10}$$

where V_{org} and V_{aq} represent the volume of the organic phase and aqueous phase respectively, and A_{org} and A_{aq} define the total astatine activities in these two phases at equilibrium. Uncertainties associated with D_{At} were calculated according to the following equation:

$$\sigma_{D_{\mathrm{At}}} = D_{\mathrm{At}} \times \sqrt{\frac{\sigma_{Aorg}^2}{A_{org}^2} + \frac{\sigma_{Aaq}^2}{A_{aq}^2} + \frac{\sigma_{Vorg}^2}{V_{org}^2} + \frac{\sigma_{Vaq}^2}{V_{aq}^2}} \tag{2.11}$$

2.2 Analytical tools

2.2.1 Liquid scintillation counter

The radioactivity of ^{211}At in solution samples are measured by the Packard 2550 TR/AB Liquid Scintillation analyzer used with the Ultima Gold LLT scintillation liquid. The measurement is based on the excitation of the scintillation liquid by emitted α-particles and the emission of light photons after de-excitation of the system. These light photons, in number proportional to the α-particles emission in the sample, and in intensity proportional to the energy of the particle, are collected by photomultipliers and recorded by electronic analysis. Therefore, this type of equipment allows both for qualitative and quantitative analysis. However, various effects can disturb the measurement leading to an under evaluation of the results, called quenching. The sources of quenching can be chemical impurities, color, ionization, *etc.*

In this work, the quenching related to the different media is taken into account to determine the activity of astatine (A). To evaluate it, an external standard is used and is

expressed by tSIE (Transformed Spectral Index of External Standard). A very pure sample (not quenched) will have a *tSIE* value close to 1000, while a very quenched sample will have a very low value, close to 50. For our measurements, a quenching curve was established to determine the counting efficiency of a sample containing ^{211}At as a function of tSIE, and the following relationship was obtained:

$$A = A_{\text{mes}} \times (8.1063 \times 10^{-10} \times tSIE^3 - 1.7581 \times 10^{-6} \times tSIE^2 + 0.0012 \times tSIE + 0.7299) \qquad (2.12)$$

with A_{mes} being the activity measured by liquid scintillation counter.

For each measurement, 1 mL At sample (aqueous solution or organic solution), together with 1.5 mL of the corresponding phase (H_2O or organic solvent) are well mixed with 2.5 mL scintillation liquid. The mixture is usually counted for 5 minutes.

2.2.2 COT measurements

A total organic carbon (TOC) meter (Shimadzu TOC V CSH) is used to determine the concentration of an organic compound in aqueous solutions. The measurements are composed of the quantification of total carbon concentration (TC) and inorganic carbon concentration (IC) in the samples. Then the total organic carbon concentration can be calculated as the difference between TC and IC. Finally, the ligand concentration can be deduced knowing the number of carbons in the molecule.

2.2.3 pH/E measurements

An electrode (Inlab) freshly calibrated with standard pH buffers (pH 4.00, 7.00 and 10.00, Merck) and a Pt combined redox electrode (Inlab) calibrated with a redox buffer ($Fe(SCN)_6^{3-}/Fe(SCN)_6^{4-}$, 220 mV/pH 7, METTLER TOLEDO) are used to measure the pH and the potential E of the aqueous phase at equilibrium, respectively.

2.3 Simulations

The experimental methodologies provide the characterizations of astatine species (such

as t_r, D_{At}) as a function of the experimental conditions. In order to obtain the quantitative parameters (stoichiometry, equilibrium constants, *etc.*) describing their formation, different approaches were used, either using the analytical expressions or JCHESS code. Moreover, the JCHESS program was used to give various presentations of interested parameters. The details of the simulation are presented below.

2.3.1 Analytical expressions

The objective is to reproduce the experimental curve obtained by the liquid/liquid competition method displaying D_{At} variation with the influent parameters considering the equilibria occurring (i) in the aqueous solution, (ii) in the organic phase and (iii) between the two phases (extraction/back extraction of the species). Once the chemical reactions are considered, an analytical expression of D_{At} is derived as a function of the experimental conditions and equilibrium constants. Naturally, one should not introduce too many equilibria, which may lead to an undetermined system of equations when one attempts to adjust the parameter values. Therefore, it is good practice to start from the known equilibria and only add a minimum number of new equilibria to fit the data. In this way, this constitutes a phenomenological approach, which thus requires extra information coming from the quantum mechanical calculations to justify the nature of the newly introduced equilibria.

Origin 9.0 was used to fit the experimental data, thus determining the values of the unknown parameters. The model is considered “good” when the model can well reproduce the experimental data with a minimum number of “predictable” equilibria and that the parameters of adjustment are not strongly correlated. The uncertainties associated with the determined parameter values were given by the software. In the framework of this thesis, the average values are given with uncertainties corresponding to a confidence interval of 95%. Note that, all the constants in aqueous solution were calculated at the given ionic strength used in the experiments with the Davies equation[118]:

$$log_{10}\gamma_i = \frac{-0.509 \times z_i^2 \times \sqrt{I}}{(1+\sqrt{I})} + z_i^2 \times 0.15 \times I \quad (2.13)$$

where γ_i is the activity coefficient, $I = \frac{1}{2}\sum_i c_i z_i^2$ is the ionic strength (in mol·L^{-}1) and z_i is the charge of species i.

2.3.1 Numerical codes

JCHESS (based on CHESS model)[119] is a scientific program specifically developed to simulate the equilibrium state of complex aquatic systems, including oxides or minerals, organics, colloids and gases. It is notably used in geochemistry, hydrology and environmental science.[119,120] In this work, JCHESS was applied to simulate the speciation of astatine in the biphasic system of liquid/liquid competition experiments for the study of halogen bonding involving astatine. An input file is used to describe the experimental conditions and the composition of the solution. The speciation of solution (other than astatine) at equilibrium is calculated using the thermodynamic database LLNL[121]. Data for astatine is added and can be divided into three types:

(i) redox processes in the aqueous solution.

(ii) equilibria describing the interactions between astatine species and components of the system, *e.g.* water (acid-base reactions, hydrolysis) or complexing agents.

(iii) equilibria describing the interaction between astatine species and complexing agents in the organic phase. Here, the extraction mechanism is considered as simple partitioning equilibria.

The details of used equilibrium are summarized in Appendix A.

2.3.3 Quantum mechanical calculations

As mentioned in Chapter 1, the experimental approaches can only offer some macroscopic parameters for describing the behaviors of At species. In this case, quantum chemistry

methods represent an appealing alternative to establish the nature of the formed species at the molecular level and to confront the theoretical calculation with the experimental results. Indeed, the molecular structure(s) can readily be determined from the (experimental) stoichiometry of a compound, as well as many other spectroscopic signatures at a desired level of accuracy. In this work, the two-component DFT approach is used, as in previous successful works.[13,16]

Since the calculations are actually performed by my colleagues Cecilia Gomez-Pech, my supervisor Rémi Maurice from the Subatech laboratory and my coauthors Nicolas Galland and Seyfeddine Rahali from the CEISAM laboratory, details concerning this methodology will not be given here, but rather a short description of the main features in the context of this PhD. First of all, the calculation outcomes depend on several degrees of freedom, such as the functional expression in DFT. The choice of the functional has to be made wisely, which requires some testing and experience. My coauthors have tested many functionals in the context of astatine chemistry,[122] and have rechecked the performance of a few of them for halogen bonding involving astatine.[16,123] Second, the equilibrium constants are computed in the gas phase in the context of the halogen bonding (the solvent polarity being here low, no much improvement would be brought by an implicit solvation model). Third, the determination of equilibrium constants requires computation of the (harmonic) vibrational frequencies, the vibrational energy entering the calculation of the Gibbs free energy at 298 K. Finally, it is hard to compute absolute equilibrium constants. Therefore, my coauthors focus more on exchange reactions. Consequently, one should look at the relative values (in log units) by changing the ligand, and not in the absolute values.

2.4 Materials

2.4.1 Chemicals

All chemicals are commercially available. They are of analytical grade or better except the following products. 1,1,3,3-tetramethylurea (Acros Organics, 99.0%), dimethyl selenide

(Alfa Aesar, 99%), (1R)-(-)-Thiocamphor (Combi-Blocks, 95%), N,N,N',N'-Tetramethylthiourea (Alfa Aesar, 98%), N,N-dimethylacetamide (Sigma Aldrich, 99.95%) and N,N-Dimethylcyanamide (Sigma Aldrich, 99%) were used as received, while N,N-Dimethylthioacetamide (Kodak) was purified by sublimation before using. All solutions were freshly prepared using Milli-Q deionized water and all experiments were performed in air-conditioned laboratories (21 ± 3°C).

2.4.2 Radioactive sources

1) ^{211}At

^{211}At sources used in the present works were produced by ARRONAX cyclotron (Nantes, France). According to the nuclear reaction ^{209}Bi(α, 2n)^{211}At, the ^{209}Bi targets were irradiated by alpha external beams accelerated and downgraded to 28.6 MeV with an average beam current of 20 μA. In these conditions, the ratio of produced ^{210}At/^{211}At is less than 10^{-3}.

Once the irradiation is completed, the produced ^{211}At was recovered using a dry distillation method. This method is based on the fact that the sublimation temperature of astatine is lower than that of bismuth and other contaminants potentially presenting in the target. In this process, the target was heated to 800°C. At this temperature, bismuth becomes liquid, whereas astatine is found in gaseous form. By using an inert gas, astatine is drawn outside the oven and condensed at the outlet in the capillary, which is placed at –45°C. Finally, ^{211}At was recovered in chloroform solution. The radionuclide purity of ^{211}At was verified by γ-ray spectroscopy with a high-purity germanium (HPGe) detector.

The production of ^{211}At source is about 2 or 3 times per months. The ^{211}At sources that we received were about 50 MBq in 0.1 mL chloroform. Two methods for recovering ^{211}At in the desired solution were applied, according to different requirements for the experiments. For the experiments which required concentrated activities or inert-gas environment, chloroform was evaporated using N_2 gas before the residue was retrieved

with the desired aqueous solution. Otherwise, astatine was back-extracted with 0.1 M NaOH. In both cases, astatine redox state was controlled by using the appropriate redox-controlling agent.

2) ^{123}I

^{123}I ($t_{1/2}$ = 13.2 h) sources were purchased from Curium (Paris, France). Sodium iodide-^{123}I (reference: I-123-S-2) with an activity of 18.5 MBq·mL^{-1} was obtained in 1 mL of solution with a radiochemical purity of ≥ 95%. This product is without a trainer and the excipients include monosodium phosphate monohydrate, thiosulfate de sodium pentahydrate, sodium chloride and water.

2.5 Summary

Three different experimental methodologies: electromobility, HPIEC and liquid/liquid competition, are used in the framework of this thesis. Each method presents its advantages and disadvantages (Table 2.1). Combining the experiments with simulations, the characterization of astatine species, *i.e.* their identification and the determination of the quantitative parameters describing their formation can be obtained.

These methods are here complementary and all can be performed in order to retrieve information on a given At speciation change. To complete the approach, quantum mechanical calculations are also performed in order to help in analyzing the experimental outcomes and interpretations, in particular with regard to the identification of the key species/equilibria.

Table 2.1 Comparison of electromigration measurements (Elc), HPIEC measurements, and liquid/liquid competition experiments (LLC).

Method	Advantages	Disadvantages	Information obtained
Elc	Avoid undesirable reactions with other phases such as extractant, ion-exchange resin	Sensitive to the experimental conditions, such as the injected volume of solution, the stability of experimental platform Large uncertainty	Negative or positive charge; mobility; complexation constants
HPIEC	Relatively good resolution	Separation performance depends on the selection of fixed phase and mobile phase	Charge of ions; complexation constants
LLC	Work in static mode (equilibria are reached); no require for a specific machine	Information may be hidden by unchanged distribution coefficient	Stoichiometry of complex; complexation constants

Chapter 3. Pourbaix diagram of astatine: Focus on alkaline conditions

The Pourbaix diagram in non-complexing medium maps out the predominant chemical redox forms of an element in an aqueous system as a function of pH and redox potential. It is of primary interest for chemists. Nevertheless, information is lacking concerning the diagram of astatine. This chapter aims at elucidating the Pourbaix diagram of astatine, with a focus on alkaline conditions.

3.1 Introduction

A Pourbaix diagram, also known as a potential-pH diagram, is a thermodynamic chart constructed using the Nernst equation and displaying the possible stable species of an element with respect to the redox potential and the pH, usually in an aqueous system. The lines in such a diagram materialize the equilibria, that is, the conditions where the activities for the predominant soluble species on each side of it are equal.

The Pourbaix diagram can help chemists shedding light on the nature of the species present in the solution and thus understand reaction mechanisms. It is not only of fundamental interest for chemists, but also for valuable practical applications, notably in corrosion studies, geoscience and environmental researches to allow a quantitative description of the behavior of the elements.[124–126] For astatine, knowing its Pourbaix diagram is a crucial issue for the development of a suitable radiolabeling strategy in medical applications. It indicates the redox form of species that can exist in aqueous solution and therefore determines the types of mechanistic approaches which can be attempted. For instance, the most used radiolabeling approaches to date are based on the EAS on either an aryl group[36,39] or a boron cluster[40,41] using an At(I) species, which is favored in acidic and slightly oxidizing conditions. Other approaches include the NAS to

form At-C bonds[37] or chelation to a transition metal ion[46–48], *i.e.* the use of an At(–I) species, as At^-, which requires reducing conditions.

Even though the Pourbaix diagrams have been well-established for most main-group elements for decades, information is limited in the case of astatine. This comes from the fact that astatine is only available at ultra-trace concentrations (below 10^{-10} mol·L^{-1}). Conventional spectroscopic tools cannot be applied to identify astatine species. A chemical form of astatine is usually established by combining diverse characterizations, such as the charge of this species, its coprecipitation behaviors and its formation from other astatine species, guided by the common knowledge on iodine chemistry. Since most experiments were performed with very diluted solutions, competitive reactions with impurities presenting in solutions may interfere with the test of specific reaction mechanisms, which may lead to irreproducible results. Actually, seven species of astatine have been identified or hypothesized in aqueous solutions, from different experimental characterizations. A detailed presentation can be found in Chapter 1.

In summary, the most clearly established form is At^- in reducing conditions over the whole pH range, following the same trend as the lighter halogens. The characterization of its –1 charge is supported by various measurements.[8,9,66,73,74,76,78,84,85] In acidic and slightly oxidizing conditions, the At^+ form was justified from its charge,[84] and indirectly supported by its formation involving the withdrawal of two electrons from At^-.[10] By further increasing the potential in acidic conditions, another positive-charged species, AtO^+, was identified, because of the charge,[84,86] its monovalent character,[85,87,88] and its formation involving two electrons and two protons from At^+ (and water).[10] When the pH was increased to weak acidic while remaining in oxidizing conditions, the first hydrolyzed species of AtO^+, a neutral species AtO(OH), was observed from HPIEC measurements.[11] Then, further increasing the pH to alkaline and non-reductive conditions led to the second hydrolyzed species of AtO^+, $AtO(OH)_2^-$. Its –1 charge was supported by HPIEC experiments.[12] Apart from the species mentioned above, two other species were reported in the literature. In strongly oxidizing conditions, AtO_3^- is

supposed to exist through the whole pH range, and AtO_4^- in alkaline conditions, by analogy with iodine (IO_3^- and IO_4^-, respectively).

The thermodynamic equilibria between different species have been experimentally studied by several authors in the literature.[10,66,69–71,78–80,89] In particular, Champion *et al.* from Nantes (Subatech and CEISAM laboratories) applied a joint experimental-computational approach, successfully determining the equilibrium constants related to the following speciation changes: At^-/At^+, At^+/AtO^+, $AtO^+/AtO(OH)$ and $AtO(OH)/AtO(OH)_2^-$.[10–12] Concerning AtO_3^- and AtO_4^-, equilibrium parameters remain qualitative or even absent. With the reliable information from the literature and the quantitative parameters reported by Champion *et al.*,[10–12] a primary version of Pourbaix diagram of astatine can be produced, as shown in Figure 3.1.

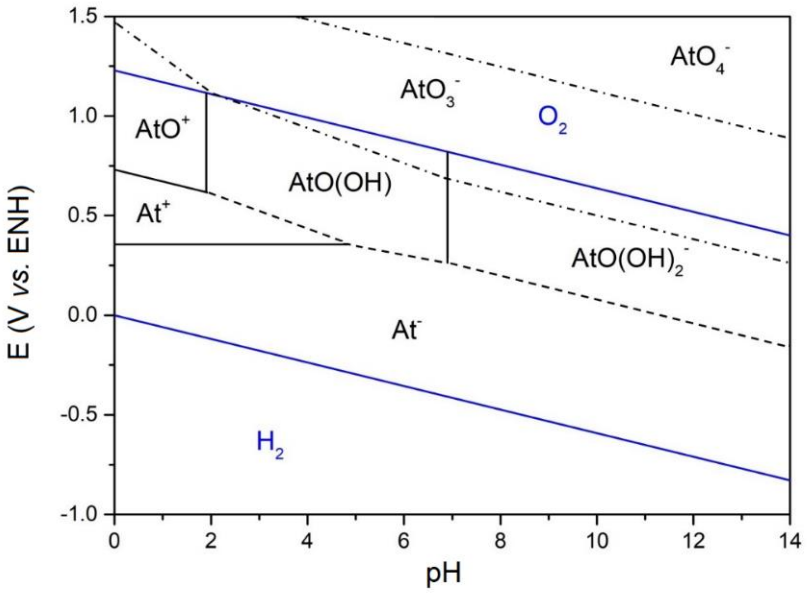

Figure 3.1 Pourbaix diagram of astatine (25°C). The blue solid lines indicate the stability zone of water; the black solid lines correspond to directly determined boundaries with data reported by Champion *et al.*[10–12]; the dashed lines indicate the boundaries deduced from known equilibria; the dashed dot lines relate to undetermined or uncertain boundaries.

3.2 Objective

It is noteworthy that in alkaline conditions, At^- and $AtO(OH)_2^-$ are both supposed to exist: At^- in reducing conditions[81] and $AtO(OH)_2^-$ in non-reductive conditions[12]. The predominance areas of these species have not been directly determined and the speciation change from one to the other has only been derived from other constants, under the hypothesis that no other species actually lie in between those two. In this context, the objective of this chapter is to find out the speciation of astatine in alkaline conditions, and to quantify the speciation change between the relevant species, only At^- and $AtO(OH)_2^-$ or not. Two cases are possible: if the direct change of $At^-/AtO(OH)_2^-$ is confirmed, then the associated constant should indeed be derivable from all the previously measured parameters (related to At^-/At^+, At^+/AtO^+, $AtO^+/AtO(OH)$, $AtO(OH)/AtO(OH)_2^-$ couples). It would thus be possible to validate the Pourbaix diagram (at least in extended range of potentials and pH). If the change cannot be simply described, this would indicate the existence of other species of At, and then at least one more speciation change would have to be characterized.

To address this question, a strategy has been set up, as shown in Figure 3.2.

Firstly, astatine species in reducing and non-reductive conditions at pH = 10 (squares and stars in Figure 3.2) were characterized by HPIEC and electromobility measurements. In order to simplify the description without presupposing the species natures, the astatine species present in alkaline and reducing conditions is (are) denoted At_{red}, and the astatine species in alkaline and non-reductive conditions is (are) denoted At_{ox} in this chapter. The aims are to identify how many species exist in each box and to obtain some key characterizations of these species. More precisely, HPIEC measurements can offer information about the number of species, the charge of the species, and also some information on their reactivity (with the exchange sites of the column). For comparison, measurements with anions carrying –1 charge (Br^-, I^-) and –2 charge ($S_2O_3^{2-}$) were performed. Electromobility measurements give not only evidence for the charge of the

species, but also their apparent mobilities, which can be compared with the mobility of iodide species ($^{123}I^-$ in this work).

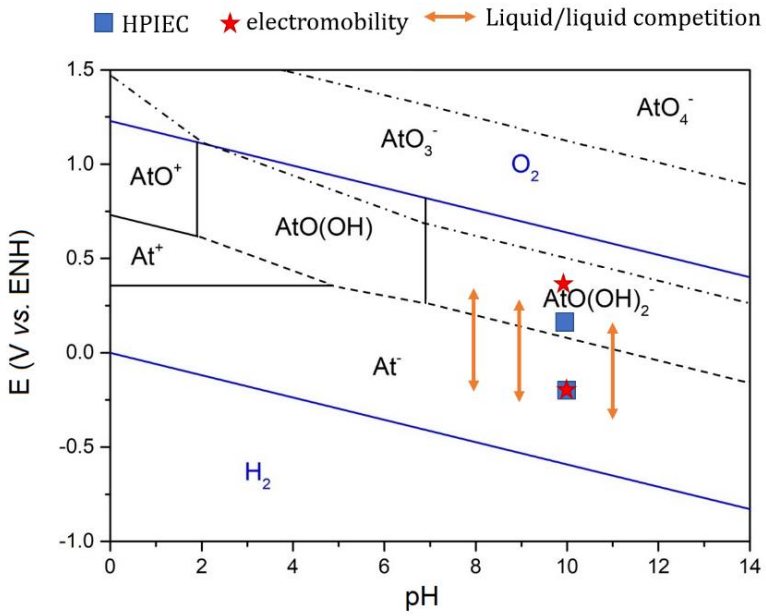

Figure 3.2 Schematic representation of the strategy for completing the Pourbaix diagram of astatine in alkaline conditions. Squares correspond to the experimental conditions for HPIEC measurements; stars indicate the conditions for electromobility measurements; arrows refer to the conditions for liquid/liquid competition experiments.

Secondly, the liquid/liquid competition experiments were applied to evidence the speciation change and to quantify the relevant thermodynamic equilibrium. Here, the experimental conditions were set to fix the pH (8, 9 or 11) of samples and to track the speciation change of astatine (by the distribution coefficient) as a function of the potential (arrows in Figure 3.2). Simulation of experimental data was used to determine the apparent potential at each pH value.

Finally, the standard potential of the equilibrium between At_{red} and At_{ox} can be deduced, and then used to compare with that predicted from the data allowing to build the current Pourbaix diagram of At in the range of water stability. The Pourbaix diagram represented in Figure 3.1 can then be validated or be completed.

3.3 Experimental details

3.3.1 Chemicals for controlling the physicochemical conditions

The objective of this work is to evidence and quantify speciation changes of astatine aroused by the change of potential and/or pH of the solution. Therefore, it is important to select chemicals which maintain or at least keep controlled the physicochemical conditions of solution while limiting the direct interaction with actual astatine species. To this end, the non-metal-complexing pH buffer piperazine-1,4-bis(propanesulfonic acid) (PIPPS, pK_{a1} = 3.73 and pK_{a2} = 7.96)[127,128] was selected to control the pH of samples when it is possible (for pH = 8 or 9). Otherwise, the pH of solution was adjusted by adding NaOH.

DL-dithiothreitol (DTT), a small-molecule redox reagent frequently applied during radiolabeling processes of astatine,[44] was used as a reducing agent. $NaClO_4$ or the redox couple $S_2O_8^{2-}/SO_4^{2-}$ was applied to maintain the oxidizing condition or to set the potential of the solutions. The possible interaction between the reducing or oxidizing agents and astatine species will be first investigated by different measurements (*vide infra*).

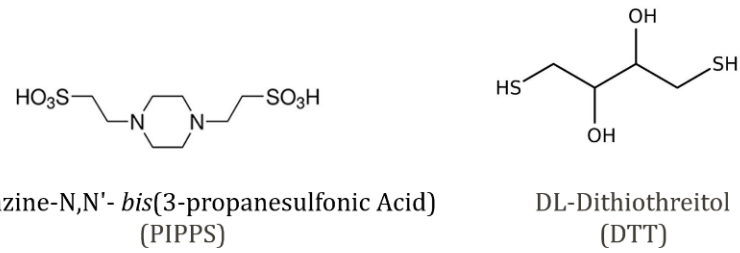

Piperazine-N,N'- *bis*(3-propanesulfonic Acid) (PIPPS)

DL-Dithiothreitol (DTT)

Figure 3.3 Molecular structure of PIPPS and DTT.

CO_2 in the air can be readily solubilized in alkaline solutions and thus be transformed into carbonate ions, a potential complexing agent for At(III). Therefore, all the solutions meant to contain astatine were prepared in a glove box under an argon or a nitrogen atmosphere

using degassed (by vacuum pump) Milli-Q deionized water. The stock solutions of DTT, PIPPS, NaCl, $NaClO_4$, $Na_2S_2O_8$, Na_2SO_4 were prepared by dissolving the corresponding salts. The stock solution of NaOH was prepared from a concentrated NaOH solution.

3.3.2 HPIEC experiments

1) Experimental procedure

The eluents were freshly prepared by dilution of stock solutions. The samples of 10^{-5} M Br^-, 10^{-5} M $^{127}I^-$ and 10^{-5} M $S_2O_3^{2-}$ were prepared by dissolving the corresponding mass of NaBr, NaI–127 and $Na_2S_2O_3$ salts, respectively.

The ^{211}At sources were initially recovered in chloroform and a series of steps was achieved to extract it in the desired medium. Firstly, chloroform was evaporated to dryness using a nitrogen gas flux. A Schott bottle containing 100 mL of 0.1 M Na_2SO_3 was then used to recover the tail gas. The recovery solution was checked by liquid scintillation counting, showing no activity loss of astatine with the nitrogen flow.[9] Secondly, about 500 µL of desired solution (reducing or non-reductive conditions) was added in the vial and the solution was left like this for at least two hours to retrieve At in solutions. At_{red} and At_{ox} were finally prepared using the reducing (10^{-4} M NaOH/10^{-4} M DTT; pH = 10.0 ± 0.2, E = –0.15 ± 0.02 V *vs.* NHE) and the non-reductive (10^{-4} M NaOH; pH = 10 ± 0.2, E = 0.19 ± 0.02 V *vs.* NHE) media, respectively. The NaI-123 source was received as an aqueous solution and it was diluted so as to lead to solutions with the same concentrations as the ^{211}At samples.

All HPIEC measurements were performed under isocratic conditions at 25°C, with an eluent flow rate fixed at 350 µL·min^{-1}. Before each measurement, the column was equilibrated with eluent for at least 30 mins. $^{123}I^-$, $^{127}I^-$, Br^-, and $S_2O_3^{2-}$ were detected online spectrophotometrically at 230, 214 nm; ^{211}At and ^{123}I were detected by a γ-ray detector.

2) Preliminary experiments

The dead time of HPIEC between the injection point and the UV detector can be readily read from the UV chromatogram. This parameter is 2.28 min when the flow rate is set to 350 µL·min^{-1}, corresponding to a dead volume of 798 µL. In order to determine the dead volume between the UV detector and the γ-ray detector for further calculations, preliminary experiments were performed. It involves the analysis of NaI-123 samples, which can be detected by both a γ detector because of the radioactive iodine and an UV one due to the excipient containing sodium thiosulfate. Therefore, without applying the separative column, the volume between the two detectors can be deduced by the time difference between the two detected peaks.

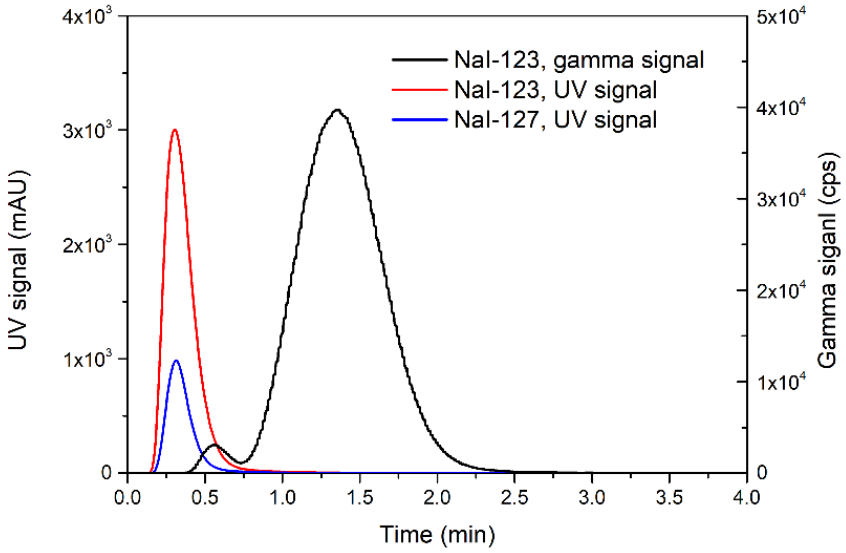

Figure 3.4 HPIEC UV-chromatograms and radio-chromatogram obtained without the separation column for a NaI-123 and a NaI-127 sample (in 0.1 M $NaClO_4$/10^{-4} M NaOH solution) with 350 µL·min^{-1} eluent containing 0.1 M $NaClO_4$/10^{-4} M NaOH.

Figure 3.4 shows the chromatograms of radioactive iodine ^{123}I and non-radioactive iodine ^{127}I obtained without entering the separation column. From the UV chromatogram, a peak at 0.3 min can be found for both ^{123}I and ^{127}I samples. Surprisingly, two peaks were observed in the γ chromatogram of the ^{123}I sample. The first peak is relatively small at 0.57 min; the second one is the principal one, present at 1.36 min. When the flow rate changed to 250 µL·min^{-1}, the same phenomenon was observed, with a longer time

difference corresponding to the same difference of volume between the two detections with the γ chromatogram. Without using a column, it is impossible to obtain two peaks for a sample simply because there is no actual separation process. Therefore, it corresponds to successive detections of the sample. In fact, this problem comes from the assemblage of the γ-ray detector. In a Raytest GabiStar system, there are two detection loops: either the conventional analytical loop of 5 µL or the "metabolites" loop of 250 µL. These loops should be connected in parallel, and only one should be selected for a measurement. However, due to an error in the setting, the two loops were connected in series, resulting in a double detection with a difference of volume of about 280 µL (corresponding to a difference of detection time of 0.8 min with the flow rate at 350 $\mu L \cdot min^{-1}$, and 1.1 min with a 250 $\mu L \cdot min^{-1}$ rate). Unfortunately, it was not practically possible to correct this setting prior to doing the actual experiments. Therefore, for the measurements detected by the γ-ray detector, only one peak of the double detection should be considered, actually the most intense one, *i.e.* the peak detected by the "metabolites" loop will be taken into account. Finally, the dead volume between UV detector and γ-ray detector is 371 µL (corresponding to a difference of detection time of 1.06 min with the flow rate at 350 $\mu L \cdot min^{-1}$).

3.3.3 Electromobility measurements

The reducing medium for the At electromobility measurements was composed of 10^{-4} M NaOH, 10^{-4} M DTT and 0.1 M NaCl (pH = 10.0 ± 0.2, E = –0.2 ± 0.02 V *vs.* NHE), while the oxidizing medium consisted of 10^{-4} M NaOH and 0.1 M $NaClO_4$ (pH = 10.0 ± 0.2, E = 0.38 ± 0.02 V *vs.* NHE). The ^{211}At and ^{123}I sources were prepared by the same method as for the HPIEC measurements, with identic compositions as the electrolytes. Note that the experiments were conducted in normal atmospheric conditions. A pre-test was performed without radioactive source; it showed that after the exposure of three hours (maximum time for a measurement) of the electrolyte in the equipment, there is no significant change in the pH and in the potential of electrolyte. Thus, it is hypothesized that there is also no evolution of the At speciation during the electromobility experiment due to the normal

atmospheric conditions.

All the electromobility measurements were performed at 25°C (maintained by a water bath system). The voltage applied to the electromigration device was set at 450 ± 3 V. The injected activity of ^{123}I (E_γ = 159.97 keV, intensity 83.25%) was about 500 kBq and for ^{211}At (E_γ = 687 keV, intensity 0.245%) it was about 1 MBq.

3.3.4 Liquid/liquid competition experiments

Two types of liquid/liquid competition experiments were performed in this work. The first one aims at studying the possible interactions between AtO^+ and redox agents ($S_2O_8^{2-}$ and SO_4^{2-}). In fact, the initial objective of this investigation is to check the possible interference of $S_2O_8^{2-}$ and SO_4^{2-} towards the $AtO(OH)_2^-$ formation – the presumed species in alkaline and non-reductive conditions. By way of reminder, $S_2O_8^{2-}$ is an oxidizing agent which is used to change the potential of samples in alkaline conditions (by changing its concentration). If it interacts with At(III), it will be difficult to identify whether the change in astatine speciation (with the change of the redox potential) is caused by a redox-type reaction or by the reactions between $AtO(OH)_2^-$ and $S_2O_8^{2-}$. Since $AtO(OH)_2^-$ is the hydrolyzed species of AtO^+, and since the conditions for AtO^+ have already been identified,[10] the reactivity between AtO^+ and $S_2O_8^{2-}$ was studied in acidic conditions.

The second type of experiment aimed at characterizing the speciation change from reducing conditions to oxidizing conditions in alkaline solutions, in order to evidence the speciation change aroused by the change of redox potential and thus by a redox-type reaction.

Considering that the samples of these two kinds of experiments were prepared in different ways, the experimental procedure is presented separately.

1) Samples of AtO^+

The ^{211}At source was recovered in aqueous medium after back-extractions in 1.5 mL of 0.1

M NaOH, AtO^+ was then obtained in a 0.1 M $HClO_4$/5·10^{-3} M $K_2Cr_2O_7$ solution (pH = 1.2 ± 0.1, E = 0.93 ± 0.02 V *vs.* NHE), in accordance with the current Pourbaix diagram of astatine (Figure 3.1).

Two liquid phases were prepared separately as the following. The organic phase was diisopropyl ether (DIPE) pre-equilibrated with a 0.1 M $HClO_4$/5·10^{-3} M $K_2Cr_2O_7$ solution. The aqueous phase was composed of 0.1 M $HClO_4$/5·10^{-3} M $K_2Cr_2O_7$; $Na_2S_2O_8$ or Na_2SO_4 was further introduced to check the potential reactivity of AtO^+ with $S_2O_8^{2-}$ and SO_4^{2-}. For a series of experiments, the concentration of $Na_2S_2O_8$ or Na_2SO_4 varies from 10^{-7} M to 0.1 M. Finally, AtO^+ was introduced into the aqueous phase from the stock solution and then one hour was left for equilibration, allowing for the occurrence of interactions, if possible.

2) Samples in alkaline conditions

The ^{211}At source was recovered in the aqueous medium after evaporation of chloroform and the addition of the desired pH buffer solution. The pH buffer solutions for pH = 8 and 9 were prepared with 0.02 M PIPPS adjusted by 1 M NaOH solution. For pH = 11, the solution was directly prepared with 10^{-3} M NaOH. The organic phase was DIPE pre-equilibrated with the corresponding pH buffer solution. The aqueous phase was prepared with a pH buffer while adding redox agents to maintain the potential. For a series of experiments, the potential of samples was modified by changing the concentration of DTT from 10^{-3} M to 10^{-7} M, and by varying the $S_2O_8^{2-}$/SO_4^{2-} redox couple proportion while fixing [$Na_2S_2O_8$] + [Na_2SO_4] = 10^{-3} M. The preparation allowed to obtain a series of aqueous solutions with the potential varied from –0.20 V to 0.35 V (see Figure 3.2). NaOH was used to re-adjust the pH of samples if it was modified after the addition of the redox agents. Finally, ^{211}At stock solution was added in each sample.

After the preparation of two phases according to the procedure described above, 5 mL of the organic phase and 5 mL of the aqueous phase were put together in a Pyrex tube (with a radioactivity of about 1000 Bq) and were shaken for two hours. The two phases were then separated and a 1 mL of aliquot of each phase was taken to measure their

radioactivity by a liquid scintillation counter. After separation of the two phases, the pH and the potential of the samples were systematically checked.

Note that the experiments in alkaline conditions were twice repeated with different At sources. The samples were prepared under the inert gas atmosphere to prevent the possible influence of CO_2 on At(III) speciation, including the preparation of samples and aliquots. The pH and the potential of the samples were also measured in the glove box as fast as possible after the separation of the two phases.

3.4 Results and discussions

3.4.1 Potential interactions between the medium chemicals and astatine species

1) Interference of DTT with astatine species

The potential interaction between DTT and astatine species was investigated by HPIEC measurement. Two astatine samples were tested. The first one was in a solution containing 0.1 M NaCl, 10^{-3} M phosphate-buffered saline (PBS), and $10^{-3}/10^{-4}$ M $S_2O_3^{2-}/SO_3^{2-}$. Sabatié-Gogova *et al.* have demonstrated that the astatine species in these conditions is At^- by HPIEC measurements.[8] The second sample was in 0.1 M NaCl, 10^{-3} M PBS, and 10^{-3} DTT solution, *i.e.*, the redox couple $S_2O_3^2/SO_3^{2-}$ controlling the potential was replaced by DTT.

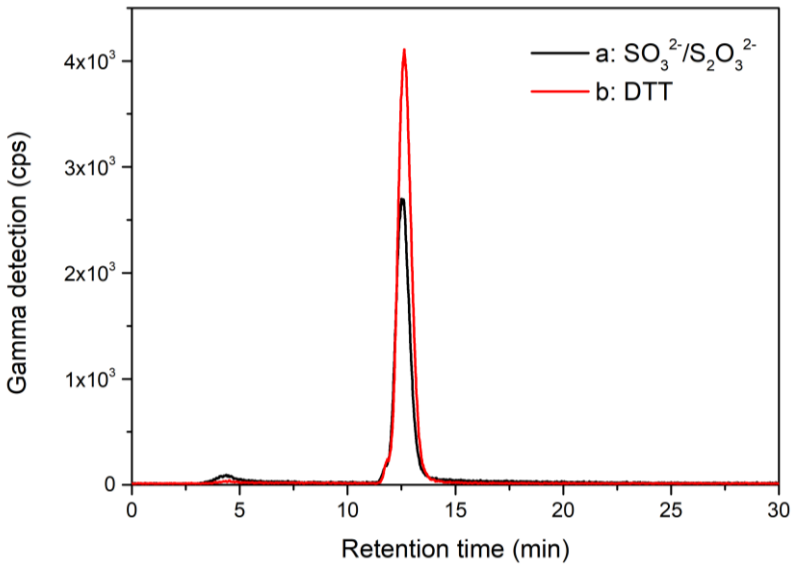

Figure 3.5 HPIEC radio-chromatograms obtained with 350 µL·min^{-1} eluent containing 0.1 M NaCl, 10^{-3} M PBS, and 10^{-3}/10^{-4} M $S_2O_3^{2-}$/ SO_3^{2-} on two samples: (a) At in 0.1 M NaCl, 10^{-3} M PBS, and 10^{-3}/10^{-4} M $S_2O_3^{2-}$/ SO_3^{2-}; (b) At in 0.1 M NaCl, 10^{-3} M PBS, and 10^{-3} M DTT.

Figure 3.5 shows the chromatograms of these samples. For the first sample (black line), one major peak at 12.6 min could be identified, which is coherent with the result of At^- reported by Sabatié-Gogova *et al.* (about 13 min).[8] Besides, a small peak appears at about 4.5 min, which is supposed to be AtO(OH) considering the applied conditions. For the second sample (red line), the same features can be observed: a principal peak at 12.6 min and a small peak at 4.5 min, which is indicative of no specific interaction between At species and DTT (for concentration ≤ 10^{-3} M). Moreover, the integration value of the peak at 4.5 min is smaller than that in the first sample, which is coherent with the fact that DTT is a potent reducing agent.

2) Interference of $Na_2S_2O_8$ and Na_2SO_4 with astatine species in acidic conditions

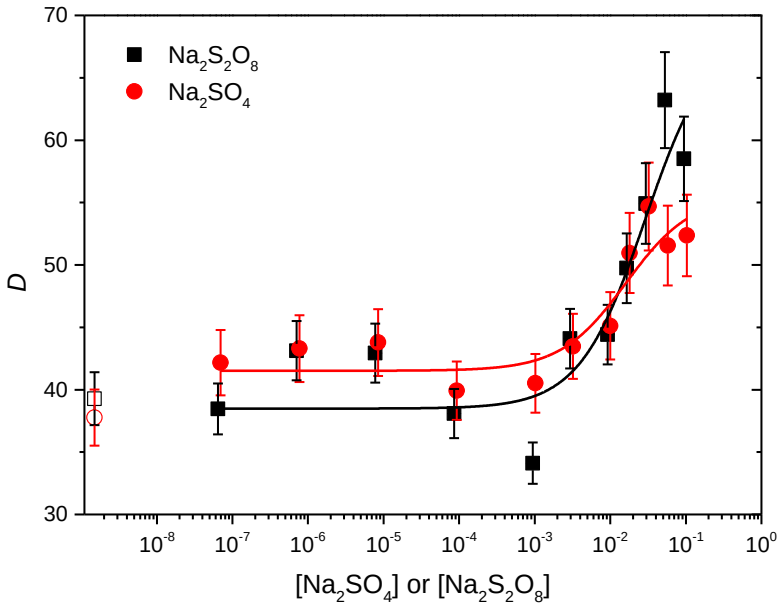

Figure 3.6 Distribution coefficient of astatine in biphasic aqueous/DIPE system with the presence of $Na_2S_2O_8$ (square) or Na_2SO_4 (circle) in the aqueous phase in acidic conditions.

Figure 3.6 shows the variation of D_{At} in function of the added concentration of $Na_2S_2O_8$ and Na_2SO_4 in the aqueous solution. At low salt concentration, D_{At} is constant with a value close to 40. With the increase of the $Na_2S_2O_8$ concentration or the Na_2SO_4 one, an increase of D_{At} can be obviously observed (for $[Na_2S_2O_8]$ or $[Na_2SO_4] > 10^{-3}$ M), implying the formation of an astatine species that is partly or totally extractable in the organic phase. According to the standard redox potential reported by Champion *et al.* in acidic conditions, AtO^+ is the predominant species. These results indicate that the influence of $Na_2S_2O_8$ or Na_2SO_4 in At(III) is minor if their concentrations are maintained smaller than 10^{-3} M. In view of the applied concentrations of Na_2SO_4 and $Na_2S_2O_8$ in alkaline conditions, *i.e.* ruled by the $[Na_2S_2O_8] + [Na_2SO_4] = 10^{-3}$ M relationship, it is hypothesized that this mechanism does not influence the formation of At_{ox} (presumably $AtO(OH)_2^-$).

3.4.2 Identification of species occurring in alkaline conditions

3.4.2.1 HPIEC

A typical γ chromatogram of At_{red} is presented in Figure 3.7. One peak can be observed in

alkaline and reducing conditions, which may be indicative of the occurrence of only one species. Note that a small peak appearing in front of the central peak with a decalage of about 0.8 min is an artifact of the experimental setup (double detection, see 3.3.2).

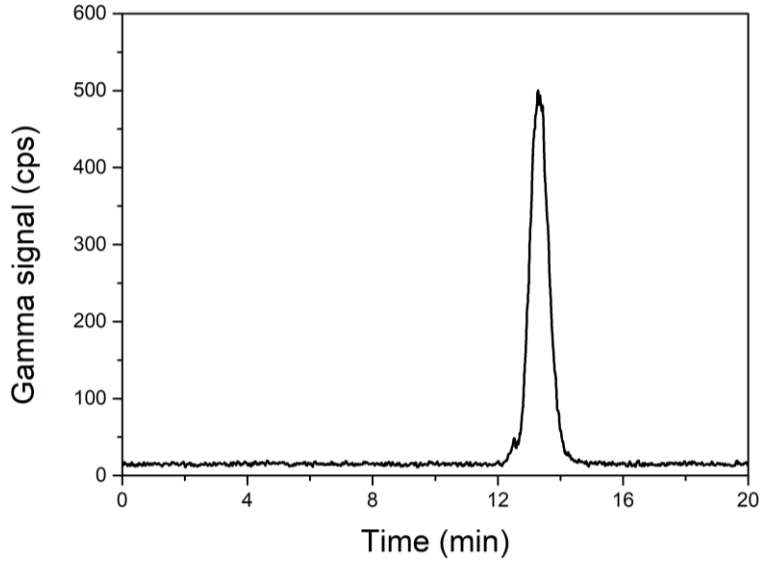

Figure 3.7 HPIEC radio-chromatogram of an At_{red} sample. Measurement of 350 µL·min^{-1} eluent containing 0.1 M NaCl/10^{-4} M M NaOH/10^{-4} M DTT on an At sample in 10^{-4} M M NaOH/10^{-4} M DTT.

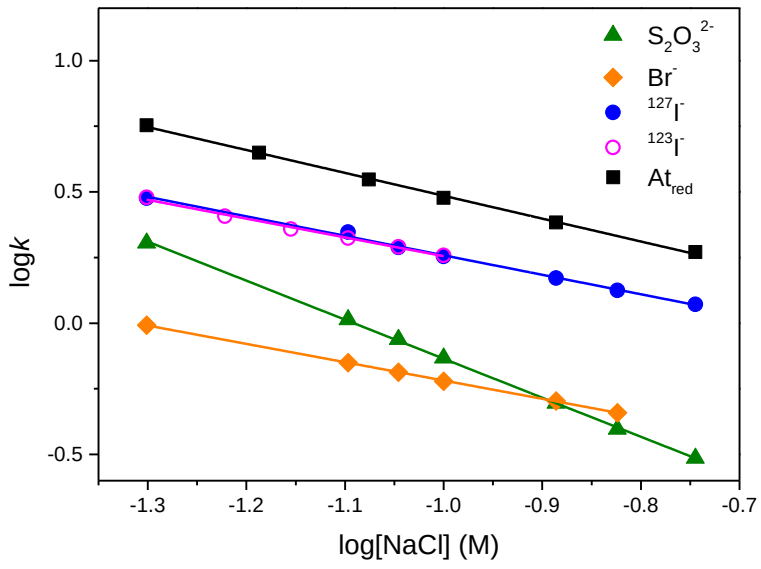

Figure 3.8 HPAEC results for At_{red} (squares), I^- (circles), and Br^- (diamond) and $S_2O_3^{2-}$ (triangles) under alkaline and reducing conditions: plot of the retention factor *k* as a function of NaCl molarity in the NaCl/10^{-4}M NaOH/10^{-4}M DTT eluent. The flow rate was fixed at 350 mL·min^{-1}.

The influence of the ionic strength (NaCl concentration) on the retention factor of Br^-, I^-, $S_2O_3^{2-}$ and At_{red} in reducing conditions is shown in Figure 3.8. The log-log representation of the retention factor as a function of the ionic strength is linear, as expected for an ionic column and ionic species.[114] The slope of astatine species is close to the ones of I^-, Br^- while is almost the half of the slope of $S_2O_3^{2-}$, as expected (the slope should match the charge value). Thus, the results leave no doubt on the charge of At_{red}: it must be –1.

The same analysis has been performed with At_{ox}. A typical γ chromatogram of At_{ox} is presented in Figure 3.9. Also, one true peak can be observed in alkaline and non-reductive conditions, which is compatible with the hypothesis of only one species.

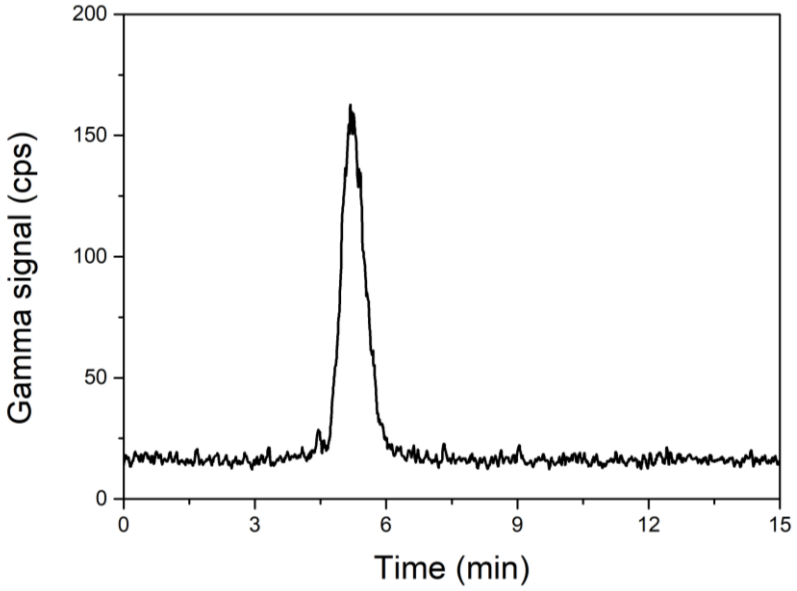

Figure 3.9 HPIEC radio-chromatogram of an At_{ox} sample. Measurement of 350 µL·min^{-1} eluent containing 0.05 M $NaClO_4$/10^{-4} M M NaOH on an At samples in 10^{-4} M NaOH.

Similarly, the influence of the ionic strength ($NaClO_4$ concentration) on the retention factor of Br^-, I^-, $S_2O_3^{2-}$ and At_{ox} is shown in Figure 3.10, showing that At_{ox} also possesses a –1 charge.

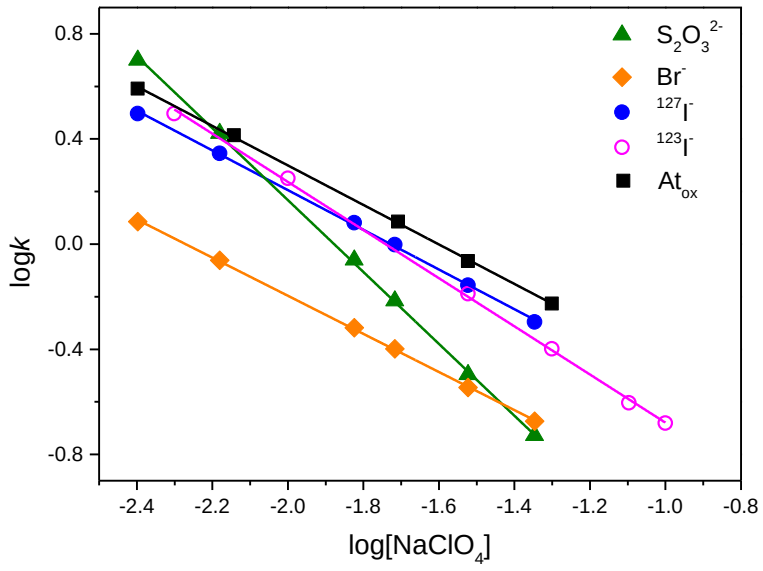

Figure 3.10 HPAEC results for At_{ox} (squares), I^- (circles), and Br^- (diamond) and $S_2O_3^{2-}$ (triangles) under alkaline and oxidizing conditions: plot of the retention factor *k* as a function of $NaClO_4$ molarity in the $NaClO_4/10^{-4}$ M NaOH eluent. The flow rate was fixed at 350 mL·min^{-1}.

At this stage, the information obtained is that (at least) one species is present in each medium, and these two species hold a –1 charge. However, their retention times cannot be directly compared since the media compositions are different (in particular Cl^- *vs.* ClO_4^-). Therefore, we cannot conclude that At_{red} and At_{ox} are different species.

In summary, from the HPIEC measurements in reducing and oxidizing conditions, the following information was obtained: (i) no sign for the occurrence of multiple species was found both in the reducing and in the oxidizing media; (ii) both At_{red} and At_{ox} hold a –1 charge.

3.4.2.2 Electromobility

As mentioned in the section 3.2, the objective of the present electromobility measurements is to compare the apparent mobility of At species with that of I^- obtained in the same conditions, while not to determine absolute mobilities of astatine species. Therefore, it is important to discuss at first the speciation of iodine in the applied conditions. From the Pourbaix diagram of iodine (Figure 3.11), I^- is the predominant

species in both the considered reducing and oxidizing conditions of electromobility measurements. Besides, the samples of NaI or KIO_3 salts diluted in 0.1 M $NaClO_4$/10^{-4} M NaOH solutions, *i.e.*, the applied oxidizing medium, are susceptible to release I^- or IO_3^- ions, respectively. To check this, HPIEC was used. Signal peak was obtained in both the cases and a clear difference in retention time was observed, indicating the stability of I^- in the applied oxidizing conditions after dissolution of NaI. As a consequence, $^{123}I^-$ is the principal species after the dilution of NaI-123 source in the electrolytes. It is possible to determine the difference of the relative mobilities of At_{ox} or At_{red} with respect to I^- to (un)validate the presence of two different species in the oxidizing and reducing conditions.

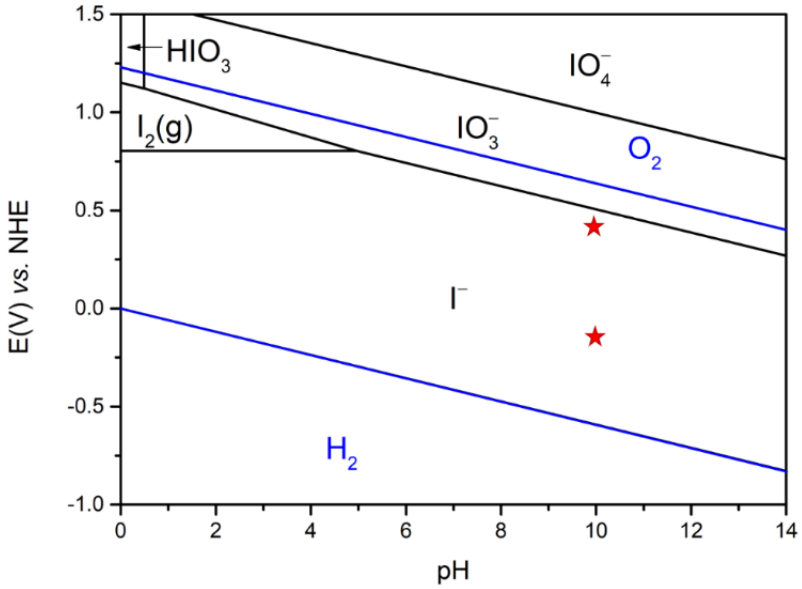

Figure 3.11 Pourbaix diagram of iodine (25°C).[121] The stars indicate the applied experimental conditions for the electromobility measurements.

Firstly, Figure 3.12 represents the peaks obtained from scans at different times for $^{123}I^-$ and ^{211}At samples in reducing or in oxidizing conditions. It shows that in both conditions, the $^{123}I^-$ and the $At_{red/ox}$ species move towards the cathode, meaning that they are negatively charged species. This characterization is coherent with the HPIEC results.

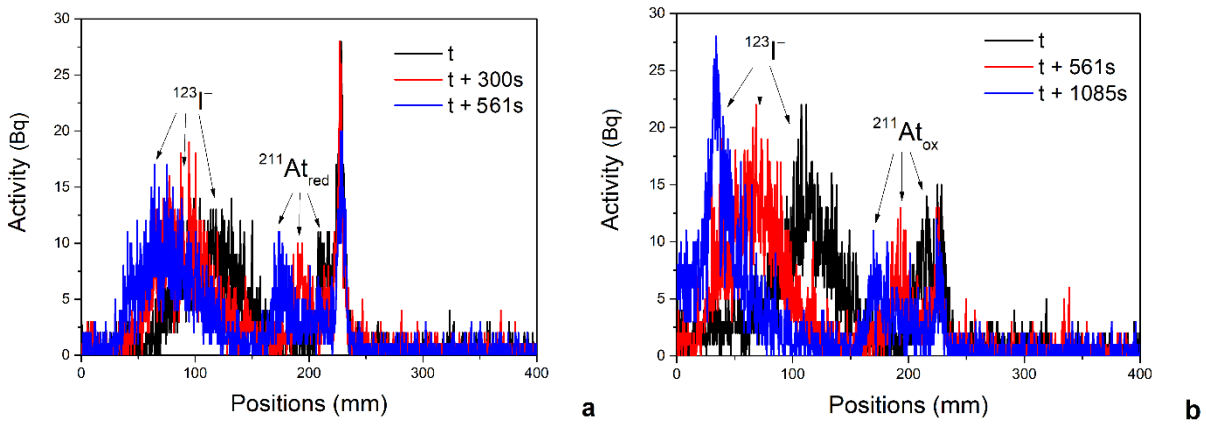

Figure 3.12 Activity of ^{123}I and ^{211}At as a function of the position along the migration tube at different times. The electrolytes and samples were prepared with (a) a 10^{-4} M NaOH/10^{-4} M DDT/0.1 M NaCl solution, (b) a 10^{-4} M NaOH/0.1 M $NaClO_4$ solution.

With the deconvolution of spectrum method presented in Chapter 2, the position of the ^{123}I and ^{211}At peaks at different times can be obtained, leading to a potential relationship between the peak position and time. Figure 3.13 displays typical results obtained in reducing conditions and in oxidizing conditions.

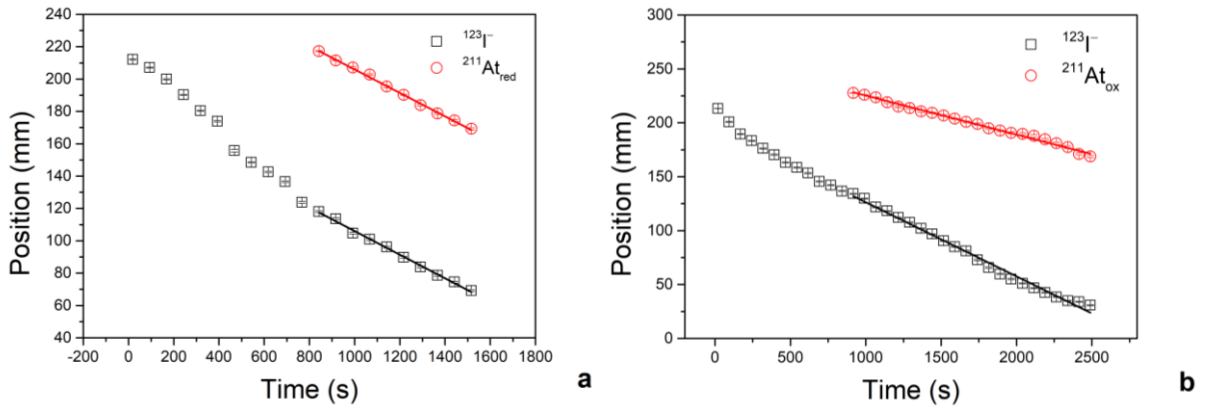

Figure 3.13 Example of data analysis: position as a function of time for ^{123}I (square) and ^{211}At (circle). The electrolytes and samples were prepared with (a) 10^{-4} M NaOH/10^{-4} M DDT/0.1 M NaCl solution, (b) 10^{-4} M NaOH/0.1 M $NaClO_4$ solution. The lines are the fitting results using Equation (2.2).

Overall, for a given peak, there is a linear relationship between the peak position and time, which suggest a constant propagation speed. However, some discontinuities may appear (see for instance Figure 3.13 a), here attributed to the use of the pump to refresh the

electrolyte around the electrodes when they were covered by bubbles.

The migration speed of I^- and the At species can be determined from the slope of the linear fitting, leading to the apparent mobility after dividing by the electric field value. Note that according to the comparison purposes, the analysis has been restricted to the time domain for which both the to be compared species are clearly distinct (*e.g.* with actual points for both species displayed in Figure 3.13). Table 3.1 shows the obtained apparent mobility of the I^- and $At_{red/ox}$ species, and then the relative mobility of $At_{red/ox}$ with respect to I^-.

From Table 3.1, it is evident that the mobility of At_{red} is very close to the mobility of I^-, with an average difference of $(0.07 \pm 0.22)\cdot10^{-4}$ $cm^2\cdot V^{-1}\cdot s^{-1}$. In a previous work, Guo et *al.* also reported that the mobility of At^- is close to that of I^- in acidic conditions (the difference being $(0.29 \pm 0.79)\cdot10^{-4}$ $cm^2\cdot V^{-1}\cdot s^{-1}$)[9], which was in accordance with a previous molecular modeling study[129]. At this stage, it is very unlikely that At_{red} would consist in two species or more since these would not be resolved with both the HPIEC and the electromobility methods (at least in the applied setups). It is also very unlikely that it would be an astatine species that is not At^- which would have both the same selectivity coefficient and the same mobility as At^-. Thus, one can reasonably conclude here that At_{red} must be At^-.

Table 3.1 Apparent mobility of At and I species in oxidizing or reducing conditions in alkaline solutions*

Sample	μ_{app} (^{211}At)	μ_{app} ($^{123}I^-$)	μ_{app} ($^{211}At - ^{123}I^-$)	Average
No.1 in reducing conditions	−7.28 ± 0.10	−7.37 ± 0.11	0.09 ± 0.15	0.07 ± 0.22
No.2 in reducing conditions	−9.34 ± 0.13	−9.39 ± 0.14	0.04 ± 0.19	
No.1 in oxidizing conditions	−4.60 ± 0.07	−8.70 ± 0.13	4.10 ± 0.14	3.32 ± 0.99
No.2 in oxidizing conditions	−9.06 ± 0.13	−11.60 ± 0.17	2.54 ± 0.21	

*All the values are in units of 10^{-4} $cm^2\cdot V^{-1}\cdot s^{-1}$

In contrast, the mobility of At_{ox} is much slower than that of I^- and the difference is significative: $(3.32 \pm 0.99)\cdot10^{-4}$ $cm^2\cdot V^{-1}\cdot s^{-1}$. As before, the fact that the astatine peaks are

not resolved by both HPLC and electromobility suggests that At_{ox} consists in one sole chemical species. Altogether, the results imply again that At_{red} and At_{ox} must be two different chemical species.

In conclusion, from the HPIEC and electromobility measurements, it is now clear that At_{red} and At_{ox} are two different species, both holding a –1 charge. Moreover, At_{red} has to be At^-, while the identification of At_{ox} remains to be performed.

3.3.3 Characterization of the At^-/At_{ox} speciation change

For characterizing the speciation change, the results of liquid/liquid competition experiments are analyzed; D_{At} is plotted as a function of measured potentials. In Figure 3.14, the case of pH = 8.4 is taken as an example.

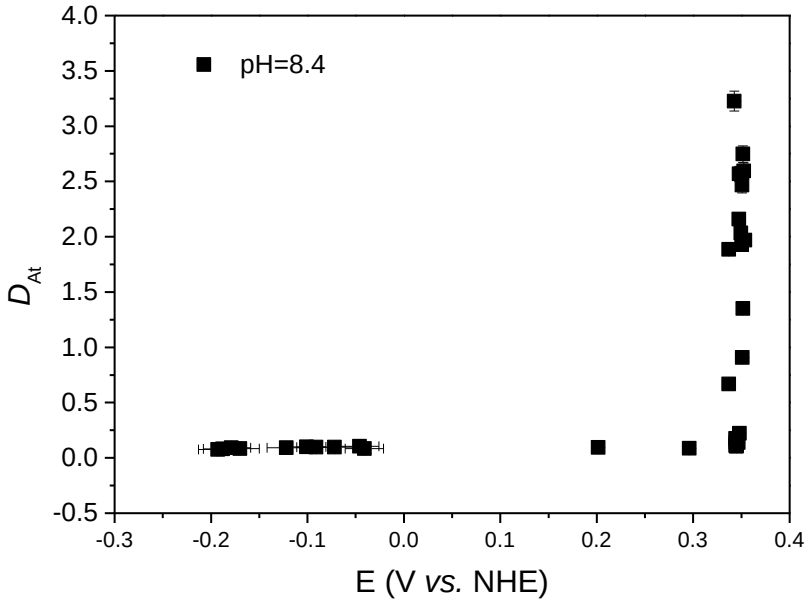

Figure 3.14 Distribution coefficient of At in biphasic aqueous/DIPE system at fixed pH (8.37) as a function of potential of the aqueous phase.

As shown in Figure 3.14, D_{At} keeps constant and close to 0 for potentials below 0.35 V before a sharp increase is observed. The change in the D_{At} values monitors a change in the astatine speciation, which is coherent with the results of HPIEC and electromobility. However, due to experimental limitations, the behavior of D_{At} beyond 0.35 V have not been

investigated.

The next step is to attempt to reproduce the D_{At} curves so as to obtain the potential of the couple At_{ox}/At^-. As shown before, At_{ox} holds a –1 charge. Supposing that At_{ox} is formed by capturing n electrons from At^-, then At_{ox} can be written as $AtO_x(OH)^-_{(n-2x)}$, and the redox process can be modeled as:

$$AtO_x(OH)^-_{(n-2x)} + ne^- + nH^+ \rightleftharpoons At^- + (n-x)H_2O \tag{3.7}$$

where n and x are both natural numbers, and $n \geq 1$ (because the speciation depends on the potential), $x \geq 0$ (obvious), and $n-2x \geq 0$ (also obvious).

The Nernst equation associated to this half reaction can be written as:

$$E = E^0 - 0.059 \times pH + \frac{0.059}{n} \lg \frac{[AtO_x(OH)^-_{(n-2x)}]}{[At^-]} \tag{3.8}$$

where E is the potential of the solution and E^0 is the standard potential of the couple.

For a fixed pH, the apparent potential is:

$$E^{0\prime} = E^0 - 0.059 \times pH \tag{3.9}$$

Therefore, the following relationship can be obtained:

$$\frac{[At^-]}{[AtO_x(OH)^-_{(n-2x)}]} = 10^{\frac{-n\times(E-E^{0\prime})}{0.059}} \tag{3.10}$$

In the other side, according to the definition, the distribution coefficient of At^-, $AtO(OH)_2^-$ and At can be defined as equation (3.11), (3.12) and (3.13), respectively, where the overlined species are related to the organic phase.

$$D_{At^-} = \frac{\overline{[At^-]}}{[At^-]} \tag{3.11}$$

$$D_{AtO_x(OH)^-_{(n-2x)}} = \frac{\overline{[AtO_x(OH)^-_{(n-2x)}]}}{[AtO_x(OH)^-_{(n-2x)}]} \tag{3.12}$$

$$D_{At} = \frac{\overline{[At^-]} + \overline{[AtO_x(OH)^-_{(n-2x)}]}}{[At^-] + [AtO_x(OH)^-_{(n-2x)}]} \quad (3.13)$$

Combining equation (3.10)–(3.13), the following expression of D_{At} can be obtained:

$$D_{At} = \frac{D_{AtO_x(OH)^-_{(n-2x)}} + D_{At^-} \times 10^{\frac{-n\times(E-E^{0\prime})}{0.059}}}{1 + 10^{\frac{-n\times(E-E^{0\prime})}{0.059}}} \quad (3.14)$$

In reducing conditions, D_{At} is ruled by the distribution of At^-. The experimental results indicate a distribution coefficient close to 0. It is therefore reasonable to suppose that $D_{At^-} = 0$ and the equation (3.14) can be re-written as:

$$D_{At} = \frac{D_{AtO_x(OH)^-_{(n-2x)}}}{1 + 10^{\frac{-n\times\left(E-E^{0\prime}\right)}{0.059}}} \quad (3.15)$$

As for $AtO_x(OH)^-_{(n-2x)}$ species, considering that D_{At} keeps increase in oxidizing conditions within the investigated potential range, $D_{AtO_x(OH)^-_{(n-2x)}}$ cannot be simply deduced like D_{At^-}. The only information is that $AtO_x(OH)^-_{(n-2x)}$ should be larger than D_{At} in any conditions. From all the experimental results (Figure 3.14 and Figure 3.16), the maximum value of D_{At} is 15 (in the case of pH = 9.2), implying that $D_{AtO_x(OH)^-_{(n-2x)}}$ should be larger than 15. In this work, the equation (3.15) is used to simulate the experimental curves, together with supposing $D_{AtO_x(OH)^-_{(n-2x)}} = 15$. Note that $D_{AtO_x(OH)^-_{(n-2x)}}$ can be larger than 15 in the reality; therefore, this model may underestimate the apparent potential.

Figure 3.15 displays the example of pH = 8.4 to illustrate the simulation results. Firstly, the value of n was imposed because it should be a neutral number. $E^{0\prime}$ and D_{At^-} were manually adjusted in order to reproduce the experimental curves. From Figure 3.15, it can be observed that with n = 1 or n = 2, the sharp increase of D_{At} in function of E cannot be well simulated. While for n ≥ 3, the simulated curves become very close to each other, and are sufficient to explain the experimental points; moreover, the obtained $E^{0\prime}$ remains very similar no matter which n value (for n ≥ 3) is imposed. At least, a good potential value is

indeed obtained.

If n = 3, the OS of At in At_{ox} is +2. Thus, the possible species are $At(OH)_3^-$ and $AtO(OH)^-$ (recall, At_{ox} has a −1 charge). These are actually hydrolyzed species of At^{2+} and AtO, respectively. Since the +2 OS has never been identified in the literature, it is quite unlikely that n = 3; thus the $At(OH)_3^-$ and $AtO(OH)^-$ identities can be discarded. With n = 4, the OS of At is +3. Three species are then possible: $At(OH)_4^-$, AtO_2^- and $AtO(OH)_2^-$. $At(OH)_4^-$ is a hydrolyzed species of At^{3+}. This is incompatible with the literature: the basic At(III) form has been identified to be AtO^+.[10] Therefore, this possibility is excluded. As for AtO_2^-, according to the quantum mechanical calculations, the occurrence of this species is quite unlikely for pH < 11[12], as in this work. The possibility of this species is thus eliminated. Finally, only $AtO(OH)_2^-$ remains as the most probable for At_{ox}, because it has already been identified in alkaline conditions and it processes the lowest stable OS for n ≥ 3.

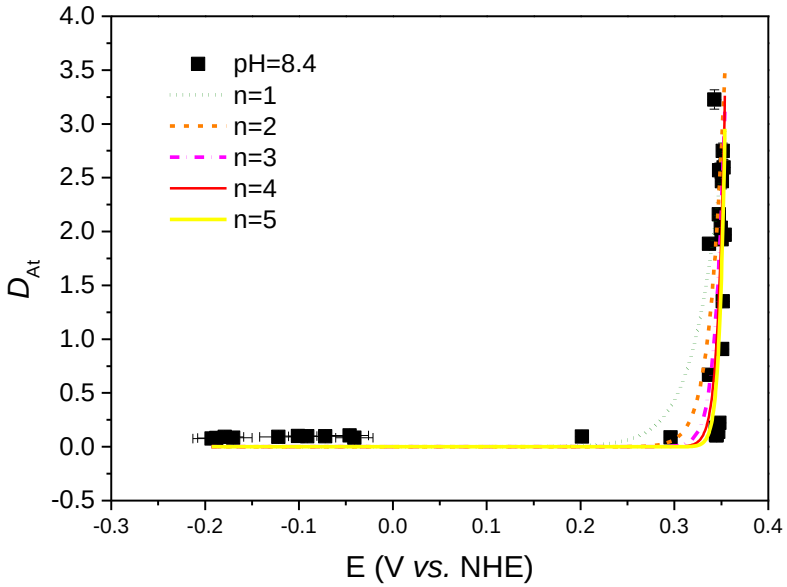

Figure 3.15 Distribution coefficient of At in the biphasic aqueous/DIPE system at fixed pH (8.37) as a function of potential of the aqueous phase. Lines correspond to the fitting with the model considering the formation of $AtO_x(OH)^-_{(n-2x)}$ by capture of n electrons from At^-.

With n = 4, all experimental results were fitted by equation (3.15) and supposing $D_{AtO_x(OH)^-_{(n-2x)}} = 15$, as shown in Figure 3.15 and Figure 3.16. The modelling fairly

reproduces the experimental data, and gives the apparent potentials listed in Table 3.2.

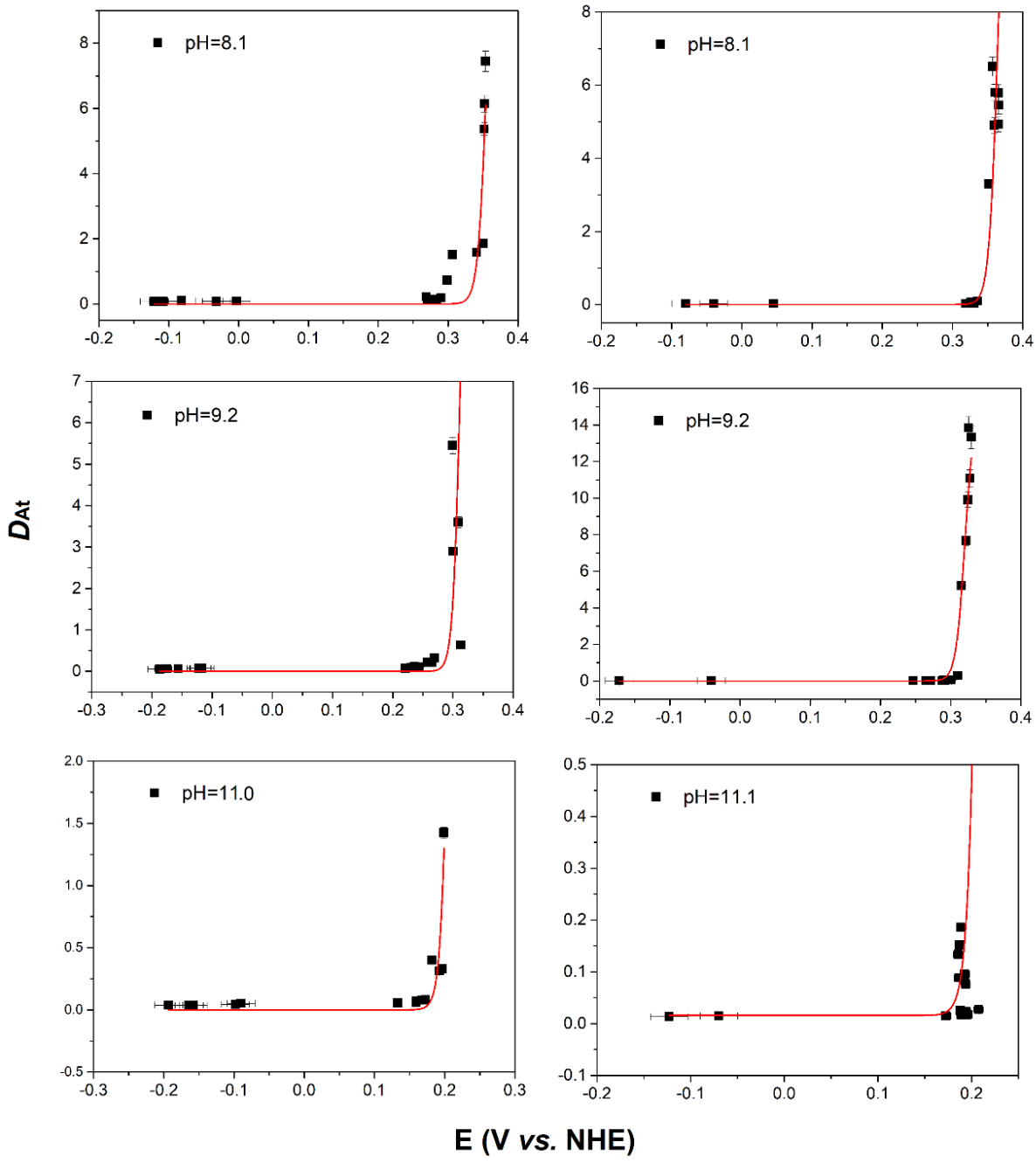

Figure 3.16 Distribution coefficient of At in the biphasic aqueous/DIPE systems at fixed pH as a function of potential of the aqueous phase. Lines correspond to the fitting with the model considering the formation of $AtO(OH)_2^-$ rom At^- by exchange of 4 electrons.

The standard potential could be deduced from each experiment by using equation (3.9). Finally, an average of E^0 = 0.86 ± 0.03 V *vs.* NHE can be obtained. The uncertainties

correspond to two standard deviations.

Table 3.2 Redox potential related to the speciation change between At^- and $AtO(OH)_2^-$ in different pH

pH	$E^{0'}$ (V *vs.* NHE)	E^0 (V *vs.* NHE)
8.1 ± 0.1	0.356	0.834
8.1 ± 0.1	0.365	0.843
8.4 ± 0.1	0.362	0.856
9.2 ± 0.1	0.313	0.853
9.2 ± 0.1	0.32	0.865
11.0 ± 0.2	0.214	0.862
11.1 ± 0.2	0.22	0.872

With the obtained standard potential value, it is found that one of the characterization of At species is improper: the applied conditions of HPAEC for At_{ox} (pH = 10 ± 0.2, E = 0.19 ± 0.02 V *vs.* NHE) species are actually not the predominant area for $AtO(OH)_2^-$ ($E^{0'}$ at pH = 10 corresponds to 0.27 V *vs.* NHE), but belong to that of At^-. Therefore, we cannot use the results of HPAEC to conclude that At_{ox} holds –1 charge. However, the characterization of –1 charge can be drawn when we plot the apparent potential as a function of the applied pH conditions, as shown in Figure 3.17. In fact, these points belong to the boundary of At^-/$AtO(OH)_2^-$ in the Pourbaix diagram of At. The linear fitting of these points gives a slope of –0.051. The slope is close to –0.059 which assuming that the half equation involves an exchange of the same number of proton and electron (*i.e.*, At_{ox} holds –1 charge).

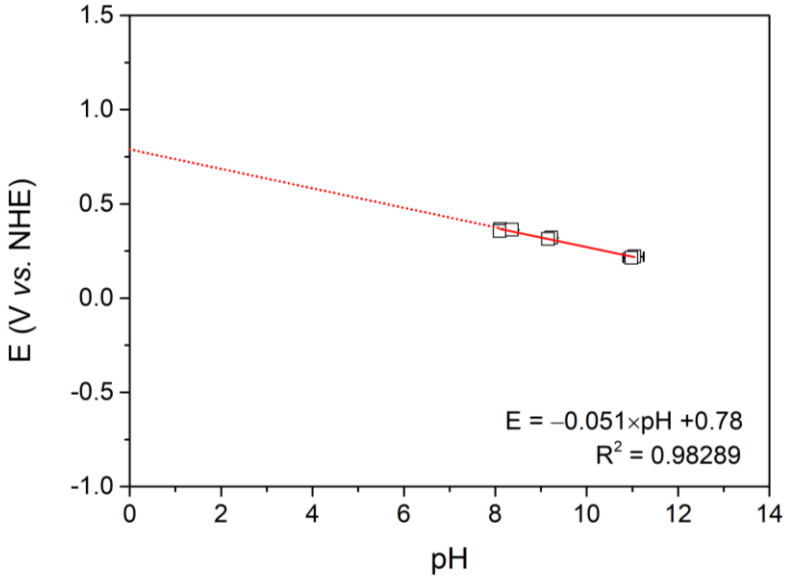

Figure 3.17 Relationship between apparent potential and pH for the reaction between At^- and $AtO(OH)_2^-$. The solid line corresponds to linear fitting.

Considering all the experimental outcomes, the following process has been justified, with a standard potential of 0.86 ± 0.03 V *vs.* NHE.

$$AtO(OH)_2^- + 4e^- + 4H^+ \rightleftharpoons At^- + 3H_2O \qquad (3.16)$$

Coming back to the hypothesis of $D_{AtO_x(OH)^-_{(n-2x)}} = 15$, it is also of interest to investigate the response of $E^{0'}$ value to a larger $D_{AtO_x(OH)^-_{(n-2x)}}$ value. A value of 60 was tested, which corresponds to the $D_{At(III)\ in\ pH\ =\ 1}$ in DIPE reported by Champion *et al.*[15] The results indicate also the necessary of n ≥ 3. Moreover, a difference of $E^{0'}$ less than 0.015 V is obtained for the imposed $D_{AtO_x(OH)^-_{(n-2x)}}$ value between 15 and 60. Consequently, the conclusions above are maintained for a large scale of the $D_{AtO_x(OH)^-_{(n-2x)}}$ value.

3.4.3 Pourbaix diagram of astatine

Qualitatively, the direct speciation change between At^- and $AtO(OH)_2^-$ was evidence, and there is no sign of the existence of other species between them from our investigations.

This indirectly confirms the nature of the species previously identified in the literature (At^-, At^+, AtO^+, $AtO(OH)$ and $AtO(OH)_2^-$). The objective of this part is to confront the quantitative parameters obtained in this work with those previously available in the literature, in order to construct a compatible Pourbaix diagram of astatine.

As a reminder, the standard potential of the $AtO(OH)_2^-/At^-$ redox couple ($E^0_{AtO(OH)_2^-/At^-}$) can be calculated from previously published data ($E^0_{At^+/At^-}$, $E^0_{AtO^+/At^+}$, $\log K_{AtO^+,hyd,1}$ and $\log K_{AtO^+,hyd,2}$) according to the following relation:

$$E^0_{AtO(OH)_2^-/At^-} = \frac{1}{2}\left(E^0_{At^+/At^-} + E^0_{AtO^+/At^+}\right) - \frac{0.059}{4}\left(\log K_{AtO^+,hyd,1} + \log K_{AtO^+,hyd,2}\right) \quad (3.17)$$

Firstly, by applying the values of $E^0_{At^+/At^-} = 0.36$ V, $E^0_{AtO^+/At^+} = 0.74$ V, $\log K_{AtO^+,hyd,1} = -1.9$ and $\log K_{AtO^+,hyd,2} = -6.9$ reported by Champion *et al.*[10–12], $E^0_{AtO(OH)_2^-/At^-}$ should be 0.68 ± 0.03 V *vs.* NHE, which is much smaller than the experimental value obtained in this work. Therefore, at least one of the five parameters above need to be revised.

Since $E^0_{AtO(OH)_2^-/At^-}$ is more sensible to both $E^0_{At^+/At^-}$ and $E^0_{AtO^+/At^+}$, and since other values exist in the literature, it is of interest to establish a diagram incorporating all reasonable experimental values, in order to have a better evaluation of the reliability of the value of each parameter. Values of redox potentials reported in the literature are given in Table 1.5. In particular, Appelman[69] proposed a potential of 0.30 V at pH 1 and Cavallero *et al.*[78] proposed 0.32 ± 0.02 V for the equilibrium between At^- and "At^0", *i.e.* At^+ according to the more recent literature[10,71,89,130]. Putting together these data and the value proposed by Champion *et al.* (0.36 ± 0.01 V), the standard potential for the redox reaction At^+/At^- should be between 0.30 and 0.37 V. In conclusion, these values are entirely consistent with each other.

Concerning the equilibrium AtO^+/At^+, the experimental values, on the other hand, are highly variable. Appelman[69] proposed 1.0 V at pH = 1 and Cavallero *et al.*[78] proposed 0.80 ± 0.05 V for the equilibrium At^+/"At^{3+}"[71,130] (*i.e.* AtO^+ because of its pH–dependent formation from At^+[10]). Combing the data reported by Champion *et al.* (0.74 ± 0.01 V), the

potential for the redox reaction AtO^+/At^+ should be in the range from 0.73 V to 1.0 V.

On the basis of these data, the At^+/AtO^+ potential value was estimated indirectly by reconstructing the diagram by considering our experimental data correct. In this approach, we fix $E^0_{At^+/At^-} = 0.37$ V[10], $E^0_{AtO(OH)_2^-/At^-} = 0.86$ V (this work), $\log K_{AtO^+,hyd,1} = -1.9$[11] and $\log K_{AtO^+,hyd,2} = -6.9$[12]. Finally, Pourbaix diagram of astatine can be constructed as the following, together with the experimental results.

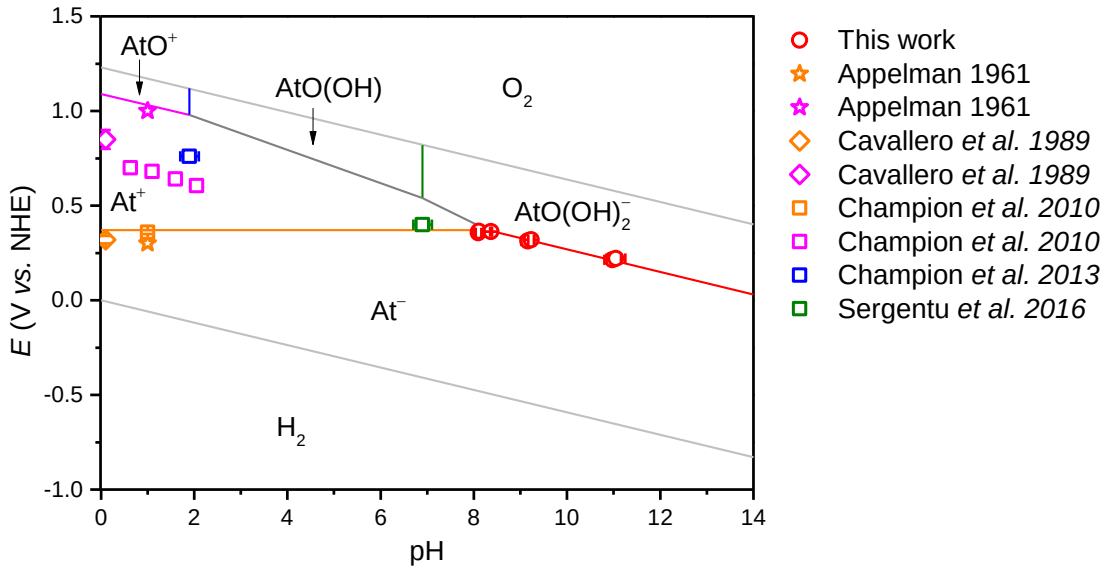

Figure 3.18 Pourbaix diagram of astatine (25°C) constructed by considering $E^0_{At^+/At^-} = 0.37$ V, $E^0_{AtO(OH)_2^-/At^-} = 0.86$ V, $\log K_{AtO^+,hyd,1} = -1.9$ and $\log K_{AtO^+,hyd,2} = -6.9$. The points in the diagram are experimental results in the literature and in this work. The color of symbols is in agreement with the considered boundary.

From this figure, we can observe that the newly established Pourbaix diagram can well incorporate the experimental points for the boundaries At^+/At^- and $AtO(OH)_2^-/At^-$. Interestingly, the experimental point initially from the study of boundary $AtO(OH)/AtO(OH)_2^-$ seems to belong to the boundary At^+/At^- according to this diagram. In fact, we are in a complex region with the possibility of finding, in non-negligible quantities, several species whose concentrations are strongly dependent on sensitivity

around the redox potential and pH. The construction gives a theoretical $E^0_{AtO^+/At^+}$ value being 1.09 V, which lies close to the results reported by Appelman[69], while above that proposed by Champion *et al.*[10] and Cavallero *et al.*[78] The discrepancy of $E^0_{AtO^+/At^+}$ value in the literature can be explained by several aspects. Firstly, in the work of Appelman,[69,70] it is observed that the photochemical reactions of astatine appear quite remarkable when the iron and vanadium redox couples are applied, because they involve a gross shift of a chemical equilibrium under the influence of light. However, this phenomenon was not considered in the work of Champion *et al.*,[10] which may lead to an underestimation of the redox potential for the AtO^+/At^+. Secondly, the samples of related experiments contain several anionic species (such as SCN^-[10]), they can interact with AtO^+ or At^+ species[13] and may lead to a modification of the apparent potential of the samples. This aspect was not taken into account the author when they analyzed the experimental outcome. Thirdly, the quality of astatine sources may play an important role. For instance, a change in recovery method and the solvent to initially recover astatine may lead to a different speciation due to differences in the radiolysis conditions. Finally, it may relate to the experimental and statistic uncertainties.

In summary, the standard potential $E^0_{AtO(OH)_2^-/At^-} = 0.86$ V obtained in this work appears compatible with most experimental data in the literature related to the Pourbaix diagram of astatine. The remaining questionable parameter is $E^0_{AtO^+/At^+}$, which may need further exploration, in particular the photochemical reactions when considering the redox reaction between AtO^+ and At^+. In the meanwhile, the quantum mechanical calculations may be a complementary approach to evaluate this parameter.

3.5 Conclusion

In the present work, the astatine species in alkaline conditions have been characterized by HPIEC and electromobility. It was found that the species in alkaline and reducing

conditions carried a –1 charge and that its mobility was close to the I^- one, indicating that this species was At^- (in accordance with the literature). The species in alkaline and non-reductive conditions also holds a –1 charge while its mobility is much smaller than that of I^-. Therefore, two different species exist, and the change in speciation is associated to a redox process. Such conclusion was also obtained from the analysis of HPIEC experimental data. The liquid/liquid competition experiments have confirmed the change of astatine speciation and the results allowed to identify the stoichiometry of At_{ox}, as well as the apparent potential of the redox equilibrium at different pH values. Finally, the species in alkaline and oxidizing conditions have been identified to be $AtO(OH)_2^-$, leading to the following redox equation:

$$AtO(OH)_2^- + 4e^- + 4H^+ \rightleftharpoons At^- + 3H_2O \qquad E^0_{AtO(OH)_2^-/At^-} = 0.86 \pm 0.03\ V\ vs.\ NHE \quad (3.18)$$

This work represents an add-on to the previous ones by (i) validating the idea of a direct speciation change between At^- and $AtO(OH)_2^-$, *i.e.* discarding the possibility for another main astatine species in alkaline medium with pH < 11, (ii) allowing to close the loop between At^- and $AtO(OH)_2^-$ (the previous works were based on successive changes starting from the standard At^- species) and (iii) providing an experimental value for the $AtO(OH)_2^-/At^-$ standard potential. Overall, it is a validation of the previous Pourbaix diagram of astatine for pH < 11.[12] From an analytical perspectives, it shows that only a combination of techniques can lead to firm conclusions, and it is a nice showcase for the electromobility technique: despite its complex implementation, it can indeed discriminate actual astatine species.

Chapter 4. Advances on the At-mediated halogen bonds: Completeness of the AtI basicity scale

The At-mediated halogen bonds – a kind of non-covalent interaction between astatine species and Lewis bases – have recently been experimentally evidenced for the first time, though only a limited number of cases have been investigated.[16] It is of fundamental interest to extend the investigations and to summarize the behaviors of At towards organic compounds. These aspects are tackled in the present chapter. Some of the results have already been published;[131] however, in order to give a more pedagogic description, it is presented here in a slightly different way.

4.1 Introduction

Halogen bonding (XB) is a type of noncovalent interaction between an electrophilic region (called σ-hole) located in the covalently-bonded halogen atom X of a Lewis acid R-X and a Lewis base B. For the formation of a XB, the σ-hole is essential. Therefore, the role of RX and B in a XB is defined regarding to the σ-hole, *i.e.*, RX is called the donor of a XB and B is called the acceptor. A typical feature of these interactions, denoted R–X···B, is the almost perfect linearity between the atom of the R group that is bound to X and B (Figure 4.1).[105]

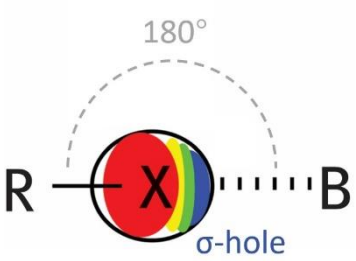

Figure 4.1 Schematic representation of an R–X···B halogen bond.[106]

XBs have been recognized as reliable and valuable non-covalent interactions, being impactful in various fields such as organocatalysis, drug design in biochemistry and

medicinal chemistry, crystal engineering and production of liquid crystal.[107–109,132,133] For chemists, it is of fundamental interest to summarize the quantitative behavior of XBs and to explore their strength range. However, because both R-X and B contribute to the XB's strength, it is impossible to represent a full scale in 2D. In this case, the diiodine basicity scale pK_{BI2} has been proposed. It considers the thermodynamic tendency of a substance to act as a XB acceptor of I_2 in terms of measured equilibrium constants. This scale is supposed to be quite general for dihalogen and interhalogen donors.[110,134]

Astatine is the heaviest natural-occurring halogen element. It was predicted to be the strongest XB donor atom[111,112,135] without experimental support. Recently, Guo *et al.*,[16] combining the liquid/liquid competition experiments and the quantum mechanical approach, have evidenced the first halogen bonds involving At as the interactions between astatine monoiodide (AtI) and nine Lewis bases. The comparison between the measured equilibrium constants (log K_{BAtI}) and the available pK_{BI2} values for the same Lewis bases, disclosed a quasi-proportional relationship: log $K_{BAtI} \approx 1.56(22) \times$ pK_{BI2}. Hence, AtI appears as a stronger XB donor than I_2, even though only a limited set of Lewis bases had been investigated. It is of prime importance to enlarge the investigation and to summarize the behavior of At towards organic compounds. One may thus expect to build a new scale, specific to astatine species, in the pK_{BI2} fashion. Here, the objective is to complete and finalize the work on At-mediated XBs. By adding more variety in terms of XB acceptors and looking for the strongest XB involving At, the present work is devoted to construct a basicity scale on a broader range, and to improve the characterization of interactions between astatine and different chemical functional groups.

As already mentioned, it is challenging to study the chemistry of astatine given its rarity. Experimental investigations are usually conducted at ultra-trace quantities, typically below 10^{-10} M, making the conventional spectroscopic tools inapplicable.[5] Most information was obtained by indirect methods and, notably, the reactivity of At-compounds has been successfully evaluated by studying the distribution of ^{211}At

radionuclide in biphasic systems formed of two immiscible solutions.[10,12,14,16]

The XB donors and acceptors in this work should be carefully selected to ensure the feasibility of the measurement. For the referential XB donor, AtI was selected because it is a typical XB donor and it is one of the "well-known" species of At,[14,76,97] following the previous experimental investigations on At-mediated XBs. Actually, among the other possibilities of dihalogen compounds with At, the At_2 and AtF species are still hypothetical, while the AtBr and AtCl display narrow predominance domains in aqueous solution and do not demonstrate miscibility for organic solvents.[13,14] Consequently, it remains to be shown if it is actually possible to consistently measure XB strengths with these two latter species. Regarding the choice of the Lewis bases, there are also many limitations because the ligands must be stable enough in the acidic and oxidizing conditions which allow the appearance of the AtI species.[10] Accordingly, nitrogen Lewis bases, such as amines, pyridines, anilines, guanidines or imines, should be avoided due to the protonation of the acceptor site under the applied conditions. Moreover, considering that AtI is distributed between aqueous and organic phases, the Lewis base is ideally only soluble in the organic phase. By increasing the Lewis base concentration, it is expected to promote the interaction between AtI and the Lewis base in the organic phase. This is translated by an increase in the value of distribution coefficient of At, which can be further used to determine the complexation constant by modelling the data. Regarding these constraints and guided by the pK_{BI2} scale, nine additional Lewis bases were selected. Their molecular structures are shown in Figure 4.2. These ligands involve more chemical functional groups of S, O and for the first time, the Se element. They should process different halogen bond acceptor abilities according to their pK_{BI2} value.

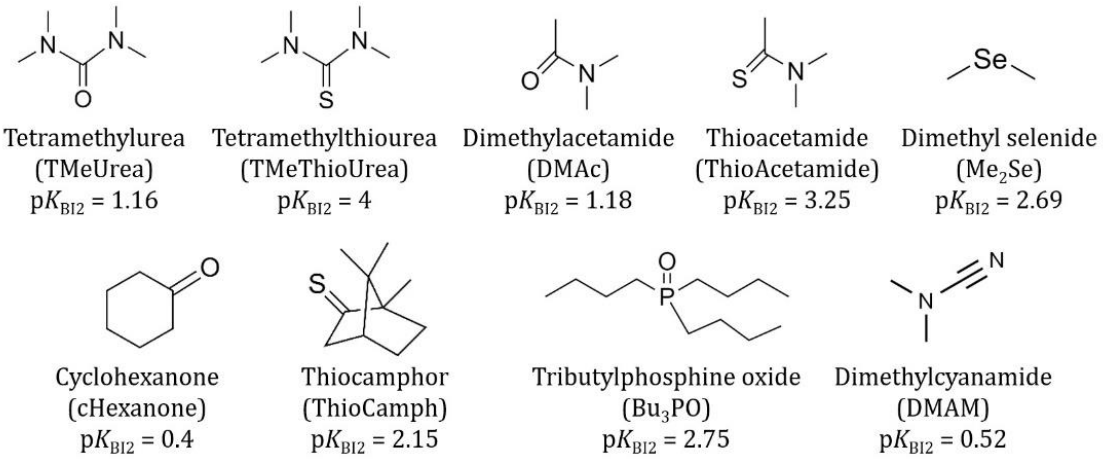

Figure 4.2 Molecular structure of selected Lewis bases. The name given is the parentheses is the abbreviation used in this chapter.

4.2 Experimental details

4.2.1 Liquid/liquid competition experiments

In this work, the liquid/liquid competition method has been applied to evidence the interactions between AtI and Lewis bases. The ^{211}At source was recovered in aqueous medium after back-extractions in 1.5 mL of 0.1 M NaOH solutions, At^+ was then obtained in 0.1 M $HClO_4$ solution (pH = 1.0 ± 0.1, E = 0.55 ± 0.05 V *vs.* NHE), in accordance with the established Pourbaix diagram of astatine from the data notably reported by Champion *et al.*[10–12], as shown in Chapter 1 (Figure 1.10).

Two liquid phases were prepared separately as the following. The aqueous phase was prepared with 0.1 M $HClO_4$ solution as a non-complexing medium. The I^- solution was obtained by adding NaI salt in the $HClO_4$ solution. Finally, the At^+ stock solution was introduced into the I^- one so that the AtI and AtI_2^- species were formed (Figure 4.3).[14]

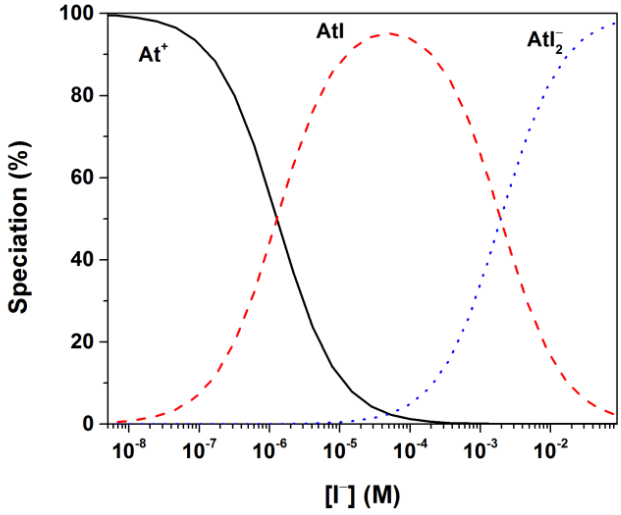

Figure 4.3 Speciation diagram of astatine in 0.1 M $HClO_4$ aqueous solution as a function of the I^- concentration, based on published equilibrium constants for the formation of AtI and AtI_2^- species.[14,16]

Note that the I^- solution should be prepared freshly in order to prevent as much as possible the oxidation of I^-. The organic phase is cyclohexane (cHex) or heptane (Hept), because they are immiscible with water and they were used to establish the pK_{BI2} scale. The solvent was pre-equilibrated with 0.1 M $HClO_4$, and then the Lewis bases were dissolved in the solvent. After preparation, 2 mL of the organic phase and 4 mL of the aqueous phase were put together in a Pyrex tube (with radioactivity about 1000 Bq) and were shaken for two hours to reach the reaction equilibrium. The two phases were then separated and 1 mL of aliquot of each phase was taken to measure their radioactivity by a liquid scintillation counter.

For each Lewis base (except Bu_3PO), two sets of experiments were performed, with NaI concentration being 0.01 and 0.1 M. For each set of experiments, only the initial ligand concentration in the organic phase was varied (from 10^{-7} to 0.1 M). The applied conditions for the Bu_3PO Lewis base were slightly different: (i) the aqueous solution was composed of 0.05 M $HClO_4$; (ii) five sets of experiments were performed, with NaI concentration being 0.01, 0.05, 0.07, 0.1 and 0.2 M. All the experiments above were repeated (at least)

twice with different astatine sources.

4.2.2 TOC meter measurements

Though the selected Lewis bases were directly dissolved in the organic phase for the competition experiments, they may actually distribute among the two phases. Their distribution coefficients (D_1), defined as the ratio of the ligand concentration in the organic phase to that in the aqueous phase, were measured by a total organic carbon (TOC) meter. First, liquid/liquid competition experiments were performed in the same conditions as described above, but without the presence of astatine. The total organic carbon concentration in the aqueous phase can be measured, thus the concentration of ligand can be deduced. Given the selected volume ratio for the two phases, D_1 at equilibrium can be eventually obtained by:

$$D_1 = \frac{1 - 2k}{k} \tag{4.1}$$

with k being the fitted slope for the detected ligand concentration in the aqueous phase as a function of the initial ligand concentration added in the organic phase.

4.3 Results

The astatine distribution coefficient (D_{At}), calculated as the ratio of the volumetric radioactivity in the organic phase to that in the aqueous one, is plotted as a function of the initial concentration of Lewis base present in the organic phase. Analytical expressions for D_{At}, based on the hypothesized key chemical equilibria in the biphasic system, were derived to fit the experimental curves. All the sets of experiments have repeatable results with different At sources, except the case of ThioCamph with the presence of 0.01 M NaI in the aqueous phase, for some unclarified reasons. Since unrepeatable behaviors of D_{At} cannot lead to a reliable analysis, the case of 0.01 M NaI for ThioCamph will not be considered hereafter. According to the different types of curves/interactions between AtI and Lewis bases, the analysis of results is divided into the following three parts.

4.3.1 Conditions for evidencing complexation and formation constants

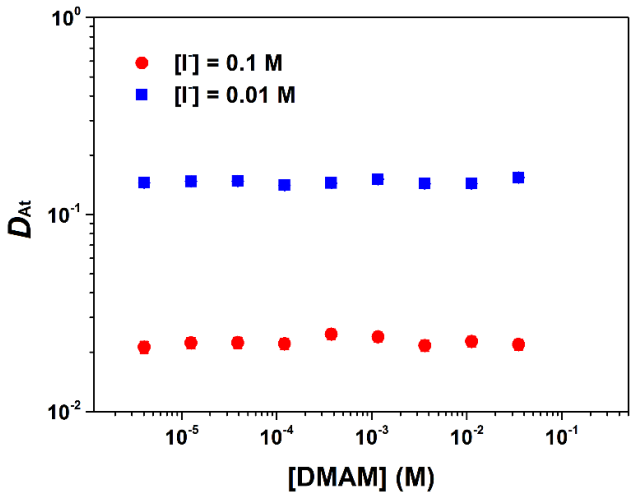

Figure 4.4 Distribution coefficient of At in biphasic aqueous/cHex system in the presence of DMAM.

The case of DMAM is quite particular. As shown in Figure 4.4, within the studied ligand concentration range, D_{At} keeps unchanged. Moreover, according to the results of TOC measurements, DMAM was found to be totally back-extracted in the aqueous solution in the studied biphasic system, *i.e.*, no ligand initially lies in the organic phase. Consequently, this ligand does not trigger any driving force to further promote astatine in the organic phase, resulting in unchanged *D* values independent of the ligand concentration. In this case, it is impossible to conclude anything on the nature and strength of the interaction between AtI and DMAM in any of the two phases.

However, this case is interesting to highlight the two main conditions for being able to evidence interactions between AtI and a given Lewis base:

(i) the D_{At} value must somehow change with the ligand concentration to evidence and characterize (at least) one interaction.

(ii) the Lewis base must be (at least partially) soluble in the organic phase to make the competition of astatine species between two phases possible (AtI being initially mostly in

the aqueous phase, transferring all the astatine to the aqueous phase by an interaction that is at play only in this phase may not lead to sufficiently accurate constants).

4.3.2 Formation of one to one complex (BAtI)

For all Lewis bases except DMAM, a distribution coefficient of the ligand in the applied biphasic system can be deduced from the TOC measurements. The values are summarized in Table 4.1. This means that the ligand remains partially in the organic phases no matter what (it is always in excess compared to AtI), which makes possible a D_{At} raise, *i.e.* an increase of the astatine concentration in the organic phase, concomitant with a change in the astatine speciation in this phase. The next step is to establish appropriate models to reproduce the experimental D_{At} values, in order to deduce the unknown thermodynamic constants. Here, the case of TMeUrea is used to illustrate the procedure to find the best fitting model (the simplest consistent one that fully explains the data). As shown in Figure 4.5, D_{At} is practically constant at low ligand concentrations, then D increases for [TMeUrea] > 10^{-2} M, which has to be elucidated.

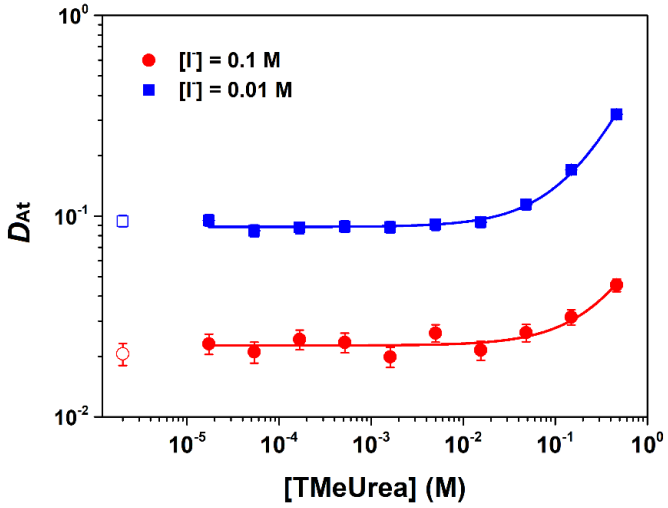

Figure 4.5 Distribution coefficient of At in biphasic aqueous/Hept system in the presence of TMeUrea. The hollow symbols indicate data without ligand (initial distribution). The solid lines correspond to the fitting with the Model 1 that considering the formation of the 1:1 complex between AtI and ligand in

the organic phase.

In the biphasic system, AtI_2^- is the initial predominant astatine species in the aqueous phase.[14] Its formation from AtI is ruled by equilibrium (4.2), with a previously determined equilibrium constant K ($10^{2.7\pm0.3}$ at zero ionic strength).[14] Note that in the analysis, since the ionic strength is non-zero in the aqueous phase, this constant is corrected ("deextrapolated") by the actual ionic strength of the sample using Davis equation.[118] Different from AtI_2^-, AtI can be partially extracted by the organic solvent.[14] The partitions of TMeUrea and AtI in the two phases are taken into account *via* equilibria (4.3) and (4.4), where overlined species relate to the organic phase. D_1 has been determined from TOC measurements in the absence of astatine, while D_2 is a parameter adjusted during the fitting process. In the organic phase, the formation of the expected 1:1 complex is considered *via* reaction (4.5).

$$\mathrm{AtI} + \mathrm{I}^- \overset{K}{\rightleftharpoons} \mathrm{AtI}_2^- \tag{4.2}$$

$$\mathrm{B} \overset{D_1}{\rightleftharpoons} \overline{\mathrm{B}} \tag{4.3}$$

$$\mathrm{AtI} \overset{D_2}{\rightleftharpoons} \overline{\mathrm{AtI}} \tag{4.4}$$

$$\overline{\mathrm{AtI}} + \overline{\mathrm{B}} \overset{K_{\mathrm{BAtI}}}{\rightleftharpoons} \overline{\mathrm{BAtI}} \tag{4.5}$$

Based on the equilibria described above, an analytical expression of D_{At} can be formulated as a function of the previously defined thermodynamic constants and, of course, of the experimental conditions. This model is denoted Model 1.

$$D_{\mathrm{At}} = \frac{D_2 + K_{\mathrm{BAtI}} \times D_2 \times [\bar{B}] \times D_1/(D_1 + 2)}{1 + K \times [I^-]} \qquad \text{Model 1}$$

The experimental data were then fitted by Model 1 with D_2 and K_{BAtI} as adjustable parameters, in a way that is similar to the previous study.[16] This model is found to satisfactorily reproduced the results of TMeUrea (solid line in Figure 4.5). Finally, the equilibrium constant K_{BAtI} and the associated uncertainties can be obtained. In the same way, Model 1 was successfully used to explain the experimental results of cHexanone and

ThioCamph (Figure 4.6).

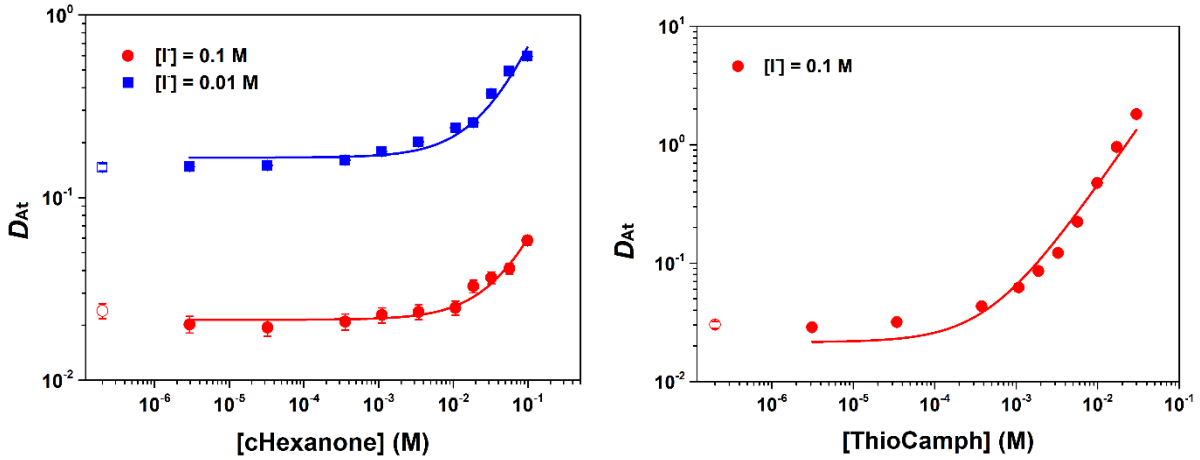

Figure 4.6 Distribution coefficient of At in biphasic aqueous/cHex system in the presence of cHexanone, and in biphasic aqueous/Hept system in the presence of ThioCamph. The hollow symbols indicate data without ligand (initial distribution). The solid lines correspond to the fitting with the model 1 that considering the formation of the 1:1 complex between AtI and ligand in the organic phase.

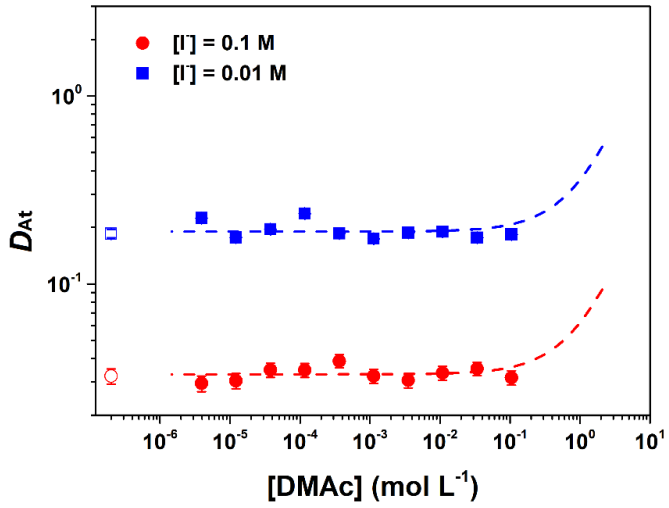

Figure 4.7 Distribution coefficient of At in biphasic aqueous/cHex system in the presence of DMAc. The hollow symbols indicate data without ligand (initial distribution). Dashed lines correspond to the simulation of D_{At} by considering the formation of the 1:1 complex between AtI and ligand in the organic phase with a formation constant being $10^{0.7}$.

Unfortunately, the interaction between AtI and DMAc has not been evidenced because there is no change in D_{At} under the applied experimental conditions (Figure 4.7). There are two possibilities: (i) no interaction occurs between AtI and DMAc; (ii) the interaction between AtI and DMAc are too weak to arise a change on D values within the studied ligand concentration range. Assuming that the interaction exists (by analogy with I_2) and using Model 1, an upper limit for the equilibrium constant can be deduced. As shown in Figure 4.7, the dashed lines are simulations using Model 1 and supposing $K_{BAtI} = 10^{0.7}$. The simulated D_{At} curves present an increase just beyond the studied maximum ligand concentration. Therefore, if the interaction between AtI and DMAc exists, the real equilibrium constant cannot be larger than $10^{0.7}$.

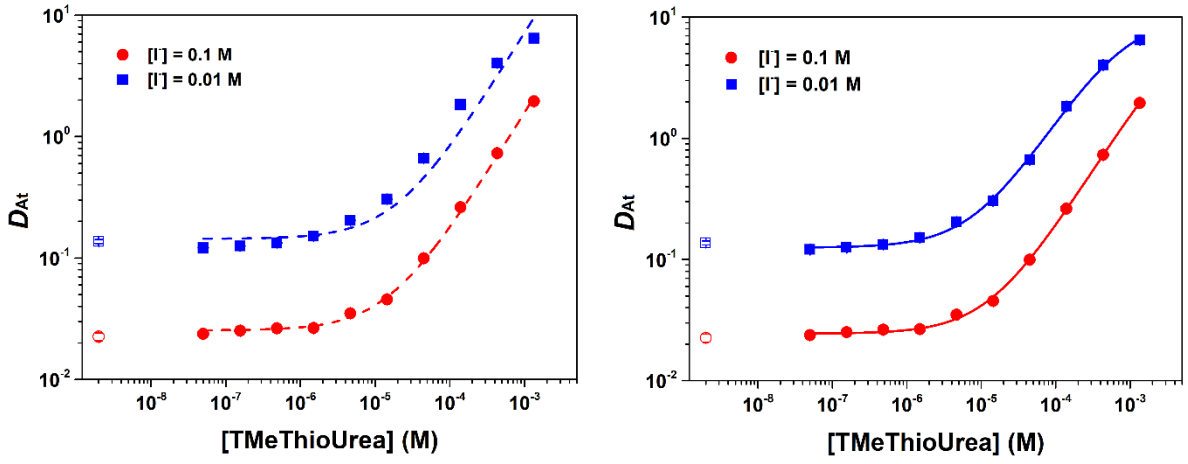

Figure 4.8 Distribution coefficient of At in biphasic aqueous/Hept system in the presence of TMeThioUrea. The hollow symbols indicate data without ligand (initial distribution). The dashed lines correspond to the fitting with the Model 1 that considering the formation of the 1:1 complex between AtI and ligand in the organic phase. The solid lines correspond to the fitting with Model 2 that considering additionally the distribution of the 1:1 complex in two phases.

The case of TMeThioUrea, ThioAcetamide and Me_2Se presents some minor differences to the former cases. Here, the results of TMeThioUrea is taken as an example. From Figure 4.8, it can be observed that after the initial plateau of D_{At} (for [TMeThioUrea] < 10^{-6} M)

and the sharp increase of D_{At} (for 10^{-6} M < [TMeThioUrea] < 10^{-4} M) as the ligand concentration is increased, the increase in D_{At} starts to slow down at high ligand concentration (for [TMeThioUrea] > 10^{-4} M), *i.e.* the derivative of D_{At} ("D_{At} slope") decreases. The dashed lines in Figure 4.8 show the fittings by Model 1. It is obvious that Model 1 is unable to present the decrease of the slope of D_{At} value and thus overestimates the D_{At} values at high ligand concentration.

Because a decrease of the D_{At} slope implies that some astatine species quit the organic phase and enter back to the aqueous phase, one may formulate the hypothesis that the formed BAtI species is partially soluble in the aqueous phase. Therefore, the distribution of the formed BAtI complex, expressed as equation (4.6), was considered in the model (Model 2).

$$\mathrm{BAtI} \overset{D_3}{\leftrightarrow} \overline{\mathrm{BAtI}} \tag{4.6}$$

$$D_{\mathrm{At}} = \frac{D_2 + K_{BAtI} \times D_2 \times [\bar{B}] \times D_1/(D_1 + 2)}{1 + K \times [I^-] + K_{B2AtI} \times D_2/D_3 \times [\bar{B}] \times D_1/(D_1 + 2)} \qquad \text{Model 2}$$

By taking account of this additional equilibrium, Model 2 was found to competently represent the experimental curves of TMeThioUrea (solid lines in Figure 4.8), as well as those of Thio Acetamide and Me_2Se (Figure 4.9).

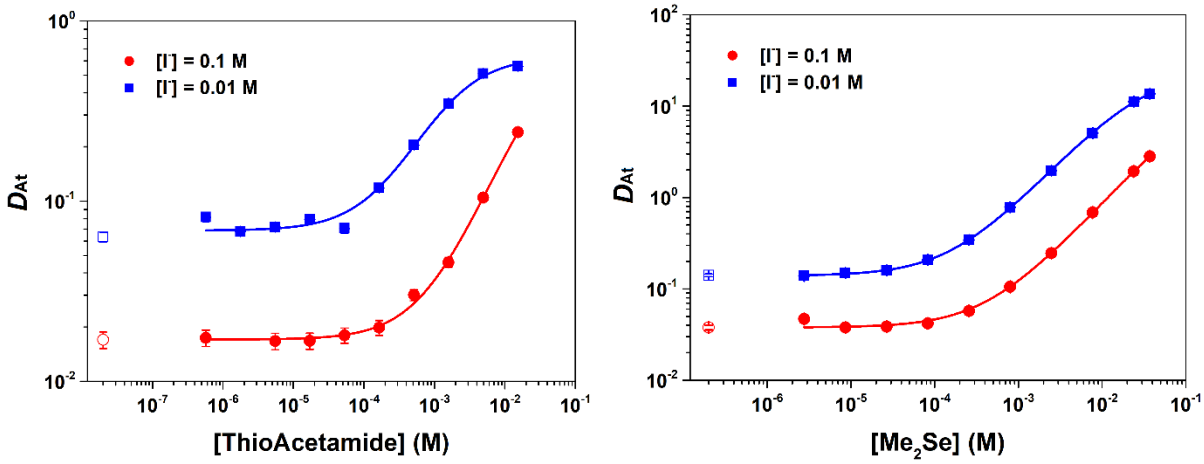

Figure 4.9 Distribution coefficient of At in biphasic aqueous/Hept system in the presence of ThioAcetamide, and in biphasic aqueous/cHex system in the presence of Me_2Se. The hollow symbols

indicate data without ligand (initial distribution). The solid lines correspond to the fitting with Model 2 that considering the formation of 1:1 complex between AtI and ligand in the organic phase plus the distribution of the 1:1 complex in two phases.

According to the analysis above, the curves of D_{At} as functions of the ligand concentration have been successfully reproduced with two models, depending on the ligand. For each Lewis base, two equilibrium constants can be obtained from the fits, corresponding to a given initially I^- concentration with two repetitions (four repetitions for ThioCamph in $[I^-]$ = 0.1 M). These four values are used to compute the average K_{BAtI} value and the associated uncertainties (for two standard deviations). All the equilibrium constants are summarized in Table 4.1 (*vide infra*).

4.3.3 Exceptional case of Bu_3PO: formation of two complexes

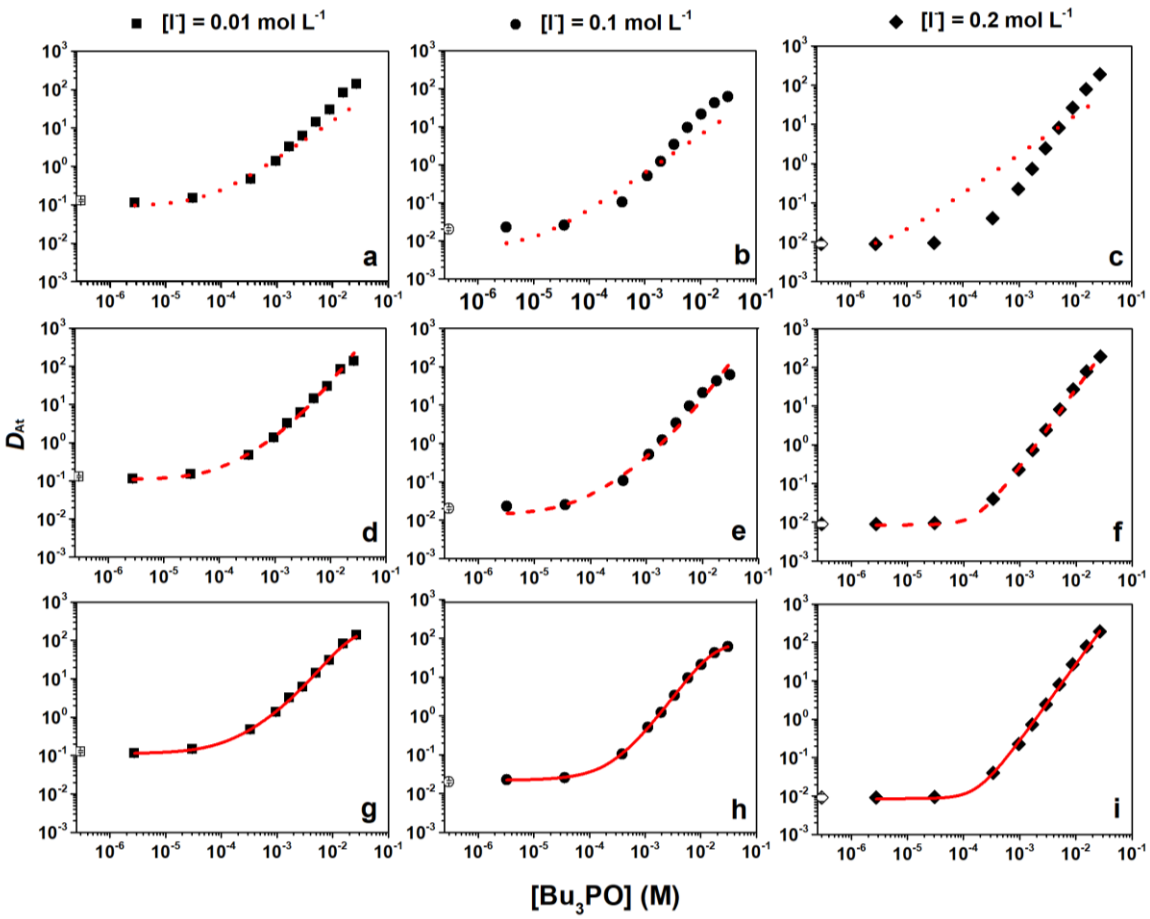

Figure 4.10 Distribution coefficient of At in biphasic aqueous/cHex system in the presence of Bu_3PO for $[I^-]$ = 0.01, 0.1 and 0.2 M. The hollow symbols indicate data without Bu_3PO (initial distribution). Data fitted with a, b, c) Model 1, considering the formation of the 1:1 $Bu_3PO\cdots AtI$ adduct in the organic phase, d, e, f) Model 3, also allowing the formation of the 2:1 $2Bu_3PO\cdots AtI$ adduct, g, h, i) Model 4, considering in addition the partial solubility of the 2:1 adduct in the aqueous phase.

Among the Lewis bases, Bu_3PO presents a distinct behavior. Three representative experimental cases with $[I^-]$ = 0.01, 0.1, and 0.2 M are displayed in Figure 4.10. As shown in Figure 4.10 a, b, c, Model 1 fails to adequately describe the experimental behaviors. In particular, the model cannot reach the high slope of D_{At} at and around the inflexion point. The unexplained D_{At} increase, corresponding to a stronger astatine transfer towards the organic phase, suggests the presence of another extractable astatine species. Under the

experimental conditions, the most probable hypothesis is that AtI and Bu_3PO can form a complex of different stoichiometry. Owing to the extremely low astatine concentration, it is assumed that a 1:2 adduct with two Bu_3PO equivalents occurs in the organic phase *via* reaction (4.7):

$$2\overline{B}+\overline{AtI} \overset{K_{B2AtI}}{\rightleftharpoons} \overline{B_2AtI} \quad (4.7)$$

$$D_{At} = \frac{D_2 + K_{BAtI} \times D_2 \times [\bar{B}] \times D_1/(D_1+2) + K_{B2AtI} \times D_2 \times [\bar{B}]^2 \times (D_1/(D_1+2))^2}{1 + K \times [I^-]} \text{ Model 3}$$

Based on equations (4.2) – (4.7), Model 3 leads to significantly improved fitted results (Figure 4.10 d, e, f), despite some imperfections at high ligand concentrations. The slight overestimation of D_{At} may imply that one of the formed species, either BAtI or B_2AtI, is back-extracted in the aqueous phase. Visual adjustments suggest that accounting for the partial solubility of B_2AtI (equation (4.8)) is enough, which results in the most refined model (Model 4) that satisfactorily fits all the experimental results (Figure 4.10 g, h, i and Figure 4.11).

$$B_2AtI \overset{D_4}{\rightleftharpoons} \overline{B_2AtI} \quad (4.8)$$

$$D_{At} = \frac{D_2 + K_{BAtI} \times D_2 \times [\bar{B}] \times D_1/(D_1+2) + K_{B2AtI} \times D_2 \times [\bar{B}]^2 \times (D_1/(D_1+2))^2}{1 + K \times [I^-] + K_{B2AtI} \times D_2/D_4 \times [\bar{B}]^2 \times (D_1/(D_1+2))^2} \text{ Model 4}$$

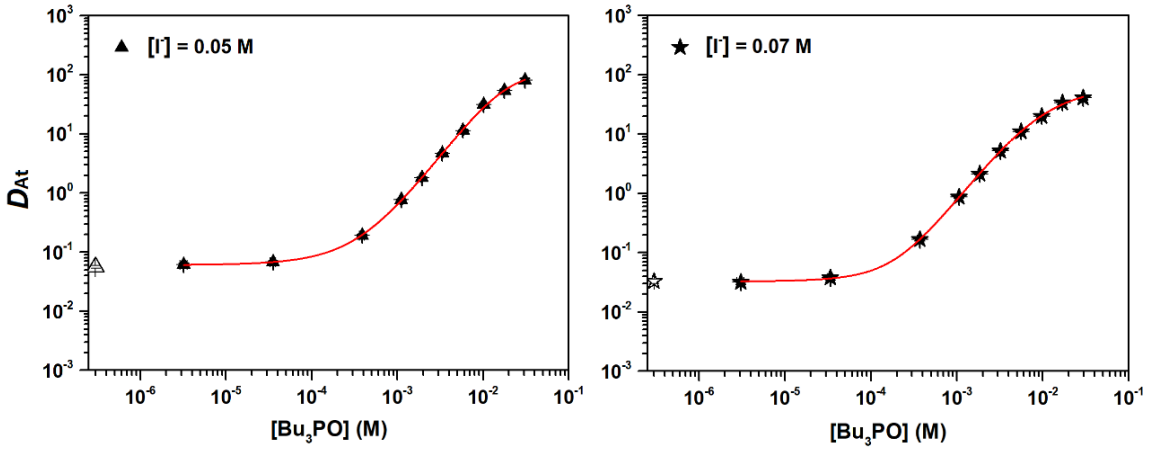

Figure 4.11 Distribution coefficient of At in biphasic aqueous/cHex system in the presence of Bu_3PO for $[I^-]$ = 0.05 and 0.07 M. The hollow symbols indicate data without Bu_3PO (initial distribution). Data fitted

with model 4, considering the formation of the 1:1 $Bu_3PO\cdots AtI$ and 2:1 $2Bu_3PO\cdots AtI$ adduct in the organic phase, plus the partial solubility of the 2:1 adduct in the aqueous phase.

The formation constants of the BAtI and B_2AtI complexes can now be derived from Model 4. Note that for $[I^-]$ = 0.2 M, the formation of the 1:1 complex does not play a significant role in the adjustment: the quality of the fit is maintained for a large interval of constrained K_{BAtI} values (including the average value obtained at other I^- concentrations), so does the adjusted value of K_{B2AtI}. Therefore, the formation constants for BAtI complex at the highest I^- concentration are excluded. Finally, the average equilibrium constant values, log K_{BAtI} = 4.24 ± 0.35 and log K_{B2AtI} = 7.95 ± 0.72, are obtained.

By considering the experimentally determined K_{BAtI} and K_{B2AtI} values, the speciation diagrams of At in the presence of I^- at a fixed concentration, as a function of the initial concentrations of Bu_3PO are obtained with the JCHESS program (Figure 4.12). No matter which I^- concentration, B_2AtI is the predominant astatine species at high ligand range. Therefore, it is necessary to take into account both the formations of BAtI and B_2AtI complexes for reproducing the experimental data. Furthermore, the AtI species being marginal at high I^- concentration, the fit is blind to K_{BAtI} for such concentrations.

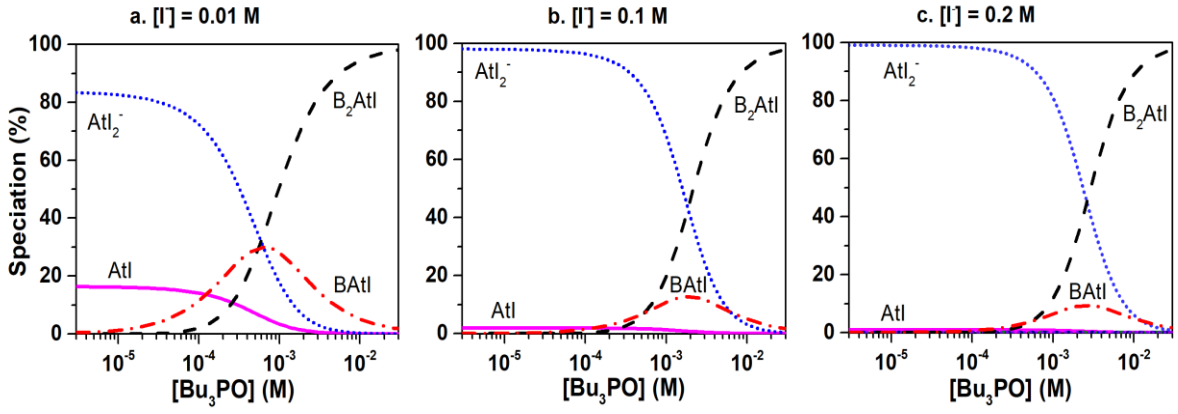

Figure 4.12 Speciation diagrams of At in the presence of I^- at a fixed concentration, as a function of the initial concentrations of Bu_3PO, obtained by considering the experimentally determined K_{BAtI} and K_{B2AtI} values. Species in the organic and aqueous phases are not distinguished. Purple solid lines correspond

to AtI, blue dot lines correspond to AtI_2^-, red dash dot lines correspond to $Bu_3PO\cdots AtI$ (noted BAtI) and black dash lines correspond to $2Bu_3PO\cdots AtI$ (noted B_2AtI). The other astatine species (< 0.1%) are not presented.

4.3.4 Summary of equilibrium constants

With various thermodynamic models, adapted to each situation, eight new formation constants have been successfully obtained, including seven for the formation of BAtI complexes and one for a B_2AtI adduct. Besides, a limit for the formation constant with DMAc has been deduced. The XB formation constant with TMeThioUrea, being $10^{5.69 \pm 32}$, is by one and a half units of log the strongest one that we have obtained so far.

Table 4.1 Distribution coefficient of Lewis bases in the alkane/aqueous system and equilibrium constants between AtI and Lewis bases in an alkane solvent.

Lewis base	Solvent	log D_1*	log K_{BAtI}*	log K_{B2AtI}*
cHexanone	cHex	0.37(02)	1.61(37)	/
TMeUrea	Hept	–0.91(02)	1.76(50)	/
ThioCamph	Hept	3.61(22)	3.25(17)	/
Me_2Se	cHex	1.40(08)	3.60(44)	/
ThioAcetamide	Hept	–0.13(01)	3.91(86)	/
Bu_3PO	cHex	0.02(02)	4.16(34)	7.95(72)
TMeThioUrea	Hept	–0.37(04)	5.69(32)	/
DMAc	cHex	–0.37(02)	< 0.7	/

*Uncertainties correspond to two standard deviations.

4.4 Discussion

4.4.1 Confrontation with theoretical calculations

As mentioned at the beginning of the chapter (and of the dissertation), there is no spectroscopic tool for characterizing astatine compounds at the molecular scale due to the deficient quantity. The application of quantum chemistry methods is thus a key alternative for determining the nature of the formed species.

A recent benchmark study focusing on At-compounds[136] has demonstrated that accurate equilibrium constants can be predicted using the two-component relativistic DFT approach, the B3LYP and PW6B95 hybrid functionals clearly appearing among the recommendable ones. For a considered system, the most stable conformers can be computed by only assuming the (experimental) stoichiometry. The formation constant can be derived by considering one or an ensemble of conformers, if necessary for the accuracy (in practice, it is the case if two or more conformers lie in a tiny free energy range). In this work, the calculations were performed and analyzed by my coauthors Seyfeddine Rahali, Jérôme Graton and Nicolas Galland (CEISAM laboratory), Cecilia Gomez-Pech (Subatech and CEISAM laboratories), and Rémi Maurice (Subatech).

1) BAtI complexes

From the experimental analysis, it is already established that AtI and seven “new” Lewis bases can form BAtI compounds. However, it is important to check if the formed species are indeed bonded by halogen bonding interactions, according to IUPAC criteria.[105]

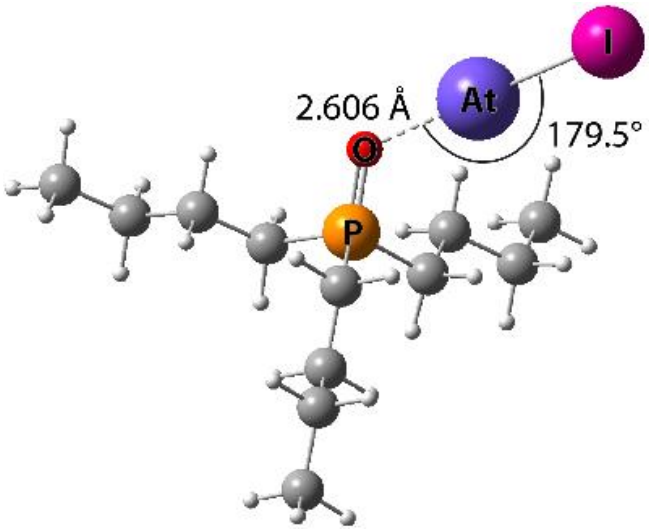

Figure 4.13 Structure of the most stable 1:1 complex between AtI and Bu_3PO calculated at the B3LYP/AVDZ level of theory.

Taking the example of Bu_3PO, the most stable conformer of the BAtI compound was computed (Figure 4.13). It is clear that the two molecular units, AtI and Bu_3PO, interact through the astatine atom and the acceptor (oxygen) atom. The interatomic distance (2.606 Å) is shorter than the sum of the Van der Waals radii of At (2.02 Å) and O (1.52 Å),[22] and the formed angle is very close to 180°. These constitute typical features of a halogen bond. Therefore, these compounds are indeed XB complexes. Same structural characterizations were obtained for the BAtI species formed with cHexanone, TMeUrea, ThioCamph, Me_2Se, ThioAcetamide and TMeThioUrea, proving the halogen bonding interactions.

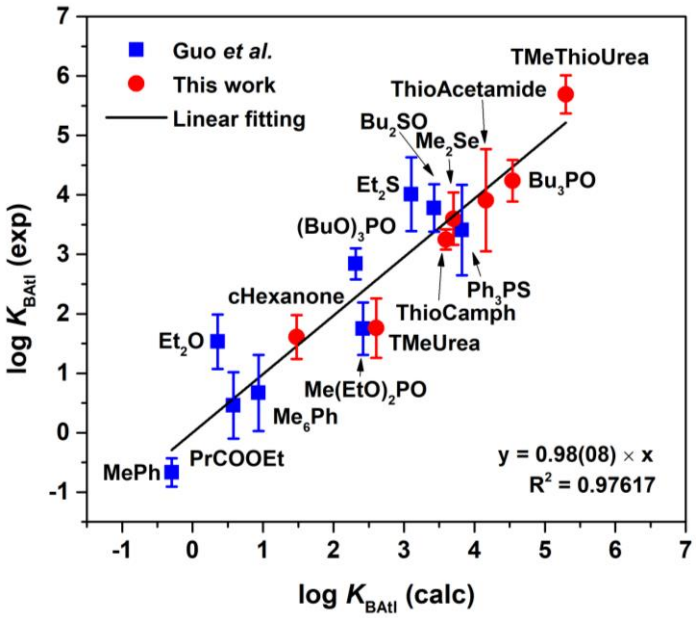

Figure 4.14 Relationship between the experimentally deduced pK_{BAtI} scale and theoretically deduced pK_{BAtI} scale for the same Lewis bases. Error bars represent two standard deviations of uncertainty.

The formation constants were calculated at the PW6B95/TZVPD level of theory, for the BAtI complexes obtained in this work, and those previously published.[16] More details concerning the calculations are available in the joint theory/experiment papers.[16,131] Here, we essentially focus on the consequences of the computational results for the interpretation of the experimental ones. Figure 4.14 presents the comparison between the theoretical calculated formation constants and the experimental ones. There is a good agreement regarding to the evolution of the measured equilibrium constants, despite some minor imperfections. The slope of the linear regression is very close to one (0.98) and the associated coefficient of determination r^2 of 0.976. Furthermore, the mean absolute deviation (MAD) between experimental log K_{BAtI} values and the ones from PW6B95/TZVPD calculations is rather small, 0.45 in log units. Hence, the theoretical results strongly support the identification of the experimentally formed species as At^- mediated XB complexes.

2) B_2AtI complex

Since it is the first time that a 1:2 adduct between AtI and a Lewis base is observed, it is of interest to investigate its nature. Several hypotheses about its nature can be formulated; with two halogens in the AtI molecule, the hot question that firstly emerges is whether this adduct exhibits two different XBs.

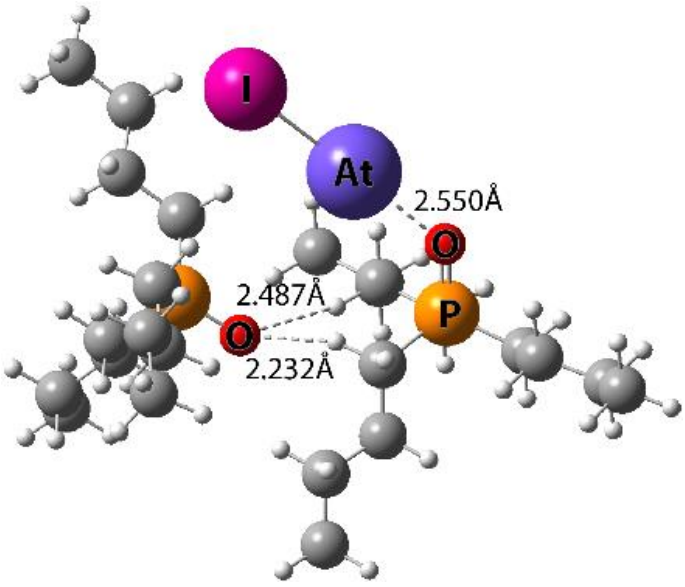

Figure 4.15 Structure of the most stable 1:2 complex between AtI and Bu_3PO calculated at the B3LYP/SVPD level of theory.

The most stable 1:2 adduct structure from the B3LYP/SVPD calculations (Figure 4.15) discloses (i) a halogen bond as described before, and (ii) two chelating hydrogen bonds involving the oxygen atom of the second Bu_3PO unit and two geminal C-H bonds of the first Bu_3PO unit. Indeed, the interatomic distances associated with the two hydrogen bonds, 2.232 and 2.487 Å, are shorter than the sum of O (1.52 Å) and H (1.20 Å) van der Waals radii.[22] Without entering into deep details, the hypothetical structures with two XBs was found to be practically unbound, and actually higher in energy by 25 kJ/mol. Thus, this plus another analysis based on the molecular electrostatic potential point toward the occurrence of one halogen plus two hydrogen bonds and not toward the occurrence of two XBs (see ref [131] for more details). Furthermore, the computations were consistent with the experimental equilibrium constants, which definitely confirmed the nature of the two

formed complexes.

4.4.2 pK_{BAtI} basicity scale

Based on the 16 equilibrium constants (obtained in this work and previous published[16]), an astatine monoiodide basicity scale, pK_{BAtI}, can be constructed by equation (4.9) in which K_{BAtI} is the equilibrium constant of equation (4.5) in an alkane at 298 K.

$$\mathrm{p}K_{BAtI} = \log_{10}(K_{BAtI}) \tag{4.9}$$

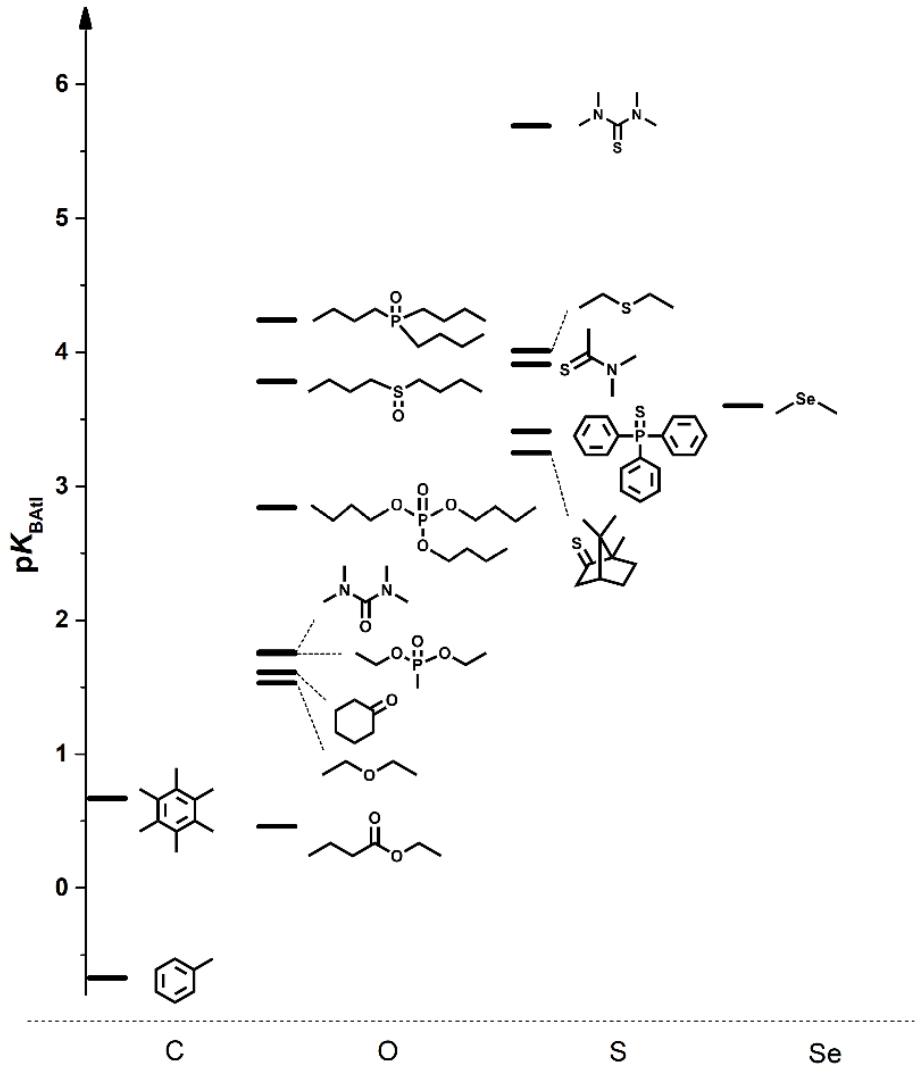

Figure 4.16 Astatine monoiodide basicity chart for functional groups. The C, O, S and Se bases are grouped on different vertical axes.

Figure 4.16 shows this basicity chart in the function of the acceptor atomic site of Lewis bases. This pK_{BAtI} scale spans over 6 log units, including the most representative XB acceptor atomic sites and functional groups, such as S, O, Se and π. The strongest XB is achieved by TMeThioUrea with the value being $10^{5.69 \pm 0.32}$. Note that the P, N based Lewis bases are not present due to experimental constraints.

The scale makes emerging the order C ≤ O ≤ S (≈ Se) for the acceptor atomic site. In particular, the comparison can be made between TMeUrea and TMeThioUrea, or Et_2O and Et_2S. These Lewis bases have exactly the same molecular structure except the acceptor atom. However, the strength of XBs formed with AtI has a significant difference, proving that S-based organic molecular has a much better affinity for At. As for the order of S and Se, Et_2S and Me_2Se are compared because they have similar structures. According to the experiments, the pK_{BAtI} value of Et_2S is larger than that of Me_2Se, while the calculations show the inverse. The difference may come from the uncertainties of experimental measurements.

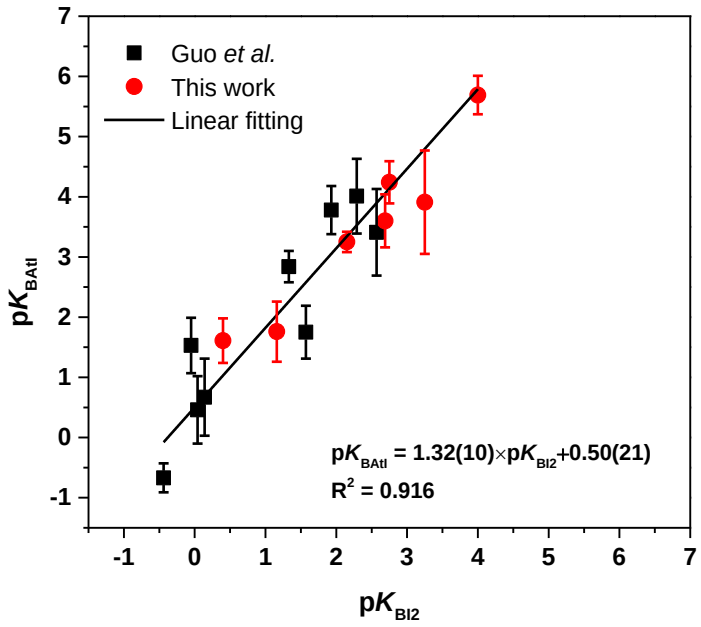

Figure 4.17 Relationship between pK_{BAtI} scale and pK_{BI2} scale for the same Lewis bases. Error bars represent two standard deviation of uncertainty. The numbers in parenthesis in the analytical

expression correspond to one standard deviation.

Finally, the pK_{BAtI} scale of astatine basicity can be compared to the pK_{BI2} scale of iodine basicity. As shown in Figure 4.17, there is an overall linearity between both sets, with R^2 = 0.916, supporting again the interactions with AtI through halogen bonding. For 15 Lewis bases among 16, the pK_{BAtI} value is larger than the pK_{BI2} value, which can only be explained by considering a stronger donor ability of At among the halogen elements. Other interhalogen donors can be indirectly compared with the AtI donor via the pK_{BI2} scale. For instance, the pK_{BICl} and pK_{BIBr} scales compared to the pK_{BI2} scale give linear relationships expressed as pK_{BICl} = 1.79 × pK_{BI2} + 1.42 and pK_{BIBr} = 1.53 × pK_{BI2} + 0.87, [110,137] which lie above the line formed by the pK_{BAtI} scale. We can deduce that the donor ability among interhalogens follows the order: I_2 < AtI < IBr < ICl.

4.5 Conclusions

In the present work, the potential halogen-bonded interactions between AtI and nine Lewis bases have been investigated through liquid/liquid competition experiments. From the analysis of the distribution coefficient of astatine, seven formation constants were successfully obtained, with a record of $10^{5.69\pm0.32}$, achieved by the Lewis base TMeThioUrea. The halogen-bonded molecular structures, as well as the equilibrium constants, were supported by the quantum mechanical calculations.

Moreover, it was evidenced for the first time the formation of a 1:2 complex between AtI and a Lewis base: Bu_3PO. Its nature is unveiled by the quantum mechanical calculations, showing that the 1:2 adduct is stabilized by one halogen bond between AtI and one Bu_3PO units, plus two hydrogen bonds sticking together the two Bu_3PO units.

Based on the formation constants obtained in this work and those previously determined,[16] an astatine monoiodide basicity scale pK_{BAtI} was proposed. This scale is composed of 16 values which spans over 6 log units, indicating that the AtI basicity follows the order C ≤ O ≤ S (≈ Se) for the acceptor atomic site.

Conclusions and perspectives

^{211}At is considered as a promising alpha-emission source for targeted alpha-particle therapy. However, limited knowledge of its physicochemical properties has impeded the attempts to label ^{211}At with cancer-cell targeting agents. Fundamental research has been triggered to obtain more information about the chemistry of astatine. Two aspects have been mainly explored in this thesis: the speciation of astatine in alkaline solution and the reactivity of AtI species towards Lewis bases (halogen bonds). Indirect methods, including HPIEC, electromobility and liquid/liquid competition, have been applied to characterize astatine species and to deduce the corresponding formation constants. The main conclusions and perspectives are presented in the following.

Conclusions

In alkaline medium, it is generally assumed that At^- is the main species (reducing conditions), in analogy with I^-. However, a recent work has shown the predominance of another species, $AtO(OH)_2^-$, in non-reductive conditions.[12] In this work, the astatine speciation in alkaline solutions has thus been further investigated. Firstly, the behaviors of astatine species existing in alkaline reducing media (At_{red}) and in alkaline non-reductive media (At_{ox}) were compared to that of the I^-, Br^- and $S_2O_3^{2-}$ species by HPIEC. The results have indicated that both At_{red} and At_{ox} hold a –1 charge. Secondly, the mobility of At_{red} and At_{ox} were measured and compared with that of the I^- species in the same conditions. At_{red} was found to exhibit a similar behavior to that of the At^- species previously reported by Guo *et al.*[9]; therefore, At_{red} was found to be At^-. In contrast, At_{ox} has a very different mobility; thus, it was concluded to be another species. The liquid/liquid competition experiments have evidenced the change in speciation with the increase of the potential, for a fixed pH. By analyzing the astatine distribution coefficient behavior as a function of the potential, At_{ox} has been presumed to be $AtO(OH)_2^-$. Moreover, the apparent potentials

associated with the redox transformation between At^- and $AtO(OH)_2^-$, obtained at different pH values, have been obtained, leading after averaging to:

$$AtO(OH)_2^- + 4e^- + 4H^+ \rightleftharpoons At^- + 3H_2O \qquad E^0_{AtO(OH)_2^-/At^-} = 0.86 \pm 0.03\ V$$

This work has thus evidenced for the first time a direct speciation change between At^- and $AtO(OH)_2^-$, allowing to close the cycle started from At^- years ago, thus involving the At^+, AtO^+ and AtO(OH) and $AtO(OH)_2^-$ species, therefore validating the Pourbaix diagram of astatine in the range of water stability and for pH < 11.

As a member of the halogen family, astatine was long supposed to possess the ability to form halogen bonds with Lewis bases, with no experimental proof for it. Following the first characterization of halogen bonds involving astatine and several Lewis bases[16], the present work has extended the set of bases, both in terms of size but also in terms of the nature of them, which has actually also led to a much wider range of halogen bond strengths. Indeed, through liquid/liquid competition experiments, the interactions between AtI and nine new Lewis bases have been investigated, and seven new equilibrium constants were obtained. The quasi-proportional relationship between the equilibrium constants and the pK_{BI2} basicity scale has thus been refined, based on both the previous[16] and the new data. The nature of the adducts, which could be already guessed from this relationship, was firmly confirmed by quantum mechanical calculations. A record for an At-mediated halogen bond was achieved with the Lewis base tetramethylthiourea (TMeThioUrea), with an equilibrium constant value of $10^{5.69 \pm 0.32}$. The new pK_{BAtI} scale is composed of 16 values and spans over 6 log units. The ligand basicity follows the order C ≤ O ≤ S (≈ Se) for the halogen bond acceptor atomic site. Moreover, the formation and the nature of a 1:2 adduct between AtI and a Lewis base has been evidenced for the first time (tributylphosphine oxide (Bu_3PO) case).

Perspectives

Despite the new advances, the current Pourbaix diagram of astatine is not yet complete,

in particular for pH > 11. In fact, this may be of interest in view of the recovery process of astatine after production. As mentioned in Chapter 1, the dry distillation approach and the wet extraction methods are commonly used to isolate astatine from the bismuth target, and finally, astatine is conditioned into an organic solvent. One of the methods to recover astatine in aqueous solution is to back-extract it with concentrated NaOH solutions. Knowing the astatine speciation in these conditions would potentially help to develop new straightforward methods. To this end, the same strategy in Chapter 3 can be used: (i) HPIEC and electromobility measures to characterize the astatine species and (ii) liquid/liquid competition experiments to study the speciation change.

Secondly, the At-mediated halogen bonds can serve for the design of new BFCs to strengthen the radiolabeling with At. To date, the labeling of At atom relies mainly on the formation of one covalent bond between At and a C or B atom of the BFC. This is not yet fully satisfactory[138], and one may attempt to use an extra halogen bond to further bind the At atom and eventually protect it by steric hindrance. Nevertheless, so far At-mediated halogen bonds have only been characterized in alkane solutions. Considering that for medicinal applications one should at some point display stability in blood, kind of a mysterious and complex aqueous solution for a chemist, a first step toward this would consist in determining halogen bond strengths in water. Of course, not every system may be suited for such a liquid/liquid extraction. A mirror setup of what has been done for measuring strengths in organic solution is a possible way: looking for a speciation change that triggers (back-)extraction to the aqueous phase, meaning that the Lewis base must be (partly) soluble in water, and so do the halogen-bonded adduct. This may require an initial step with a high concentration of astatine in the organic phase (e.g. by interaction with another reagent that has less affinity for the astatine moiety than the Lewis base). For this, one may play with three main degrees of freedom: the choice of the astatine moiety (perhaps the At-labeled organic compounds as SAB[39], ethyl 3-astatobenzoate[139], *etc.* are interesting candidates), the Lewis base, and the organic solvent; this would thus require a new extensive study.

Appendix A. Supplementary data

Table A.1 List of equilibria and their associated thermodynamic constants added in the JCHESS database for modeling astatine behaviors.

Equilibrium	log$k$
$At^- + 2H^+ + 0.5O_2 \rightleftharpoons At^+ + H_2O$	31
$At^- + 2H^+ + O_2 \rightleftharpoons AtO^+ + H_2O$	48.8
$AtO^+ + H_2O \rightleftharpoons AtO(OH) + H^+$	1.9
$AtO^+ + 2H_2O \rightleftharpoons AtO(OH)_2^- + H^+$	8.8
$At^+ + I^- \rightleftharpoons AtI$	6.1
$At^+ + 2I^- \rightleftharpoons AtI_2^-$	8.8

Table A.2 Adjustable parameters obtained from the fitting of the distribution coefficient measurements with different models presented in chapter 4 for all experimental data related to the halogen bonding between AtI and Lewis bases.

Lewis base	$[I^-]$ ($molL^{-1}$)	log K_{BAtI}[a]	D_2[a]	D_3[a]
cHexanone	0.01	1.78 ± 0.14	0.12 ± 0.06	/
		1.75 ± 0.10	0.08 ± 0.04	/
	0.1	1.40 ± 0.10	0.37 ± 0.04	/
		1.52 ± 0.08	0.14 ± 0.04	/
TMeUrea	0.01	1.95 ± 0.10	-0.19 ± 0.02	/
		2.00 ± 0.04	-0.19 ± 0.02	/
	0.1	1.51 ± 0.10	0.16 ± 0.02	/
		1.58 ± 0.12	0.16 ± 0.02	/
ThioCamph	0.1	3.29 ± 0.24	0.11 ± 0.22	/
		3.31 ± 0.38	0.14 ± 0.34	/
		3.28 ± 0.34	0.16 ± 0.30	/
		3.13 ± 0.18	0.22 ± 0.16	/
Me_2Se	0.01	3.78 ± 0.04	-0.02 ± 0.04	1.38 ± 0.12
		3.80 ± 0.02	0.01 ± 0.00	1.40 ± 0.04
	0.1	3.43 ± 0.12	0.30 ± 0.08	1.38 ± 0.72
		3.39 ± 0.06	0.38 ± 0.08	1.37 ± 0.68
ThioAcetamide	0.01	4.31 ± 0.14	-0.30 ± 0.04	-0.20 ± 0.04
		4.23 ± 0.20	-0.17 ± 0.06	-0.12 ± 0.08
	0.1	3.64 ± 0.06	0.04 ± 0.02	-0.06 ± 0.14
		3.44 ± 0.06	0.19 ± 0.02	0.05 ± 0.28
TMeThioUrea	0.01	5.80 ± 0.06	-0.04 ± 0.04	1.01 ± 0.04
		5.85 ± 0.06	-0.04 ± 0.04	1.01 ± 0.08

	0.1	5.60 ± 0.04	0.19 ± 0.02	1.08 ± 0.16
		5.52 ± 0.04	0.27 ± 0.04	0.98 ± 0.18

[a] Uncertainties correspond to two standard errors.

Table A.3 Adjustable parameters obtained from the fitting of the distribution coefficient measurements with Model 3 presented in chapter 4 for all experimental data related to the halogen bonding between AtI and Bu_3PO.

$[I^-]$ (mol L^{-1})	log K_{BAtI}[a]	log K_{B2AtI}[a]	D_2[a]	D_4[a]
0.01	4.41 ± 0.12	7.47 ± 0.12	-0.09 ± 0.08	2.30 ± 0.38
	4.24 ± 0.10	7.41 ± 0.08	-0.01 ± 0.04	2.41 ± 0.34
0.05	4.04 ± 0.12	7.71 ± 0.04	0.29 ± 0.04	2.00 ± 0.08
	3.98 ± 0.10	7.80 ± 0.04	0.25 ± 0.04	1.98 ± 0.06
0.07	4.51 ± 0.20	8.13 ± 0.12	0.18 ± 0.10	1.59 ± 0.10
	4.30 ± 0.26	8.17 ± 0.12	0.13 ± 0.12	1.56 ± 0.10
0.1	4.19 ± 0.14	8.03 ± 0.06	0.14 ± 0.06	1.89 ± 0.06
	4.26 ± 0.48	7.96 ± 0.24	0.19 ± 0.24	2.00 ± 0.28
0.2	-28.83[b]	8.44 ± 0.34	0.03 ± 0.34	98.34[b]
	-48.47[b]	8.42 ± 0.26	0.06 ± 0.26	49.78[b]
Average[c]	4.24 ± 0.35	7.95 ± 0.72		

[a] Uncertainties correspond to 95% confidence intervals. [b] Unreliable. [c] The average value is the average of the eight or ten values obtained by fitting the experimental data, and the uncertainties correspond to two standard deviations.

Appendix B. Résumé de la thèse en français

Lorsque Dmitri Mendeleïev publia son tableau périodique en 1869, l'espace sous l'iode, c'est-à-dire l'élément 85, était vide. En 1940, Dale R. Corson, Kenneth R. MacKenzie et Emilio G. Segrè ont synthétisé pour la première fois l'élément 85 en bombardant du bismuth-209 avec des particules alpha accélérées dans un cyclotron à l'université de Californie, Berkeley (États-Unis).[1] Cet élément est ensuite appelé « astate », du grec astatos (ἄστατος), qui signifie « instable ».[2,3] Comme le reflète son nom, l'astate est un radioélément. Depuis sa découverte, 39 isotopes ayant les masses atomiques de 191 à 229 ont été identifiés expérimentalement, tous radioactifs, avec une courte durée de vie ($t_{1/2}$ ≤ 8,1 h).[4] L'astate existe naturellement. Il est l'un des éléments les plus rares présents dans la croûte terrestre (moins de 30g[5]). Il est donc difficile de le récupérer à partir de cette source. La voie principale pour obtenir de l'astate passe par des réactions nucléaires, qui conduisent à la production de quantités infimes. Ainsi, toutes les études chimiques sur l'astate sont menées à des concentrations d'ultra-traces (entre 10^{-10} et 10^{-15} mol·L^{-1}), ce qui rend les outils spectroscopiques classiques inapplicables pour étudier les structures moléculaires. Même 80 ans après la découverte de l'astate, sa chimie reste méconnue.

Parmi les isotopes de l'astate, l'astate-211 (^{211}At) attire une attention particulière en raison de son application potentielle en médecine nucléaire. En effet, ^{211}At a une demi-vie de 7,21 heures. Il émet des particules α avec une énergie moyenne de 6,8 MeV.[6] Le transfert d'énergie linéique moyen dans les tissus est de 97 keV·µm^{-1},[7] ce qui est suffisamment efficace pour détruire des cellules cancéreuses. Ces propriétés favorables font de ^{211}At un candidat prometteur pour la radiothérapie alpha ciblée. Cette thérapie est basée sur l'injection d'isotopes radioactifs dans le corps du patient tout en ciblant préférentiellement des cellules malades pour les détruire à proximité immédiate. Une condition préalable à l'injection est de marquer un agent ciblant à l'^{211}At de manière stable,

ce qui nécessite bien entendu des connaissances sur la chimie de base de l'astate.

Le cyclotron ARRONAX à Nantes permet entre autres la production de ^{211}At par la réaction nucléaire ^{209}Bi(α, 2n)^{211}At. Autour du cyclotron, plusieurs équipes, notamment des chimistes expérimentateurs et théoriciens, collaborent pour étudier la chimie de l'astate. Le projet déployé au sein du laboratoire Subatech (UMR 6457), en collaboration avec le laboratoire CEISAM (UMR 6230), vise à explorer la chimie de l'astate en solution en combinant des approches expérimentales et théoriques. Subatech a initié ces recherches il y a plus de quinze ans. Les efforts consentis par Julie Champion et Ning Guo, les premières doctorantes sur ce sujet à Subatech, ont permis de commencer à comprendre la spéciation de l'astate en solution aqueuse et la réactivité des espèces. Plus précisément, trois états d'oxydation ont été identifiés en phase aqueuse : –1, +1 et +3 pour respectivement At^-, At^+ et AtO^+,[8–10] ainsi que des produits d'hydrolyse de AtO^+.[11,12] Ceci a finalement contribué à la construction d'un diagramme de Pourbaix pour l'astate. Les interactions des espèces cationiques de l'astate avec des ligands inorganiques (Cl^-[13], Br^-[13,14], I^-[14] et SCN^-[15]) et avec certains ligands organiques[15,16] ont été caractérisées. Ceci a notamment permis de confirmer le caractère métallique de l'astate et la mise en évidence de l'espèce AtI a conduit à l'étude de liaisons halogènes impliquant l'astate. Mon projet de doctorat cherche à approfondir les connaissances sur ces deux aspects.

Comme l'astate n'est disponible qu'en faibles quantités (ultra-traces), trois méthodes expérimentales indirectes couplées avec des systèmes de détection de radioactivité ont été utilisées dans le cadre de cette thèse : l'électromobilité, l'HPIEC (« High-Performance Ion Exchange Chromatography ») et la compétition liquide/liquide.

La technique d'électromobilité est basée sur le principe de l'électrophorèse. Une haute tension est appliquée dans une solution électrolytique, créant un champ électrique homogène. L'échantillon contenant ^{211}At est injecté dans l'électrolyte. En balayant par un détecteur de rayons γ, la position de ^{211}At peut être suivie au cours du temps. Les ions se déplacent vers la cathode ou vers l'anode, ce qui donne une première indication sur leur

charge (négative ou positive). De plus, le changement de position de ^{211}At en fonction du temps permet une évaluation de la mobilité des ions dans l'électrolyte, caractéristique de leur rapport charge/taille.

Le principe des mesures HPIEC repose sur l'utilisation d'une colonne contenant une résine échangeuse d'ions (phase stationnaire). La colonne est couplée à un détecteur de rayons γ qui génère des signaux de radio-chromatogramme en raison de l'élution des espèces contenant ^{211}At. Dans une expérience typique de HPIEC, un éluant qui contient le milieu souhaité (phase mobile) est tout d'abord introduit à travers le système. L'échantillon contenant ^{211}At est ensuite injecté et est emmené par l'éluant à traverser la colonne. Les analytes cibles (anions ou cations) sont retenus sur la phase stationnaire, mais peuvent être détachés de celle-ci en ajoutant une espèce de charge similaire dans l'éluant. En fonction du débit de l'éluant et de l'affinité d'une espèce de At donnée pour la résine d'échange, il faut un certain temps pour que cette espèce sorte de la colonne. Ce temps est défini comme le temps de rétention (t_r) et peut être visualisé sur le radio-chromatogramme. Des informations importantes telles que le nombre d'espèces et leur charge peuvent ainsi être déduites.

La répartition de l'astate entre deux phases non miscibles dans des conditions expérimentales données est un moyen de caractériser les changements de spéciation. La méthode de compétition liquide/liquide est basée sur le suivi du coefficient de distribution de l'astate (D_{At}) dans deux phases liquides. Il est calculé comme le rapport de l'activité volumique de ^{211}At entre ces deux phases. Une variation de la valeur D_{At} causée par le changement des conditions expérimentales (pH, Eh, concentration en ligand, *etc.*) permet de mettre en évidence un changement de spéciation dans au moins une des deux phases.

Pour obtenir des paramètres quantitatifs permettant de décrire la formation des espèces de l'astate, différentes simulations ont été réalisées. Elles sont basées sur les processus chimiques connues (distribution, complexation, redox) à partir des expressions

analytiques simples ou des codes numériques. Ces derniers font appel à des bases de données thermodynamiques. De plus, puisque la chimie quantique apparaît comme une méthode de « spéciation » alternatif pour aider à établir la nature des espèces de l'astate à l'échelle moléculaire, certain de mes résultats expérimentaux sont comparées aux résultats obtenus par de tels calculs.

Avec les méthodologies mentionnées ci-dessus, deux objectifs ont été fixés dans le cadre de ma thèse, dont les contextes et résultats obtenus vont être présentés ci-dessous.

Le premier objectif était de collecter des informations manquantes dans le diagramme de Pourbaix de l'astate, en conditions alcalines. Le diagramme de Pourbaix cartographie les domaines de prédominance des différentes espèces d'un élément en fonction du pH et du potentiel redox. Sa connaissance est primordiale pour les chimistes. D'ailleurs, connaître le diagramme de Pourbaix de l'astate dans les milieux non complexant est crucial pour le développement de stratégies de radiomarquage adaptées aux applications médicales. Il indique les formes redox des espèces qui peuvent prédominer en solution aqueuse et donc déterminer les types d'approches de marquage envisageables. Dans la littérature, les études sur la spéciation de l'astate ont commencé en présupposant existence de At^- dans des conditions réductrices, comme pour les halogènes plus légers. En augmentant le potentiel en conditions acides, deux espèces ont été proposées avec les états d'oxydation +1 et +3, correspondant à At^+ et AtO^+.[10,71] Lorsque le pH de la solution augmente tout en restant dans des conditions oxydantes, une espèce neutre, AtO(OH), a été observée.[11] En continuant à augmenter le pH vers des conditions alcalines, l'espèce $AtO(OH)_2^-$ a été récemment identifiée comme prédominante dans les milieux non réducteurs.[12] À ce jour, les changements de spéciation pour les couples At^-/At^+, At^+/AtO^+, $AtO^+/AtO(OH)$ et $AtO(OH)/AtO(OH)_2^-$ ont été caractérisés et quantifiés. Cependant, le passage entre At^- et $AtO(OH)_2^-$ n'a pas encore été étudié et l'existence d'espèces intermédiaires n'est pas démontrée. Dans ce contexte, mon objectif est de caractériser la spéciation de l'astate en conditions alcalines, et de quantifier le changement de spéciation entre les différentes

espèces d'intérêt. Deux cas sont possibles : si le changement direct entre At^- et $AtO(OH)_2^-$ est confirmé, alors la constante associée doit pouvoir être déterminée en combinant tous les paramètres mesurés précédemment. Il serait ainsi possible de valider le diagramme de Pourbaix (du moins pour pH < 11). Si le changement ne peut pas être décrit simplement, cela indiquerait l'existence d'autres espèces de l'astate qu'il faudrait identifier.

Pour ce faire, les espèces de At présentes dans les milieux basiques réducteur (appelées At_{red}) et non réducteur (appelées At_{ox}) ont été caractérisées par HPIEC. Leurs comportements sont comparés avec ceux des ions de charge –1 (I^- et Br^-) et de charge –2 ($S_2O_3^{2-}$). Les résultats indiquent l'existence d'une seule espèce et que At_{red} et At_{ox} sont toutes de charge –1. Ensuite, la mobilité de At_{red} et de At_{ox} a été mesurée, et a été comparée à la mobilité de l'espèces $^{123}I^-$ obtenue dans les mêmes conditions. Comme pour les expériences de HPIEC, seulement une espèce est identifiée. La mobilité de At_{red} est très proche de celle de $^{123}I^-$, avec une différence de $(0{,}07 \pm 0{,}34)\cdot10^{-4}$ $cm^2\cdot V^{-1}\cdot s^{-1}$, ce qui est cohérant avec le comportement de At^- publié par Guo *et al.*[9]. Il est donc raisonnable de supposer que At_{red} est At^-. En revanche, At_{ox} a une mobilité très différente par rapport à $^{123}I^-$ avec une différence de $(3{,}32 \pm 0{,}99)\cdot10^{-4}$ $cm^2\cdot V^{-1}\cdot s^{-1}$. At_{ox} est donc différent de At_{red}. Les expériences de compétition liquide/liquide ont mis en évidence le changement de spéciation de l'astate avec l'augmentation du potentiel pour un pH fixe. En analysant le comportement du D_{At}, At_{ox} a été identifié comme étant $AtO(OH)_2^-$. De plus, le potentiel apparent pour l'équilibre entre At^- et $AtO(OH)_2^-$ à différents pH a été obtenu, permettant de déduire le potentiel standard pour la demi-réaction suivante :

$$AtO(OH)_2^- + 4e^- + 4H^+ \rightleftharpoons At^- + 3H_2O \qquad E^0_{AtO(OH)_2^-/At^-} = 0{,}86 \pm 0{,}03\ V$$

Le potentiel standard du couple $AtO(OH)_2^-/At^-$ obtenu est confronté avec les paramètres quantitatives liées aux autres couples d'espèces afin de construire un digramme de Pourbaix compatible.

Figure A.1 est le digramme de Pourbaix de l'astate construit en considérant $E^0_{At^+/At^-} =$

0,37 V[10], $E^0_{AtO(OH)_2^-/At^-} = 0{,}86$ V (le travail présent), $\log K_{AtO^+,hyd,1} = -1{,}9$[11] et $\log K_{AtO^+,hyd,2} = -6{,}9$[12], avec les points expérimentaux correspondant à chaque ligne dans la littérature.[10–12,69,78]

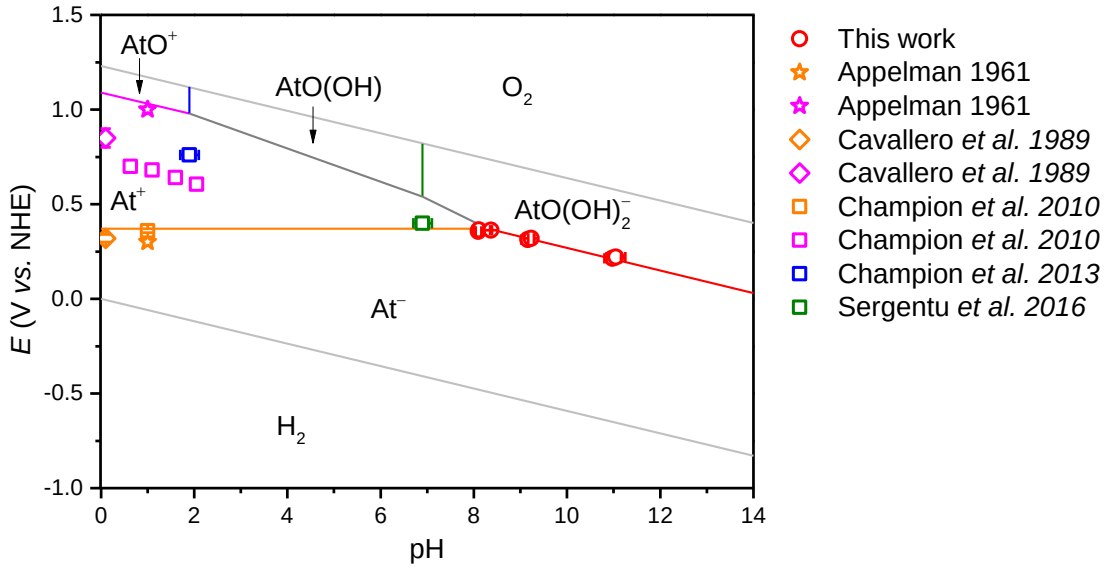

Figure A.1 Diagramme de Pourbaix de l'astate (25°C) construit en considerant $E^0_{At^+/At^-} = 0{,}37$ V, $E^0_{AtO(OH)_2^-/At^-} = 0{,}86$ V, $\log K_{AtO^+,hyd,1} = -1{,}9$ et $\log K_{AtO^+,hyd,2} = -6{,}9$. Les points du diagramme sont des résultats expérimentaux dans la littérature et dans ce travail. La couleur des symboles est en accord avec les frontières des espèces considérée.

Sur cette figure, on peut observer que le diagramme nouvellement établi peut bien incorporer pour la plupart des points expérimentaux, et la construction donne une valeur de potentiel standard pour le couple AtO^+/At^+ de 1,09 V. Cette value est proche de la valueur poblie par Appelman[69], alors que plus elevee que celles propose par Champion *et al.*[10] et Cavallero *et al.*[78]

Pour conclure, ce travail complète les travaux précédents en validant l'idée d'un changement de spéciation direct entre At^- et $AtO(OH)_2^-$, c'est-à-dire en écartant la possibilité de l'existence d'une autre espèce de l'astate en milieu alcalin et pH < 11. Une valeur expérimentale du potentiel du couple $AtO(OH)_2^-/At^-$ est donnée.

Le deuxième objectif de cette thèse était de poursuivre l'étude sur la capacité de l'astate (sous la forme AtI) à former des liaisons halogènes avec différentes bases de Lewis. En effet, la liaison halogène (« XB », pour « halogen bond » en anglais) est une interaction électrostatique locale entre un halogène en déficit d'électrons (donneur de XB) et une base de Lewis (accepteur de XB). Étant l'halogène « naturel » le plus lourd, l'astate est considéré comme l'atome donneur de XB le plus puissant.[111,112,135] Les premières liaisons halogènes induites par l'astate ont été récemment mises en évidence par Guo *et al.* au travers d'une interaction de l'espèce AtI et plusieurs bases de Lewis.[16] Néanmoins, un nombre limité de bases de Lewis a été étudié. Il est primordial d'élargir l'étude et de rationaliser le comportement de l'astate vis-à-vis des composés organiques. Pour se faire, neuf bases de Lewis ayant des groupes fonctionnels chimiques contenant S, O, et pour la première fois, l'élément Se ont été sélectionnées. Par la méthode de compétition liquide/liquide, les interactions entre AtI et ces ligands ont été étudiées. En analysant le comportement du D_{At} en fonction de la concentration initiale en ligand, sept nouvelles constantes d'équilibre ont été obtenues. Les interactions de type liaison halogène sont caractérisées par la relation quasi proportionnelle entre les constantes d'équilibre obtenues et l'échelle de basicité de la liaison halogène (construite avec le donneur I_2). De plus, ces données ont été confrontées avec succès à des calculs de mécanique quantique. Un record en terme de force d'interaction de la liaison halogène impliquant l'astate est atteint. Il s'agit de l'interaction entre AtI et le ligand tétraméthylthiourée dont la constante de formation est $10^{5,69 \pm 0,32}$. De plus, la formation d'un complexe 1:2 entre AtI et une base de Lewis a été mise en évidence pour la première fois (le cas de l'oxyde de tributylphosphine, Bu_3PO). Sa nature est dévoilée par des calculs de mécanique quantique, montrant qu'il est stabilisé par une liaison halogène entre AtI et une unité Bu_3PO, plus deux liaisons hydrogènes liant les deux unités Bu_3PO. A partir des constantes de formation obtenues dans ce travail et de celles déterminées précédemment[16], une échelle de basicité du monoiodure d'astate pK_{BAtI} a été construite (Figure A.2). Cette échelle est composée de 16 valeurs de constante qui s'étendent sur 6 unités log, indiquant que la

basicité de AtI suit l'ordre C ≤ O ≤ S (≈ Se) pour le site atomique de l'accepteur.

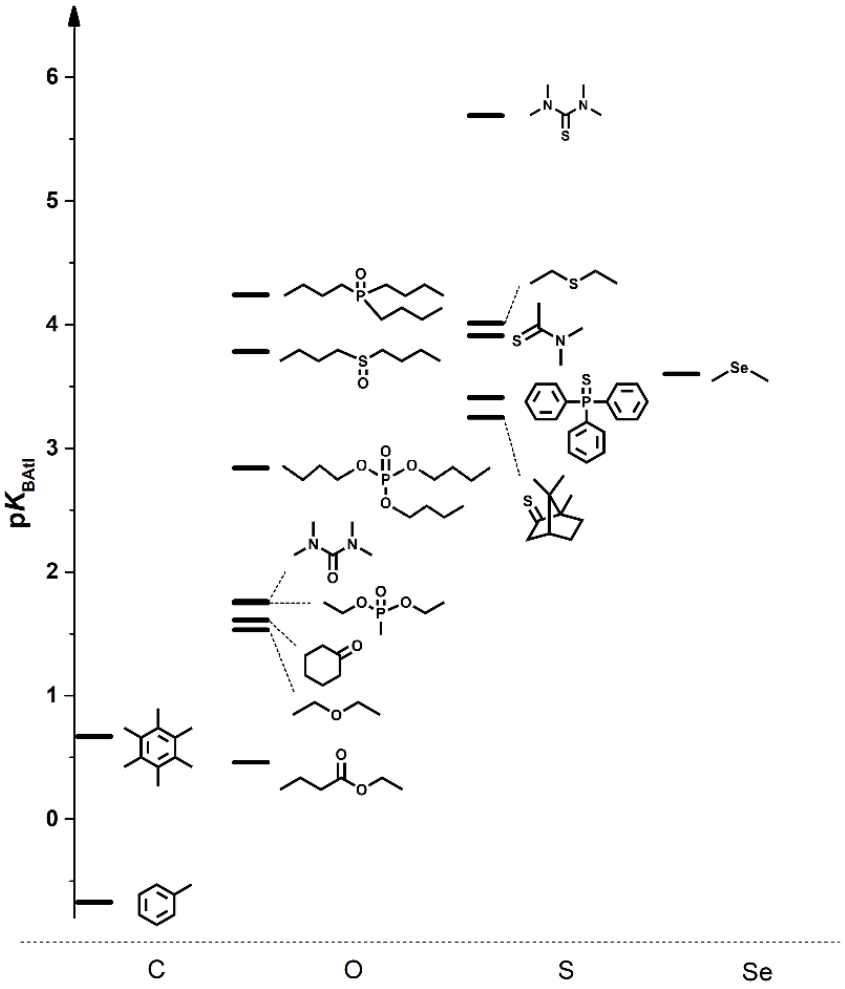

Figure A.2 L'échelle de basicité pK_{BAtI} pour les bases de Lewis. Les bases de C, O, S et Se sont regroupées sur différents axes verticaux.

Pour conclure, cette thèse a permis de compléter le diagramme de Pourbaix de l'astate et de rationaliser l'affinité d'une espèce de l'astate, AtI, envers des molécules organiques via la formation de liaisons halogènes. Sans nul doute, ce travail devra être prolongé par d'autres études pour améliorer à moyen terme les techniques de radiomarquage à l'^{211}At.

References

[1] D. R. Corson, K. R. MacKenzie, E. Segrè, *Phys. Rev.* **1940**, *58*, 672–678.

[2] D. R. Corson, K. R. MacKenzie, E. Segrè, *Nature* **1947**, *159*, 24.

[3] A. Weights, M. Perey, *Chem. Eng. News* **1949**, *27*, 2996–3000.

[4] C. Fry, M. Thoennessen, *At. Data Nucl. Data Tables* **2013**, *99*, 497–519.

[5] D. S. Wilbur, *Nat. Chem.* **2013**, *5*, 246–246.

[6] M. R. Zalutsky, M. Pruszynski, *Curr. Radiopharm.* **2011**, *4*, 177–185.

[7] M. R. Zalutsky, D. A. Reardon, O. R. Pozzi, G. Vaidyanathan, D. D. Bigner, *Nucl. Med. Biol.* **2007**, *34*, 779–785.

[8] A. Sabatié-Gogova, J. Champion, S. Huclier, N. Michel, F. Pottier, N. Galland, Z. Asfari, M. Chérel, G. Montavon, *Anal. Chim. Acta* **2012**, *721*, 182–188.

[9] N. Guo, F. Pottier, J. Aupiais, C. Alliot, G. Montavon, J. Champion, *Inorg. Chem.* **2018**, *57*, 4926–4933.

[10] J. Champion, C. Alliot, E. Renault, B. M. Mokili, M. Chérel, N. Galland, G. Montavon, *J. Phys. Chem. A* **2010**, *114*, 576–582.

[11] J. Champion, A. Sabatié-Gogova, F. Bassal, T. Ayed, C. Alliot, N. Galland, G. Montavon, *J. Phys. Chem. A* **2013**, *117*, 1983–1990.

[12] D.-C. Sergentu, D. Teze, A. Sabatié-Gogova, C. Alliot, N. Guo, F. Bassal, I. Da Silva, D. Deniaud, R. Maurice, J. Champion, N. Galland, G. Montavon, *Chem. - A Eur. J.* **2016**, *22*, 2964–2971.

[13] J. Champion, M. Seydou, A. Sabatié-Gogova, E. Renault, G. Montavon, N. Galland, *Phys. Chem. Chem. Phys.* **2011**, *13*, 14984.

[14] N. Guo, D.-C. Sergentu, D. Teze, J. Champion, G. Montavon, N. Galland, R. Maurice, *Angew. Chemie Int. Ed.* **2016**, *55*, 15369–15372.

[15] J. Champion, C. Alliot, S. Huclier, D. Deniaud, Z. Asfari, G. Montavon, *Inorganica Chim. Acta* **2009**, *362*, 2654–2661.

[16] N. Guo, R. Maurice, D. Teze, J. Graton, J. Champion, G. Montavon, N. Galland, *Nat. Chem.* **2018**, *10*, 428–434.

[17] F. Allison, E. J. Murphy, E. R. Bishop, A. L. Sommer, *Phys. Rev.* **1931**, *37*, 1178–1180.

[18] H. G. MacPherson, *Phys. Rev.* **1935**, *47*, 310–315.

[19] B. F. Thornton, S. C. Burdette, *Bull. Hist. Chem.* **2010**, *35*, 86–96.

[20] W. Minder, *Helv. Phys. Acta.* **1940**, *13*, 144–152.

[21] A. Leigh-Smith, W. Minder, *Nature* **1942**, *150*, 767–768.

[22] M. Mantina, A. C. Chamberlin, R. Valero, C. J. Cramer, D. G. Truhlar, *J. Phys. Chem. A* **2009**, *113*, 5806–5812.

[23] A. K. Lavrukhina, A. A. Pozdniakov, *Analytical Chemistry of Technetium, Promethium, Astatine and Francium*, Ann Arbor-Humphrey Science Publishers, **1970**.

[24] I. Asimov, *J. Chem. Educ.* **1953**, *30*, 616.

[25] J. Harrison, R. Leggett, D. Lloyd, A. Phipps, B. Scott, *J. Radiol. Prot.* **2007**, *27*, 17–40.

[26] D. E. Milenic, E. D. Brady, M. W. Brechbiel, *Nat. Rev. Drug Discov.* **2004**, *3*, 488–499.

[27] E. Hallaba, H. El-Asrag, Y. A. Zeid, *Int. J. Appl. Radiat. Isot.* **1970**, *21*, 107–110.

[28] G. Sugiura, H. Kühn, M. Sauter, U. Haberkorn, W. Mier, *Molecules* **2014**, *19*, 2135–2165.

[29] S. Liu, *Adv. Drug Deliv. Rev.* **2008**, *60*, 1347–1370.

[30] R. J. M. Fry, E. J. Hall, *Radiat. Res.* **1995**, *141*, 347.

[31] E. L. Johnson, T. G. Turkington, R. J. Jaszczak, D. R. Gilland, G. Vaidyanathan, K. L. Greer, R. E. Coleman, M. R. Zalutsky, *Nucl. Med. Biol.* **1995**, *22*, 45–54.

[32] T. G. Turkington, M. R. Zalutsky, R. J. Jaszczak, P. K. Garg, G. Vaidyanathan, R. E. Coleman, *Phys. Med. Biol.* **1993**, *38*, 1121–1130.

[33] M. R. Zalutsky, D. A. Reardon, G. Akabani, R. E. Coleman, A. H. Friedman, H. S. Friedman, R. E. McLendon, T. Z. Wong, D. D. Bigner, *J. Nucl. Med.* **2007**, *49*, 30–38.

[34] H. Andersson, E. Cederkrantz, T. Back, C. Divgi, J. Elgqvist, J. Himmelman, G. Horvath, L. Jacobsson, H. Jensen, S. Lindegren, S. Palm, R. Hultborn, *J. Nucl. Med.* **2009**, *50*, 1153–1160.

[35] A. T. M. Vaughan, J. H. Fremlin, *Int. J. Nucl. Med. Biol.* **1978**, *5*, 229–230.

[36] G. Vaidyanathan, D. J. Affleck, K. L. Alston, X.-G. Zhao, M. Hens, D. H. Hunter, J. Babich, M. R. Zalutsky, *Bioorg. Med. Chem.* **2007**, *15*, 3430–3436.

[37] Y. V. Norseev, *J. Radioanal. Nucl. Chem.* **1998**, *237*, 155–158.

[38] M. R. Zalutsky, D. A. Reardon, G. Akabani, R. E. Coleman, A. H. Friedman, H. S. Friedman, R. E. McLendon, T. Z. Wong, D. D. Bigner, *J. Nucl. Med.* **2007**, *49*, 30–38.

[39] A. S. Narula, M. R. Zalutsky, *Radiochim. Acta* **1989**, *47*, 131–136.

[40] T. Ayed, J. Pilmé, D. Tézé, F. Bassal, J. Barbet, M. Chérel, J. Champion, R. Maurice, G.

Montavon, N. Galland, *Eur. J. Med. Chem.* **2016**, *116*, 156–164.

[41] D. S. Wilbur, M.-K. Chyan, D. K. Hamlin, M. A. Perry, *Bioconjug. Chem.* **2009**, *20*, 591–602.

[42] D. S. Wilbur, M.-K. Chyan, D. K. Hamlin, B. B. Kegley, R. Risler, P. M. Pathare, J. Quinn, R. L. Vessella, C. Foulon, M. Zalutsky, T. J. Wedge, M. F. Hawthorne, *Bioconjug. Chem.* **2004**, *15*, 203–223.

[43] D. S. Wilbur, M.-K. Chyan, D. K. Hamlin, R. L. Vessella, T. J. Wedge, M. F. Hawthorne, *Bioconjug. Chem.* **2007**, *18*, 1226–1240.

[44] D. S. Wilbur, M.-K. Chyan, D. K. Hamlin, H. Nguyen, R. L. Vessella, *Bioconjug. Chem.* **2011**, *22*, 1089–1102.

[45] Y. Li, D. K. Hamlin, M.-K. Chyan, R. Wong, E. F. Dorman, R. C. Emery, D. R. Woodle, R. L. Manger, M. Nartea, A. L. Kenoyer, J. J. Orozco, D. J. Green, O. W. Press, R. Storb, B. M. Sandmaier, D. S. Wilbur, *PLoS One* **2018**, *13*, e0205135.

[46] M. Pruszyński, A. Bilewicz, B. Wąs, B. Petelenz, *J. Radioanal. Nucl. Chem.* **2006**, *268*, 91–94.

[47] M. Pruszyński, A. Bilewicz, M. R. Zalutsky, *Bioconjug. Chem.* **2008**, *19*, 958–965.

[48] M. Pruszyński, M. Łyczko, A. Bilewicz, M. R. Zalutsky, *Nucl. Med. Biol.* **2015**, *42*, 439–445.

[49] R. G. Pearson, *J. Am. Chem. Soc.* **1963**, *85*, 3533–3539.

[50] D. Wilbur, *Curr. Radiopharm.* **2008**, *1*, 144–176.

[51] S. Morzenti, M. L. Bonardi, F. Groppi, C. Zona, E. Persico, E. Menapace, Z. B. Alfassi, *J. Radioanal. Nucl. Chem.* **2008**, *276*, 843–847.

[52] S. Lindegren, P. Albertsson, T. Bäck, H. Jensen, S. Palm, E. Aneheim, *Cancer Biother. Radiopharm.* **2020**, *35*, 425–436.

[53] A. T. Yordanov, O. Pozzi, S. Carlin, G. Akabani, B. Wieland, M. R. Zalutsky, *J. Radioanal. Nucl. Chem.* **2004**, *262*, 593–599.

[54] J. D. Burns, E. E. Tereshatov, M. A. McCarthy, L. A. McIntosh, G. C. Tabacaru, X. Yang, M. B. Hall, S. J. Yennello, *Chem. Commun.* **2020**, *56*, 9004–9007.

[55] C. Ekberg, H. Jensen, S. P. Mezyk, B. J. Mincher, G. Skarnemark, *J. Radioanal. Nucl. Chem.* **2017**, *314*, 235–239.

[56] C. Alliot, M. Chérel, J. Barbet, T. Sauvage, G. Montavon, *Radiochim. Acta* **2009**, *97*, 161–165.

[57] S. Lindegren, T. Bäck, H. J. Jensen, *Appl. Radiat. Isot.* **2001**, *55*, 157–160.

[58] M. R. Zalutsky, X. G. Zhao, K. L. Alston, D. Bigner, *J. Nucl. Med.* **2001**, *42*, 1508–1515.

[59] E. Maeda, A. Yokoyama, T. Taniguchi, K. Washiyama, I. Nishinaka, *J. Radioanal. Nucl. Chem.* **2020**, *323*, 921–926.

[60] J. R. Crawford, P. Kunz, H. Yang, P. Schaffer, T. J. Ruth, *Appl. Radiat. Isot.* **2017**, *122*, 222–228.

[61] G.-J. Meyer, R. M. Lambrecht, *Int. J. Appl. Radiat. Isot.* **1980**, *31*, 351–355.

[62] M. Milanov, W. Doberenz, A. Marinov, V. A. Khalkin, *J. Radioanal. Nucl. Chem. Artic.* **1984**, *82*, 101–109.

[63] J. Schubert, *J. Am. Chem. Soc.* **1951**, *73*, 4488–4489.

[64] J. Schubert, J. W. Richter, *J. Phys. Colloid Chem.* **1948**, *52*, 350–357.

[65] D.-C. Sergentu, Geometries, Electronic Structures and Physico- Chemical Properties of Astatine Species: An Application of Relativistic Quantum Mechanics, **2016**.

[66] G. L. Johnson, R. F. Leininger, E. Sergè, *J. Chem. Phys.* **1949**, *17*, 1–10.

[67] E. H. Appelman, *J. Phys. Chem.* **1961**, *65*, 325–331.

[68] E. H. Appelman, E. N. Sloth, M. H. Studier, *Inorg. Chem.* **1966**, *5*, 766–769.

[69] E. H. Appelman, *J. Am. Chem. Soc.* **1961**, *83*, 805–807.

[70] E. H. Appelman, Chemical Properties of Astatine, **1960**.

[71] G. W. M. Visser, *Radiochim. Acta* **1989**, *47*, 97–104.

[72] S. Fischer, R. Dreyer, S. Albrecht, *J. Radioanal. Nucl. Chem. Lett.* **1987**, *117*, 275–283.

[73] I. Dreyer, R. Dreyer, V. A. Chalkin, M. M., *J. Radiochem. Radioanal. Lett.* **1979**, *40*, 145–154.

[74] I. Dreyer, R. Dreyer, V. A. Chalkin, *J. Radiochem. Radioanal. Lett.* **1978**, *35*, 257–262.

[75] R. Dreyer, I. Dreyer, M. Pfeiffer, F. Rösch, *J. Radiochem. Radioanal. Lett.* **1982**, *55*, 207–214.

[76] R. Dreyer, I. Dreyer, F. Rosch, G.-J. Beyer, *J. Radiochem. Radioanal. Lett.* **1982**, *54*, 165–176.

[77] A. Cavallero, Contribution to the Study of Some Fundamental Chemical Properties of Astatine, Louvain Univ. Catholique, Louvain-la-Neuve (Belgium), **1981**.

[78] A. Cavallero, K. Roessler, *Radiochim. Acta* **1989**, *47*, 113–117.

[79] A. Cavallero, K. Roessler, *Radiochim. Acta* **1989**, *47*, 109–112.

[80] K. Berei, H. W. Eberle, Siegfried H. Kirby, H. Munzel, K. Rossler, A. Seidel, L. Vasáros,

Gmelin Handbook of Inorganic Chemistry Astatine, Springer-Verlag Berlin Heidelberg, **1985**.

[81] T. J. Ruth, M. Dombsky, J. M. D'auria, T. E. Ward, *Radiochemistry of Astatine*, Office Of Scientific And Technical Information, Tennessee, **1988**.

[82] I. Nishinaka, K. Hashimoto, H. Suzuki, *J. Radioanal. Nucl. Chem.* **2018**, *318*, 897–905.

[83] I. Nishinaka, K. Hashimoto, H. Suzuki, *J. Radioanal. Nucl. Chem.* **2019**, *322*, 2003–2009.

[84] I. Dreyer, R. Dreyer, V. A. Chalkin, *J. Radiochem. Radioanal. Lett.* **1978**, *36*, 389–398.

[85] K. Rössler, W. Tornau, G. Stöcklin, *J. Radioanal. Chem.* **1974**, *21*, 199–209.

[86] M. Milanov, V. Doberenz, V. A. Khalkin, A. Marinov, *J. Radioanal. Nucl. Chem. Artic.* **1984**, *83*, 291–299.

[87] F.-C. Wang, Y. V. Norseev, V. A. Khalkin, T. Chao, *Radiokhinmiya.* **1963**, *5*, 351–355.

[88] D. K. Tyung, I. V. Dudova, V. A. Khalkin, *Radiokhimiya.* **1973**, *15*, 548–553.

[89] G. W. M. Visser, E. L. Diemer, *Radiochim. Acta* **1983**, *33*, 145–151.

[90] T. K. Hung, M. Milanov, F. Rösch, V. A. Khalkin, *Radiochim. Acta* **1989**, *47*, 105–108.

[91] D. Schumann, S. Milesz, M. Jovchev, B. C. So, V. Khalkin, *Radiochim. Acta* **1992**, *56*, 173–176.

[92] O. R. Pozzi, M. R. Zalutsky, *J. Nucl. Med.* **2007**, *48*, 1190–1196.

[93] E. Aneheim, S. Palm, H. Jensen, C. Ekberg, P. Albertsson, S. Lindegren, *Sci. Rep.* **2019**, *9*, 15900.

[94] Y. V. Norseyev, V. A. Khalkin, *J. Inorg. Nucl. Chem.* **1968**, *30*, 3239–3243.

[95] D. K. Tyung, I. V. Dudova, V. A. Khalkin, *Sov. Radiochem.* **1973**, *15*, 552–556.

[96] R. Dreyer, I. Dreyer, S. Fischer, H. Hartmann, F. Rösch, *J. Radioanal. Nucl. Chem. Lett.* **1985**, *96*, 333–341.

[97] R. Ludwig, S. Fischer, H. Hussein, M. Frind, R. Dreyer, *J. Radioanal. Nucl. Chem. Artic.* **1989**, *134*, 141–149.

[98] S. Milesz, M. Jovchev, D. Schumann, V. A. Khalkin, M. Milanov, *J. Radioanal. Nucl. Chem. Lett.* **1988**, *127*, 193–198.

[99] S. Milesz, Y. V. Norseev, Z. Szücs, L. Vasáros, *J. Radioanal. Nucl. Chem. Lett.* **1989**, *137*, 365–372.

[100] L. Ning, J. Jiannan, M. Shangwu, C. Hengliu, Y. Yanping, *J. Radioanal. Nucl. Chem.* **1998**, *227*, 187–190.

[101] S. Fischer, R. Dreyer, H. Hussein, M. Weber, H. Hartmann, *J. Radioanal. Nucl. Chem. Lett.* **1987**, *119*, 181–191.

[102] R. Luding, R. Dreyer, S. Fischer, *Radiochim. Acta* **1989**, *47*, 129–130.

[103] R. Ludwig, S. Fischer, R. Dreyer, R. Jacobi, J. Beger, *Polyhedron* **1991**, *10*, 11–17.

[104] A. T. Yordanov, K. Deal, K. Garmestani, H. Kobayashi, B. Herring, T. A. Waldmann, M. W. Brechbiel, *J. Label. Compd. Radiopharm.* **2000**, *43*, 1219–1225.

[105] G. R. Desiraju, P. S. Ho, L. Kloo, A. C. Legon, R. Marquardt, P. Metrangolo, P. Politzer, G. Resnati, K. Rissanen, *Pure Appl. Chem.* **2013**, *85*, 1711–1713.

[106] P. J. Costa, *Phys. Sci. Rev.* **2017**, *2*, 1–16.

[107] G. Cavallo, P. Metrangolo, R. Milani, T. Pilati, A. Priimagi, G. Resnati, G. Terraneo, *Chem. Rev.* **2016**, *116*, 2478–2601.

[108] F. Meyer, P. Dubois, *CrystEngComm* **2013**, *15*, 3058–3071.

[109] S. M. Walter, F. Kniep, E. Herdtweck, S. M. Huber, *Angew. Chemie Int. Ed.* **2011**, *50*, 7187–7191.

[110] C. Laurence, J. Graton, M. Berthelot, M. J. El Ghomari, *Chem. - A Eur. J.* **2011**, *17*, 10431–10444.

[111] J. G. Dojahn, E. C. M. Chen, W. E. Wentworth, *J. Phys. Chem.* **1996**, *100*, 9649–9657.

[112] I. Alkorta, F. Blanco, M. Solimannejad, J. Elguero, *J. Phys. Chem. A* **2008**, *112*, 10856–10863.

[113] J. G. Sunderland, *J. Appl. Electrochem.* **1987**, *17*, 889–898.

[114] D. T. Gjerde, G. Schmuckler, J. S. Fritz, *J. Chromatogr. A* **1980**, *187*, 35–45.

[115] J. E. Madden, P. R. Haddad, *J. Chromatogr. A* **1998**, *829*, 65–80.

[116] M. J. Van Os, J. Slanina, C. L. De Ligny, W. E. Hammers, J. Agterdenbos, *Anal. Chim. Acta* **1982**, *144*, 73–82.

[117] A. D. McNaught, A. Wilkinson, *IUPAC. Compendium of Chemical Terminology, 2nd Ed. (the "Gold Book").*, Blackwell Scientific Publications, **1997**.

[118] B. J. Colston, V. J. Robinson, *J. Environ. Radioact.* **1995**, *29*, 121–136.

[119] J. Van der Lee, **2010**.

[120] M. Maloubier, P. L. Solari, P. Moisy, M. Monfort, C. Den Auwer, C. Moulin, *Dalt. Trans.* **2015**, *44*, 5417–5427.

[121] J. Johnson, F. Anderson, D. L. Parkhurst, **2000**.

[122] P. Atkins, J. De Paula, *Physical Chemistry*, Oxford, **2006**.

[123] S. Sarr, J. Graton, G. Montavon, J. Pilmé, N. Galland, *ChemPhysChem* **2020**, *21*, 240–250.

[124] V. Marimuthu, I. Dulac, K. Kannoorpatti, *J. Bio- Tribo-Corrosion* **2016**, *2*, 17.

[125] M. F. Ashby, D. R. H. Jones, *Wet Corrosion of Materials*, Elsevier Ltd., **2012**.

[126] B. Yang, Z. Zeng, X. Wang, X. Yin, S. Chen, *Acta Oceanol. Sin.* **2014**, *33*, 58–66.

[127] Q. Yu, A. Kandegedara, Y. Xu, D. B. Rorabacher, *Anal. Biochem.* **1997**, *253*, 50–56.

[128] A. Kandegedara, D. B. Rorabacher, *Anal. Chem.* **1999**, *71*, 3140–3144.

[129] F. Réal, A. Severo Pereira Gomes, Y. O. Guerrero Martínez, T. Ayed, N. Galland, M. Masella, V. Vallet, *J. Chem. Phys.* **2016**, *144*, 124513.

[130] G. W. M. Visser, Some Aspects of the Organic, Biological and Inorganic Chemistry of Astatine, **1982**.

[131] L. Liu, N. Guo, J. Champion, J. Graton, G. Montavon, N. Galland, R. Maurice, *Chem. – A Eur. J.* **2020**, *26*, 3713–3717.

[132] R. Wilcken, M. O. Zimmermann, A. Lange, A. C. Joerger, F. M. Boeckler, *J. Med. Chem.* **2013**, *56*, 1363–1388.

[133] P. Metrangolo, G. Resnati, *Chem. Commun.* **2013**, *49*, 1783.

[134] L. Christian, J.-F. Gal, *Lewis Basicity and Affinity Scales: Data and Measurement*, John Wiley & Sons Ltd, **2010**.

[135] F. Zhou, Y. Liu, Z. Wang, T. Lu, Q. Yang, Y. Liu, B. Zheng, *Phys. Chem. Chem. Phys.* **2019**, *21*, 15310–15318.

[136] D.-C. Sergentu, G. David, G. Montavon, R. Maurice, N. Galland, *J. Comput. Chem.* **2016**, *37*, 1345–1354.

[137] L. Christian, J.-F. Gal, *Lewis Basicity and Affinity Scales: Data and Measurement*, John Wiley & Sons Ltd, **2010**.

[138] F. Guérard, J.-F. Gestin, M. W. Brechbiel, *Cancer Biother. Radiopharm.* **2013**, *28*, 1–20.

[139] D. Teze, D. C. Sergentu, V. Kalichuk, J. Barbet, D. Deniaud, N. Galland, R. Maurice, G. Montavon, *Sci. Rep.* **2017**, *7*, 1–9.

UNIVERSITE MATIERE BRETAGNE MOLECULES LOIRE ET MATERIAUX

IMT Atlantique
Bretagne-Pays de la Loire
École Mines-Télécom

Titre : Exploration de la chimie de l'astate en solution : Focalisation sur le diagramme de Pourbaix en milieu non complexant et caractérisation de liaisons halogènes induites par l'astate

Mots clés : astate, spéciation, diagramme de Pourbaix, liaisons halogènes

Résumé : L'astate (At, Z = 85) est un élément halogène rare, tous ses isotopes étant radioactifs. En raison des quantités disponibles limitées, aucun outil spectroscopique n'est applicable pour identifier la nature moléculaire des espèces de At. En conséquence, la chimie de At reste méconnue. L'un de ses isotopes, ^{211}At, est un candidat potentiel pour le traitement de cancers par thérapie alpha ciblée. Cependant, la connaissance limitée de ses propriétés chimiques a entravé les tentatives de marquage de ^{211}At avec des molécules porteuses ciblant la maladie. Cela a conduit au développement d'un programme de recherches sur la chimie de base de At. Cette thèse s'intéresse plus particulièrement au diagramme de Pourbaix de l'astate et à la caractérisation de liaisons halogènes avec l'espèce AtI, au moyen de divers outils expérimentaux (chromatographie ionique, méthode de compétition et électromobilité). Dans une première partie, des études de spéciation de At en milieu alcalin confirment la présence de l'espèce At^- en conditions réductrices. Lorsque le potentiel augmente, l'espèce $AtO(OH)_2^-$ se forme. Le changement de spéciation entre ces deux espèces est décrit pour la première fois. Dans une deuxième partie, la formation de liaisons halogènes entre l'espèce AtI et divers composés organiques a été étudiée. La réactivité se résume par une échelle de basicité nouvellement établie dont la force entre le donneur (AtI) et l'atome accepteur varie suivant l'ordre C ≤ O ≤ S (≈ Se).

Title: Exploration of astatine chemistry in solution: Focus on the Pourbaix diagram in non-complexing medium and characterization of astatine-mediated halogen bonds

Keywords: astatine, speciation, Pourbaix diagram, halogen bonds

Abstract: Astatine (At, Z = 85) is a scarce halogen element, all of its isotopes being radioactive. Due to the limited available quantities, no spectroscopic tool is applicable to identify the molecular nature of At species. Consequently, the chemistry of At remains poorly known. One of its isotopes, ^{211}At, is a potential candidate for the treatment of cancers by targeted alpha therapy. However, the limited knowledge of its chemical properties has hindered attempts to label ^{211}At with disease-targeting carrier molecules. This led to the development of a research program on the basic chemistry of At. This thesis focuses more particularly on the Pourbaix diagram of astatine and the characterization of halogen bonds with the AtI species, by means of various experimental tools (ion chromatography, competition method and electromobility). In the first part, speciation studies of At in alkaline medium confirm the presence of the At^- species under reducing conditions. As the potential increases, the $AtO(OH)_2^-$ species is formed. The speciation change between these two species is described for the first time. In a second part, the formation of halogen bonds between the AtI species and various organic compounds was studied. The reactivity is summarized by a newly established basicity scale, with the strength between the donor (AtI) and the acceptor atom following the order of C ≤ O ≤ S (≈ Se).